The Destabilising Effects of Various Cations on a Surfactant Derivative of Poly Iso-butenyl Succinic Anhydride

by

Christine Elizabeth Rutherford

Submitted in partial fulfilment of the requirements for the degree of Masters of Science, in the Department of Chemistry and Applied Chemistry, University of Natal, 1990

Durban

1990

PREFACE

This thesis presents work carried out by the author and has not been submitted in part, or in whole, to any other University. Where use has been made of the work of others it has been duly acknowledged in the text.

The work described in this thesis was performed in the Department of Chemistry and Applied Chemistry, University of Natal, King George V Avenue, Durban, 4001, from February 1989 to September 1990 under the supervision of Prof L. F. Salter.

ACKNOWLEDGEMENTS

I am indebted to African Explosives and Consolidated Industries, (AECI), Modderfontein, South Africa, and the Council of Scientific and Industrial Research for the financial assistance provided during the course of this work.

I am grateful to my supervisor, Prof L.F. Salter, for his guidance and interest in the progress of this work. To my colleagues, Mr M. Malone (MSc 1989), Mr S. J. Foster (Ph.D 1990) and Mr K. Bolton (MSc 1990), I thank you for the interesting discussions and friendly support during the difficult times.

Thanks also to Mr P. Houlden, the University glassblower, for the construction of glassware and Mr L. Murugas for the use of laboratory equipment.

The loan of equipment from the Departments of Biological Sciences and Civil Engineering, University of Natal, Durban, is gratefully acknowledged.

ABSTRACT

The interfacial behaviour of two amphiphillic poly iso-butenyl succinic anhydride (PIBSA)-derived surfactants and the effect of their interaction with various nitrate salts on the stability of a water-in-oil type emulsion has been investigated.

The adsorption of the esterification product of PIBSA and coco-diethanolamide (PICDEA) and of Experse-70 (E-70) at the equilibrated aqueous-fuel oil interface was investigated via the measurement of interfacial tension using the ring detachment method.

The interfacial pressure of PICDEA decreased in the presence of excess unreacted coco-diethanolamide (CDE) and for both PICDEA and E-70 interfacial pressure decreased with an increase in the length of the poly iso-butenyl (PIB) hydrocarbon tail. Interfacial tension-concentration curves and the Gibbs Equation were used to determine surfactant surface excess concentration and the packing efficiency of the surfactant in the interphase. The double hydrocarbon PICDEA molecule was found to occupy a larger interfacial area than the single hydrocarbon E-70 molecule.

The pH of the aqueous phase effects the interfacial activity and nature of PICDEA and E-70 at the interface. PICDEA is protonated at pH values less than 4.6 and deprotonated at higher pH values. E-70 is neutral at low pH and deprotonated at pH values greater than approximately 2.

The effect of sodium, calcium and ferric nitrate salts on the interfacial free energy of the surfactant saturated interface

was also determined. The interfacial tension at the E-70 aqueous nitrate interface was dependent on ionic strength alone with a general decrease in interfacial free energy as nitrate concentration was increased. In the case of PICDEA, however, a surfactant-cation orientation effect was observed. The divalent Ca^{2+} cation attracts two adjacent PICDEA anions resulting in the adverse interaction of hydrocarbon tails in the interphase. This produces an interface with a higher than expected interfacial free energy. The Na^{+} cation produces an interface with a more energetically stable orientation.

PICDEA in the presence of a ferric nitrate solution (pH 1 to 2) is protonated and therefore the univalent nitrate anion forms the counterion layer at the positively charged surfactant interface.

Stability studies were carried out on aqueous nitrate salt in diesel emulsions using PICDEA as the stabilizing surfactant. Droplet coalescence rates were determined from droplet size distribution data in the presence of varying concentrations of sodium, calcium and ferric nitrate salts. Droplets were sized microscopically at progressive time intervals and the rate of coalescence determined from the change in droplet concentration with time.

Coalescence was found to follow two or more consecutive first order reactions. After an initial period of rapid droplet coalescence, involving small droplets with diameters of 5μm and less, a droplet distribution is attained conducive to a more stable emulsion which then undergoes a slower rate of coalescence involving larger droplets.

The effect of the nitrate salt type on the initial droplet

coalescence rate (in order of increasing rate) is as follows: $Ca^{2+} < Na^{+} < Fe^{3+}$. The opposite trend was observed for the slower long term rate of coalescence, i.e. $Fe^{3+} < Na^{+} < Ca^{2+}$. These trends are explained in terms of the surfactant cation orientation effect, the effect of the droplet's radius of curvature on the potential energy barrier against coalescence and the effect of the droplet distribution of the emulsion system.

LIST OF CONTENTS

LIST OF FIGURES

LIST OF TABLES

ABBREVIATIONS

A.A.	: Acetic Acid
Ac	: Acetone
ACN	: Acetonitrile
EtOAc	: Ethyl Acetate
EtOH	: Ethanol
Iso-p	: Iso-propanol
mag.	: magnification
MeOH	: Methanol
Tlc	: Thin layer chromatography
UV	: Ultra-violet

CHAPTER I

INTRODUCTION

This thesis investigates the interfacial region between two immiscible liquids. This region, often referred to as the interphase, has a finite thickness over which there is a graduation in property. The structure and energies of such an interface are vital in the formation, stabilisation and properties of emulsion systems.

It is difficult to give a full, concise definition of the term "emulsion". Although many definitions exist[1,2,3,4] only one, given by Becher[5], can be considered a complete definition:

"An emulsion is a heterogenous system, consisting of at least one immiscible liquid intimately dispersed in another in the form of droplets, whose diameters in general, exceed 0.1 μm. Such systems possess a minimal stability, which may be accentuated by such additives as surface active agents, finely divided solids, etc."

When considering a mixture of oil and water there are two distinct emulsion types; either an oil-in-water emulsion in which the oil is dispersed throughout a water continuous phase, or a water-in-oil emulsion in which water is the dispersed phase. The investigation covered in this thesis is concerned with the latter emulsion type.

The most fundamental characteristic of an emulsion is its overall thermodynamic instability[6]. The large interfacial area associated with a dispersion of tiny droplets of one liquid in another represents a system of high interfacial free energy. The emulsion will always tend to reduce this free energy by reducing its interfacial area. This is achieved by the merging of small droplets to produce a smaller number of larger droplets. This phenomenon is known as droplet coalescence[7]. Coalescence is a thermodynamically spontaneous process and generally the free energy of a binary system is minimized when two component phases have coalesced into two separate bulk liquid masses.

It is the aim of the emulsion manufacturer to slow down this approach to thermodynamic equilibrium and so prevent the breakdown of the emulsion. It is therefore essential to create a large energy barrier in the coalescence "reaction path"[8]. This is achieved by the addition of surface active agents.

Of considerable importance to the theory of emulsion stability is the interfacial tension between the two liquid phases[9]. The tension of an interface is defined as:

$$\gamma = \left(\frac{dG}{d\Omega}\right)_{T,P,n_i} \qquad (1)$$

where G = the Gibbs energy of the system

Ω = the interfacial area

γ = the interfacial tension

T, P and n_i have their usual meaning

Thus the interfacial tension is the work necessary in forming a unit area of interface which is dimensionally equivalent to force per unit length. The units of surface and interfacial tension used throughout this thesis are mN m^{-1}.

In 1870 Quincke[10] showed that stable emulsions could be readily formed by the incorporation of solutes which greatly lower the interfacial tension. In 1906 Gibbs[11] showed that such surface active solutes accumulate at the droplet interface where they are strongly adsorbed to produce an interfacial film. Bancroft[12] noted the importance of this film to droplet stability. It is the physico-chemical properties of this film and the reduction in interfacial tension which provide the mechanical and energy barriers against coalescence resulting in the stabilization of emulsion droplets.

The adsorption of surface active molecules at an interface always causes a reduction in the interfacial tension[13]. An example of this is the lowering of the interfacial tension between paraffin oil and water from 40.6 mN m^{-1} to 31.05 mN m^{-1} when the aqueous phase is made 0.001M in oleic acid[14]. Consequently, less work is required to produce an emulsion containing adsorbed surfactant molecules. Ruckenstein[15] has shown that if the interfacial tension is of the order of 10^{-2} mN m^{-1} then ΔG_f, the free energy of emulsion formation, is negative and the two separate liquid phases will emulsify spontaneously producing a thermodynamically stable emulsion commonly referred to as a microemulsion. Systems with interfacial tensions greater than 10^{-2} mN m^{-1}

require mechanical work to form a thermodynamically unstable macroemulsion. It follows that the lower the interfacial tension the more stable the emulsion will be. A reduction in interfacial tension reduces the need for the emulsion to minimize droplet interfacial area. Such an emulsion is kinetically rather than thermodynamically stable, but will ultimately form two separate phases[16].

There are various categories of surface active agents[17] the most common of which are the amphiphilic[18] organic compounds, eg. soaps and detergents. These compounds consist of two distinct regions - one possessing polar characteristics and the other non-polar. The polar portion is preferentially water soluble and is therefore referred to as hydrophilic (water-loving) whereas the non-polar region is hydrophobic (water-hating) or lipophilic (oil-loving). Figure (1)[19] is a schematic representation of stearic acid illustrating its amphiphilic nature.

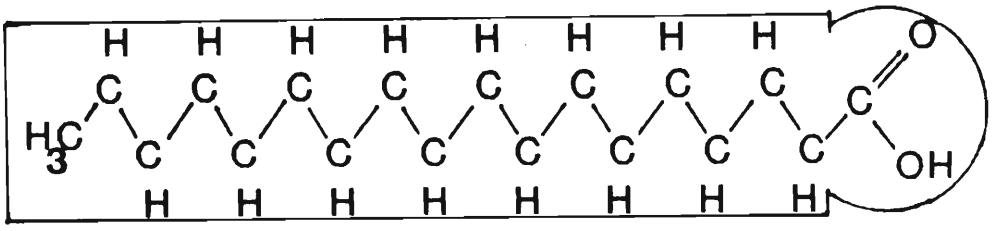

Figure 1. The structure of stearic acid. The section in the rectangle is the hydrophobic hydrocarbon tail; the section in the circle is the hydrophilic carboxylic head.

The surface active agents investigated in this thesis are classified as organic amphiphilic compounds and are used to stabilize water-in-oil emulsion explosives.

1.1. Water-in-oil Emulsion Explosives

In 1967 Bluhm[20] showed that a commercially usable explosive could be produced by forming a water-in-oil emulsion from a hot nitrate salt solution, a paraffinic oil or wax and various emulsifiers (surface active agents) including certain fatty acid derivatives of sorbitol.

The reaction producing a chemical explosion[1] occurs between an oxidiser containing weakly bound oxygen (eg. ammonium nitrate) and a fuel containing atoms which bind strongly with oxygen (such as carbon and hydrogen).

The redox stoichiometry of the reaction between ammonium nitrate and a hydrocarbon is as follows[21]:

$$3nNH_4NO_3 + (CH_2)_n \rightarrow nCO_2 + 7nH_2O + 3nNO_2$$

This reaction requires approximately ten times as much ammonium nitrate by volume as the fuel oil[21]. This requirement is met by using a large volume of a highly supersaturated (and therefore metastable) nitrate salt

---

[1] An explosion is generally understood as an event characterised by a rapid and violent release of energy. A chemical explosion, more specifically, is when the liberated energy is derived from an oxidation/reduction reaction[22].

solution which is finely dispersed in a small volume of hydrocarbon fuel oil. Such a system is referred to as a high internal phase emulsion.

A typical emulsion explosive has the following basic composition[23]:

Constituent	Typical Proportion	Principle Function
Water	15%	Solvent for oxidiser
Ammonium nitrate	70%	Oxidiser
Sodium nitrate	5%	Oxidiser / stability
Calcium nitrate	5%	Alternative to sodium nitrate
Hydrocarbon	5%	Fuel
Surfactant	1%	Emulsifier and stabilizer / fuel

The aqueous phase, ~94% (v/v), consists of a melt of ammonium nitrate, sodium nitrate and/or calcium nitrate with a little water to lower the melting point. This solution is supersaturated and has a crystallisation point of approximately 70 ^{o}C. Sodium and calcium nitrate are added to improve the emulsion stability by lowering the fudge point (crystallisation point) without reducing the nitrate (oxidiser) content of the explosive. In a well prepared emulsion the droplets remain liquid at temperatures as low as -20^{o}C. This can be attributed to the large degree of sub-division of the dispersed phase which ensures that a minute percentage of the droplets contain heterogenous nuclei, i.e. dust particles. According to Bampfield and Cooper[24], a system containing

10^{13} to 10^{15} droplets dm^{-3} has a small percentage of the droplets containing heterogenous nuclei and therefore homogenous nucleation becomes predominant. For ammonium nitrate emulsions with droplet diameters of 1 to 2 μm rapid homogenous nucleation occurs at -30 to -40 ^{o}C. The inclusion of calcium or sodium nitrate salts can lower this temperature further because they increase the complexity of the supersaturated solution and therefore decrease the probability of assembling a critical nucleus.

1.2. The Detonation of an Emulsion Explosive

In the detonation of an emulsion explosive the redox reaction proceeds through the emulsion at a velocity greater than that of sound through the same material[25]. Detonation is initiated by a supersonic shock wave which is propagated through the emulsion via the chemical reaction.

A fast detonation reaction is a function of two factors[26]:

1. The degree of mixing of fuel and oxidiser components, i.e. size distribution of droplets.
2. Supersaturation; most of the droplets must be in liquid form. Liquids react faster than solids in heterogenous detonation.

At normal storage temperatures, where homogenous nucleation is not a major threat, the manufacturer is concerned with two processes which ultimately destroy the detonation sensitivity of the emulsion. First,

heterogenous crystal nucleation on dust particles. This can be overcome by filtration of the aqueous phase prior to emulsification[27]. As previously mentioned, however, the greater the droplet concentration, i.e. the smaller the droplets, the smaller the proportion of droplets containing heterogenous nuclei thus limiting crystal growth. Second, droplet coalescence which reduces the degree of contact between oxidiser and fuel. The larger the droplets the smaller the overall interfacial area between the phases which reduces the degree of contact between fuel and oxidiser phases.

If the manufacturer can minimise the rate of droplet coalescence, then heterogenous crystal growth can be limited (or confined) and the intimate mixing of oxidiser and fuel can be maintained. Consequently, the emulsion will remain sensitive to detonation for longer.

One of the primary objectives of explosive emulsion manufacturers is, therefore, to develop a surface active agent (from inexpensive starting materials) which is capable of minimizing droplet coalescence. Furthermore, the surfactant must not nucleate nitrate crystal growth and, in droplets where nucleation is inevitable, it must restrict crystal growth to individual droplets.

The commonly used surfactants that are effective in fulfilling these requirements are oleic acid esters of sorbitol, glycerides and oxazoline derivatives. More recently certain amphiphilic polymers have been developed including a number of surface active species derived from poly iso-butenyl succinic anhydride (PIBSA). These derivatives offer improved stability over the

conventional emulsifier systems such as SMO (sorbitan mono-oleate). Appendix I shows the molecular structures of a number of PIBSA-derived surfactants. This thesis will describe the investigation of the interfacial properties of two amphiphilic PIBSA-derived surfactants currently used to a limited extent by ICI and AECI in emulsion explosive stabilisation.

1.3. Poly Iso-butenyl Succinic Anhydride (PIBSA)

PIBSA is the malenised product of poly iso-butenyl (PIB). Figure (2) shows the molecular structure of PIBSA. X-ray diffraction on stretched PIB has shown that repeats in the chain occur every eighth $C(CH_3)_2$ unit, i.e. each unit is offset by 45^o from the next which causes the spiralling of the PIB chain[28]. Consequently one would expect the hydrocarbon chain to acquire a relatively bulky configuration. It has been suggested[28], however, that the spiral formation provides the PIBSA chain with good packing potential. PIBSA has a typical amphiphilic structure and is known to be an excellent emulsifier. It is, however, a less efficient emulsion stabilizer[29].

Figure 2. The molecular structure of Poly iso-butenyl succinic anhydride (PIBSA) Adibis (BP): x = 14
Aktol (Exon): x = 22

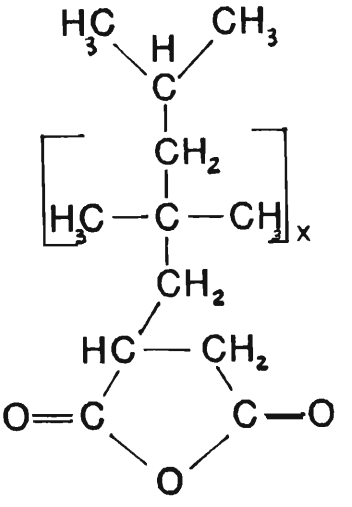

PIBSA is obtained by AECI, Modderfontein from two different sources:

1. BP Chemicals (Additives) Pty. Ltd. (United Kingdom). This PIBSA will be referred to as Adibis PIBSA throughout this thesis. Adibis is an acronym for Additives British Industrial Solvents. The full code name for this PIBSA is Adibis ADX 101 PIBSA. Adibis PIBSA is quoted to have an average molecular weight of 950 $gmol^{-1}$. Therefore it must have an average hydrocarbon chain length of 30 carbons, i.e. x in Figure (2) will be equal to 14. The original sample is blended with a diluent oil and the final composition of Adibis PIBSA supplied by AECI for this investigation has the following composition:

Constituent	Approximate Percentage
PIBSA	55%
PIB (unreacted)	15%
HVI 55	30%

Where HVI 55 (Shell) is a process oil which is believed to have the following approximate composition:

Hydrocarbon	Approximate Percentage
aromatic	2%
paraffinic	65%
naphthenic	32%

(This information was provided by the Chemical Resources Division, AECI, Modderfontein)

2. Exon (Singapore) provide AECI with Aktol ECA 6774 PIBSA. The meaning of Aktol is unknown. The quoted molecular weight of Aktol PIBSA is 1400 g mol^{-1}. Therefore the average hydrocarbon chain length is 47 carbons, i.e. x in Figure (2) will be 22. Aktol PIBSA therefore has a hydrocarbon chain which is ~36% longer than that of Adibis PIBSA. The sample of Aktol PIBSA supplied by AECI for this investigation was quoted as being 100% active. However, a thin layer chromatographic study (Chapter II, Section 2.2.2.1.) showed the presence of a substantial amount of unreacted PIB, indicating that the percentage activity of PIBSA was in fact less than 100%.

1.4. PIBSA-derived Amphiphilic Surface Active Agents

The investigation presented in this thesis is primarily concerned with the interfacial action of the esterification product of PIBSA and coco-diethanolamide (CDE) which is referred to as PICDEA. This derivative's molecular structure is shown in Figure (3). CDE has an average hydrocarbon chain length of 12.3 carbons and an

average molecular weight of 287 g mol^{-1} (Appendix II), i.e. n in Figure (3) will be 11.3. CDE, like PIBSA, is also an amphiphilic molecule. Consequently, PICDEA has a double hydrocarbon structure unlike the conventional single tailed PIBSA-derived surfactants (Appendix I).

PICDEA, prepared from Aktol PIBSA, was supplied by AECI as a 45% active solution in diesel. The average molecular weight of Aktol PICDEA is 1700 g mol^{-1}. PICDEA based on Adibis PIBSA was prepared in this laboratory according to the technique described in Chapter II, Section 2.2.4. The average molecular weight of Adibis PICDEA is approximately 1240 g mol^{-1}.

Most of the work presented in this thesis involves the study of PICDEA, however, when necessary the interfacial activity of PICDEA has been compared with that of Experse-70 (E-70). E-70 is the imide reaction product of PIBSA and monoethanolamine (MEA). The molecular structure of E-70 is shown in Figure (4). E-70 is a single hydrocarbon amphiphilic surfactant and is currently used by AECI in the production of explosive emulsions. E-70 samples based on both Adibis and Aktol PIBSA were supplied by AECI as 50% active solutions in an unspecified diluent.

Figure 3. The molecular structure of PICDEA, the esterification product of PIBSA and CDE

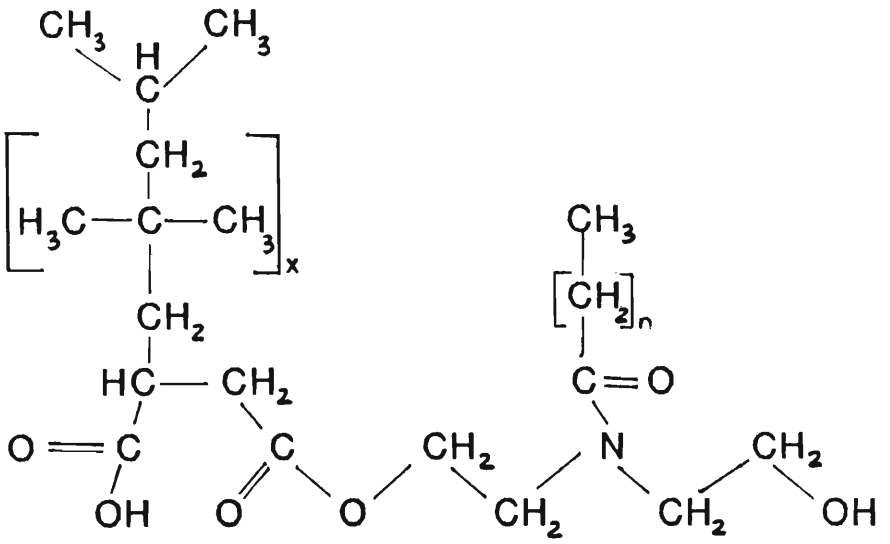

Figure 4. The molecular structure of Experse-70 (E-70)

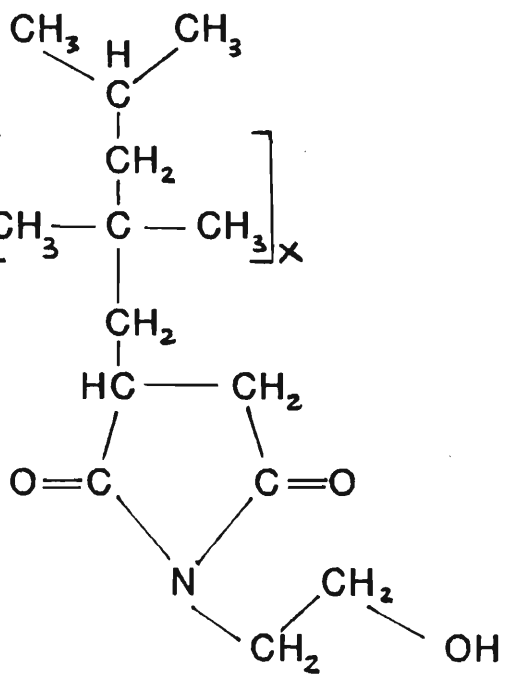

PIBSA surfactants are essentially blends of different PIB chain lengths. The minimum chain length is thought to be approximately 20 carbons, i.e. x = 9 in Figure (1). The maximum length has not been specified. This range in hydrocarbon chain length introduces a large degree of uncertainty in the determination of surfactant concentration. In the experimental chapter of this thesis (Chapter II, Sections 2.2.1 to 2.2.5) surfactant concentrations are quoted to three decimal places. Consequently, the margin of error, although unknown, is expected to be high. Progressive dilutions of a surfactant stock solution, however, enables a relatively accurate determination of the differences in surfactant concentration from one solution to the next. Parameters such as surface excess concentration (defined in Chapter III, Section 3.1) which is dependent on the change in surfactant concentration rather than the actual concentration should therefore have a relatively low, acceptable margin of error.

Chattopadhyay[30] pointed out that coco-alkyl chain derivatives such as PICDEA (Figure (3)) and PICMEA (Appendix I) produce emulsions with a smaller droplet size and higher viscosity than single hydrocarbon PIBSA derivatives, i.e E-70 and others. Furthermore, PICDEA produces emulsions which are less sensitive to shock and shear than other emulsions. Small droplet size, high viscosity and shock/shear stability are all desirable emulsion properties. Chattopadhyay suggests that this is largely due to the double hydrocarbon structure of PICDEA which may promote a more organised, tighter packing at the interface. Chattopadhyay also determined that PICDEA occupies a smaller area at the interface

($67Å^2$) than other PIBSA derivatives[31] even though it has a double hydrocarbon structure and a larger hydrophilic head group than other PIBSA derivatives. Consequently, it was suggested that an interface saturated with PICDEA molecules would be more compact, an interfacial property which Shah[32] has shown helps to reduce the possibility of surfactant hydrolysis. Chattopadhyay[33] showed that PIBSA derivatives are hydrolysed at the aqueous ammonium nitrate interface at a temperature of 80°C. Hydrolysis converts a percentage of the derivative to the original PIBSA anhydride or dicarboxylic form, both of which are less efficient stabilisers. Table (1) is a list of derivatives showing percentage hydrolysis at the aqueous ammonium nitrate interface. Note that double hydrocarbon derivatives, PICDEA and PICMEA as well as the imide E-70 are indeed less susceptible to hydrolysis.

Table 1. Percentage hydrolysis of PIBSA-derived surfactants at the aqueous ammonium nitrate interface at 80°C (After Chattopadhyay[31]).

SURFACTANT	% HYDROLYSED
E476	26
E-70	13
PICMEA	6
PICDEA	13
PNADEA	20
PNBDEA	28

In South Africa (at AECI, Modderfontein) calcium nitrate is added to the ammonium nitrate solution to reduce the fudge point. It has been observed that emulsions stabilised with PIBSA derivatives experience increased instability in the presence of calcium nitrate[34]. Using a spectrophotometric technique Chattopadhyay[35] showed that the dicarboxylic acid form (a hydrolysis product) of the PIBSA derivative is a potential ligand for complexation with the divalent calcium cation. Such a complexation will change the properties of the hydrophilic moiety of the surfactant molecule which could make it less efficient as an emulsion stabiliser.

Table (1) shows that only 13% of both PICDEA and E-70 are hydrolysed at the aqueous ammonium nitrate interface. However, emulsions prepared from PICDEA show a greater instability in the presence of calcium nitrate than E-70 emulsions. The hydrophilic head group of PICDEA has a free carboxylic group which, if deprotonated, could possibly be made available for complexation with Ca^{2+} cations. E-70, on the other hand, does not have a free carboxyl group unless it is hydrolysed.

The aim of this investigation was to determine the effect of such an interaction or complexation between calcium and PICDEA on the properties and structure of the PICDEA interfacial film which as already mentioned has been found to produce and sustain a better quality emulsion than any other PIBSA surfactant.

CHAPTER II

EXPERIMENTAL

The experimental work described in this thesis is divided into three main sections. First, the investigation of the interfacial properties of PIBSA-derived surfactants at an oil-water interface (Section 2.2.1.). Second, the attempts to separate and identify the components of crude surfactant samples using various chromatographic techniques (Section 2.2.2.), and last an investigation of the effects of varying concentrations of different nitrate salts on emulsion stability (Section 2.2.3.). Experimental procedures will be described in the sections that follow the lists of materials and equipment used.

2.1. MATERIALS AND EQUIPMENT

Details of the chemicals and equipment are listed below. Materials used in each separate experimental technique are listed together in alphabetical order. Materials are displayed together with the specific grade used, the supplier's name, the minimum assay quoted by the supplier and any other relevant information.

2.1.1. Materials

2.1.1.1. Chemicals for Surface and Interfacial Tension Measurements.

Acetone	(AR)	SAARCHEM	Assay 99.5%
Ammonium nitrate	(AR)	BDH	Assay 99.5%
Calcium nitrate	(AR)	Merck	Assay 98.0%
Coco-diethanolamide		MANRO	Assay 84.0%
Diesel	AECI: Modderfontein		
Diesel	AECI: Umbogintwini		
Experse-70	(Aktol)	AECI	Assay ~58.0%
Experse-70	(Adibis)	AECI	Assay ~58.0%
Ferric nitrate	(AR)	SAARCHEM	Assay 98.0%
Milli-Q water	Water passed through a Millipore apparatus to remove inorganic and organic contaminants.		
n-Hexane	(HPLC)	May & Baker	Assay 95.0%
Nitric Acid	(AR)	BDH	Assay 99.7%
PICDEA (Batch A)	(Aktol)	AECI	Assay ~45.0%
PICDEA (Batch B)	(Aktol)	AECI	Assay ~45.0%
PICDEA	(Adibis)		Assay ~54.7%
PIBSA, ECA 6774	(Aktol)	AECI	Assay ~100%
PIBSA, ADX 101	(Adibis)	AECI	Assay ~50.0%
Potassium dichromate	(GPR)	BDH	Assay 98.5%
Shellsol PA mineral oil		AECI	
Shellsol PA mineral oil (CLK)		AECI	
Sodium Hydroxide	(AR)	HOLPRO	Assay 98.0%
Sodium nitrate	(AR)	BDH	Assay 99.5%

2.1.1.2. Chemicals used in Chromatographic Separations.

Acetic Acid	(AR)	BDH	Assay 99.7%
Acetone	(AR)	SAARCHEM	Assay 99.5%
Acetonitrile	(HPLC)	Waters	UV cut off 190 nm
			Assay 99.0%
Acid Washed Sand	(AR)	SAARCHEM	
Ammonium Solution	(AR)	BDH	Assay 25%
C18 Silica Gel		Bondapak	
Carbon Tetrachloride	(AR)	BDH	Assay 99.5%
Chloroform	(HPLC)	Waters	UV cut off 245 nm
			Assay 99.0%
Dichloromethane	(LAB)	SAARCHEM	Assay 99.5%
Diesel	AECI: Modderfontein		
	AECI: Umbogintwini		
Ethanol	(LAB)	SAARCHEM	Assay 99.5%
Ethyl Acetate	(LAB)	KLEBER	
Experse-70	(Aktol)	AECI	Assay ~58%
Experse-70	(Adibis)	AECI	Assay ~58%
Filter paper, No.1		WHATMAN	dia. 15 mm
Filter paper, 0.45 µm		MILLIPORE	Type HV
Iodine crystals			
Iso-propanol	(HPLC)	SAARCHEM	UV cut off 210 nm
			Assay 99.7%
Methanol	(HPLC)	WATERS	UV cut off 205 nm
			Assay 99.9%
Milli-Q Water			
Mono-ethanolamine		MERCK	Assay 98.0%
n-Heptane	(AR)	MERCK	Assay 99.0%
n-Hexane	(LiChrosolv)	MERCK	UV cut off 200 nm
			Assay 95.0%
	(HPLC)	MAY & BAKER	Assay 95.0%
			UV cut off 200 nm

PICDEA (Batch A & B)	(Aktol)	AECI	Assay ~45%
PICDEA	(Adibis)	AECI	Assay ~54.7%
PIBSA ADX 101	(Adibis)	AECI	Assay ~100%
PIBSA ECA 6774	(Aktol)	AECI	Assay ~50%
Potassium Bromide	(Spectrosol)	BDH	
Toluene	(AR)	SAARCHEM	Assay 99.8%
TLC Silica plates	(Grade 60)	MERCK	
Tetrahydrofuran	(UV grade)	WATERS	UV cut off 215 nm
			Assay 99.0%
Sephadex LH-20	Pharmacia Fine Chemicals Co. Lot. 59F-0462		

2.1.1.3. Chemicals for the Preparation of Adibis PICDEA

PIBSA ADX 101	(Adibis)	AECI	Assay ~50.0%
Coco-diethanolamide		MANRO	Assay 84.0%

2.1.1.4. Chemicals for the Preparation of Dodecenyl Succinic Anhydride/Coco-diethanolamide Esterification Product

Dodecenyl succinic anhydride		MERCK	Assay 98.0%
Coco-diethanolamide		MANRO	Assay 84.0%

2.1.1.5. Chemicals used in the Preparation of Emulsions.

Calcium nitrate	(AR)	Merck	98.0%
Diesel	AECI: Umbogintwini		
Ferric nitrate	(AR)	SAARCHEM	98.0%
Milli-Q water			
PICDEA	(Adibis)		54.7%
Sodium nitrate	(AR)	BDH	99.5%

2.1.1.6. Chemicals for Photomicrographic Development.

Acufix rapid fixer	Paterson
Anti-static wetting agent	Paterson
Rodinal film developer	Agfa
Neutol Liquid NE	Agfa
35 mm Pan F black and white photographic film	Ilford
Brovira speed photographic paper grade 4	Agfa

2.1.2. Equipment

DMS 300 UV/VIS Double Beam Spectrophotometer (VARIAN)
Serial No. 809139

IR-408 Spectrophotometer Serial No. 00104 (SHIMADZU)

Torsion Balance Serial No. 41682F (WHITE)

Volac High Precision Micro-pipetters 100-1000 µl
5-50 µl

Rotary Evaporator Type RV05 (JUNK & KUNKEL)
Serial No.153191

Overhead Stirrer Serial No. 501104 (HEIDOLPH)

Photographic Enlarger Type IIa (OSRAM)
Serial No. 586389

Developing Tank (PATERSON)

2.1.3. Names and Addresses of Chemical Suppliers

BDH Chemicals Ltd
Broom Road
Poole, Dorset, BH12 4NN
England

Kleber Chemicals
P.O. Box 12018
Jacobs, 4026
South Africa

SAARCHEM (Pty) Ltd
P.O. Box 144
Muldersdrift, 1747
South Africa

Waters (Division of
Millipore): Agent
P.O. Box 2268
Pinetown, 3600

Holpro
P.O. Box 7868
Johannesburg
2000
South Africa

Manro Products (Pty) Ltd
P.O. Box 515
Bergvlei
2001
South Africa

E. Merck
D-6100 Darmstadt
F.R. Germany

AECI
Explosives Division
Private Bag X2
Modderfontein 1645
Johannesburg

2.2. EXPERIMENTAL TECHNIQUES

2.2.1. Surface and Interfacial Tension Measurements

In this work interfacial and surface tensions were determined using the ring detachment method. In using this method a platinum wire ring is placed in the liquid surface (or interface) and the force required to detach the ring from the surface is measured.

Prior to 1926 the false assumption was made that the maximum pull (P) per cm on the ring at the point of detachment from a liquid surface was equal to the surface tension of that liquid[36] and therefore:

$$P = Mg = 2\pi\gamma R' + 2\pi\gamma(R' + 2r)$$

$$= 4\pi\gamma(R' + r)$$

and hence,

$$\gamma = \frac{Mg}{4\pi R} \qquad (2)$$

where M = mass of liquid supported by the ring
R' = outside radius of the ring
r = radius of the wire of the ring
R = average radius of the ring (R' + r)
γ = surface tension
g = acceleration due to gravity

This equation assumes that as the ring is pulled up it supports a perfect cylinder of liquid. However, the shape of liquid observed experimentally is shown in Figure (5)[37], thus falsifying this assumption. Figure (5) illustrates the distension of the surface film just before detachment.

Figure 5. The distortion of the surface or interfacial film by a tensiometer ring immediately before detachment of the ring from the film. R is the radius of the ring and r is the radius of the wire from which the ring is made

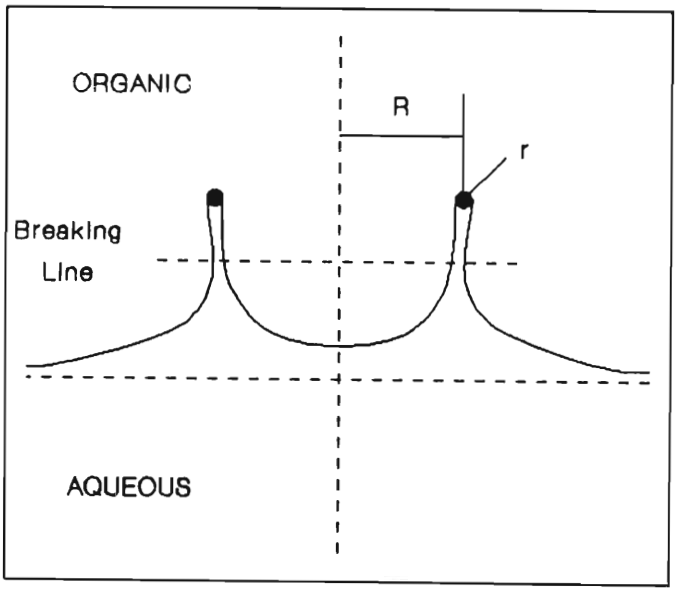

In 1926 Harkins, Young and Cheng[38] showed that the shape of the liquid supported by the ring is a function of two dimensionless variables. These are the ratio of the cube of the radius of the ring to the volume of the liquid (R^3/V), and the ratio of the radius of the ring to the radius of the wire from which it is made (R/r).

The shape is also a function of the liquid's surface tension so that Equation (2) becomes:

$$\gamma = \frac{Mg}{4\pi R} \cdot f\left(\frac{R^3}{V}, \frac{R}{r}\right)$$

and hence,

$$\gamma = \frac{Mg}{4\pi R} \cdot F \qquad (3)$$

where M,R and g are the same variables as previously defined in Equation (2)

F = the correction factor

The correction factor F can be obtained from tables calculated by Harkins and Jordan[36] and Freud and Freud[39]. Use of the correction factor may be obviated entirely by determining the values of P for a number of pure liquids in order to construct a calibration curve[40]. This curve will then be characteristic of the particular ring being used. Alternatively, the balance used for the measurement of P can be calibrated for use with one particular ring.

The most common apparatus used to measure the pull on a ring is the torsion balance originally devised by P. L. Du Nouy[41] in 1919. Du Nouy designed this torsion balance specifically for the determination of surface tension via the ring detachment method. The White torsion balance used in this work is a modified version of Du Nouy's original design.

The White torsion balance, illustrated in Figure 6(a), was supplied with its own platinum ring, Figure 6(b), for which the balance is calibrated. Consequently surface and interfacial tensions can be determined directly without incorporating the correction factor.

Before discussing the specific experimental procedures adopted in this work there are a number of important experimental requirements which need to be emphasised. These requirements are essential if the ring method is to be used with an acceptable degree of accuracy. Small deviations from these requirements can lead to large errors in the results obtained. These requirements[36,41,43] which are discussed below, were taken into careful consideration in this work and have aided in giving more meaningful, reproducible results.

1. The ring method requires that the vessel containing the liquid be large enough so that any curvature of the free surface of the liquid would not be great enough to affect the shape of the liquid raised by the ring. Harkins and Jordan[36] have shown that this requirement is met if the diameter of the vessel is not less than 8 cm. The vessel used for the purpose of surface tension measurement in this work was a crystallisation dish with a diameter of 8.5 cm. It is not clear from the literature what diameter vessel should be used for the measurement of interfacial tensions. The beaker supplied with the White torsion balance has a diameter of 5.5 cm and was used for all interfacial tension measurements ensuring a fixed water-oil interfacial area.

Figure 6(a). The White torsion balance

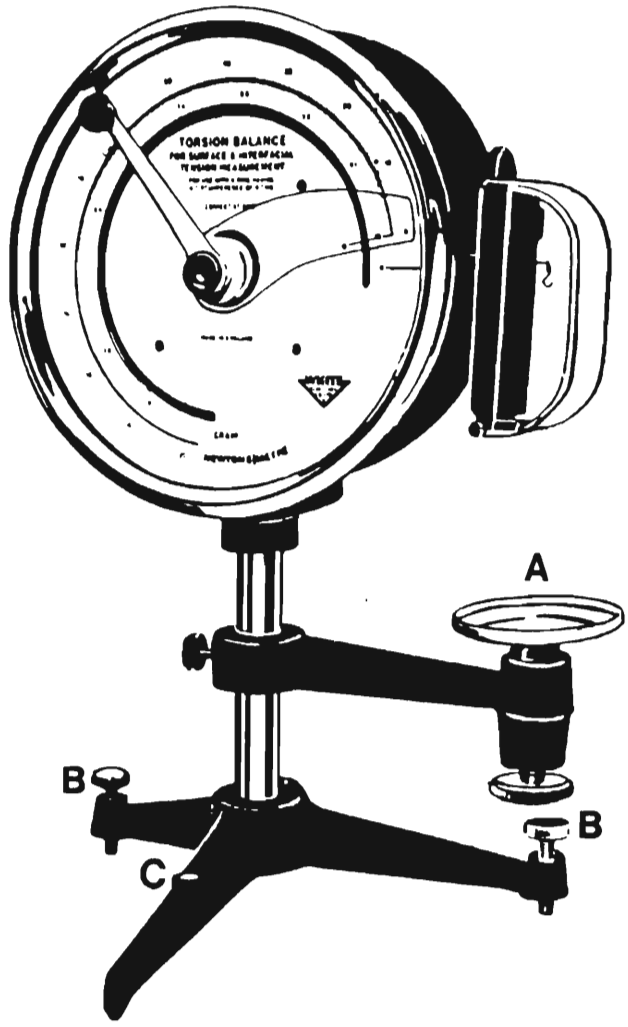

A is the horizontal vertically moveable platform, B are levelling screws and C is a built in spirit level.

Figure 6(b). The Platinum ring supplied with the White torsion balance

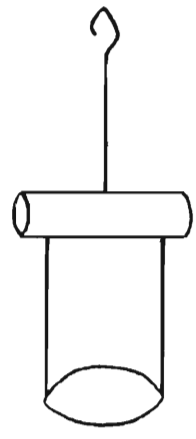

2. The most significant source of error arises when the ring is not kept horizontal. When the ring is tilted by small angles ($< 1.5^{o}$), as are liable to be encountered during experimentation, the error introduced is proportional to the square of the angle, i.e.

$$\Delta P = k\alpha^2 \qquad (4)$$

where α = angle of tip of the ring

$k = 0.36$ when $\alpha < 1.5^{o}$

In order to maintain an error below 0.1% the angle of tip must be less than 0.47^{o}. In this work levelling of the ring was approximated as closely as possible using the following method. The ring was suspended below and within 1 mm of the surface of water in a beaker placed on the tensiometer's vertically moveable platform (A). The platform was made level with the aid of two levelling screws (B) and a spirit level (C) in the base of the apparatus illustrated in Figure 6(a). By sighting between the surface of the water and the ring in two mutually perpendicular directions small degrees of tip could be determined. The glass rod from which the ring is suspended (Figure 6(b)) was then carefully tilted until the plane of the ring appeared to be perfectly horizontal.

3. The wire of the ring must lie in one plane otherwise consistently lower readings are obtained due to a reduction in the pull on the ring. The wire of the ring was aligned by positioning the ring on a smooth flat

surface and sighting it from various directions to ensure complete contact of the ring with the surface. In this manner any bend in the ring is easily detected and could then be straightened by lightly tapping the bent area with a glass rod.

4. The surface of the liquid must be free from wave motion and there must be no motion of the ring. Both of these requirements can only be met with extreme care and a steady hand whilst lowering the platform. The screw mechanism (D) was kept well greased so that minimal force was needed in lowering the platform.

When all of these requirements are met the ring method is considered to be highly accurate in the measurement of surface tensions[42,44]. However it is reputably less precise in the measurement of interfacial tensions.[42,45] It has been noted[46] and observed experimentally in this work that the exact point of detachment of the ring from the liquid interface is less rapid and less pronounced than it is at the liquid surface. Consequently, experimental error is expected to be greater when taking interfacial tension measurements than with surface tension measurements.

In this study of PIBSA surfactants, the organic-aqueous interface experiences an ageing effect due to the slow migration of these bulky amphiphilic molecules from the interior of the bulk oil phase to the interface. This is due to the high energies involved in their transportation through the diluent phase[47]. The adoption of the ring method enables one to take this ageing phenomenon into account and measurements were taken once the interface

had reached equilibrium. This was achieved by immersing the platinum ring in the aqueous phase before the addition of the upper organic-surfactant phase and then allowing the system to equilibrate before a measurement was taken. In using this technique one is able to prevent the unavoidable disturbance of the equilibrated interface which would result if the ring were lowered through the interface into the aqueous phase. Furthermore, this method ensures the complete wetting of the ring by the aqueous phase, i.e. it eliminates the possibility of oil droplets adhering to the ring which would probably occur if the ring were lowered through the oil phase. Consequently, because of the extended ageing required for measurements in this system it is thought that the ring method is the most appropriate for the investigation of the systems considered in this work.

The only other method which could have been successful for this system is that described by McGee[48] using equipment designed by Harkins and Humphrey[49], in which the drop weight method is used to determine interfacial tensions taking interfacial ageing into account. In this method the drop weight is measured as a function of the period of drop fall and the results are extrapolated to an infinite time of fall. Unfortunately the type of apparatus necessary for this technique was not available in this laboratory.

The following pages in this section describe the systems examined and the experimental procedures followed for interfacial tension measurement.

Before each set of measurements was taken the torsion balance was zeroed. Klopsteg[50] argued that the zero weight should be taken as the weight of the ring plus the weight of the drops of liquid which adhere to it, whilst MacDougal[51] considers that such a correction is not justified. Theory indicates that the zero point should be taken as the weight of the dry ring in air. Harkins and Jordan[36] observed that the weight of liquid that adheres to a ring is constant only if the air is saturated with the vapour. In this work the air is not saturated with vapour so for the purpose of surface tension measurements, the zero point was taken as the weight of the dry ring in air. For the purpose of interfacial tension measurements the balance was zeroed when the ring was immersed in the upper oil layer, so that the weight of the oil on the ring is taken into account. In both cases the "zero adjuster" knob was turned until the small beam pointer and the large index pointer were set accurately at zero.

In using the tensiometer for surface tension measurements, a crystallisation dish was placed on the platform and overflowed with the liquid, thus ensuring a uniformly clean surface. The dish was elevated until the ring made contact with the liquid surface. Tension was then applied to the torsion wire by rotating the knurled knob whilst the dish was slowly lowered at a rate such that the beam pointer remained zeroed. This reduced the distortion of the film prior to detachment and thus increased the accuracy[52]. When the tension on the wire was equal to the pull required to detach the ring from the surface or interface, the beam pointer would spring up. The tension was then read directly from the scale.

To check the accuracy of the apparatus (set up according to the requirements previously mentioned) and the experimental procedure, the surface tension of Milli-Q water was measured and compared to the literature value. Figure (7) is a calibration curve constructed from literature values[53], showing the change in surface tension (mN m^{-1}) of pure water as a function of temperature. From this graph the surface tension at 23°C for pure water is 72.9 mN m^{-1}. Using the White torsion balance the average surface tension for Milli-Q water at 23°C was measured as 71.96 mN m^{-1} with a standard deviation of 0.22 mN m^{-1}. The experimental error observed when measuring surface tensions using this procedure is therefore 1.3 %. Although this error is relevant only to the experimentally obtained surface tension values for Milli-Q water, it indicates that the apparatus and procedure are correctly set up. The measurement of the surface tension of Milli-Q water was repeated on several occasions ensuring that the experimental error never exceeded 1.3%.

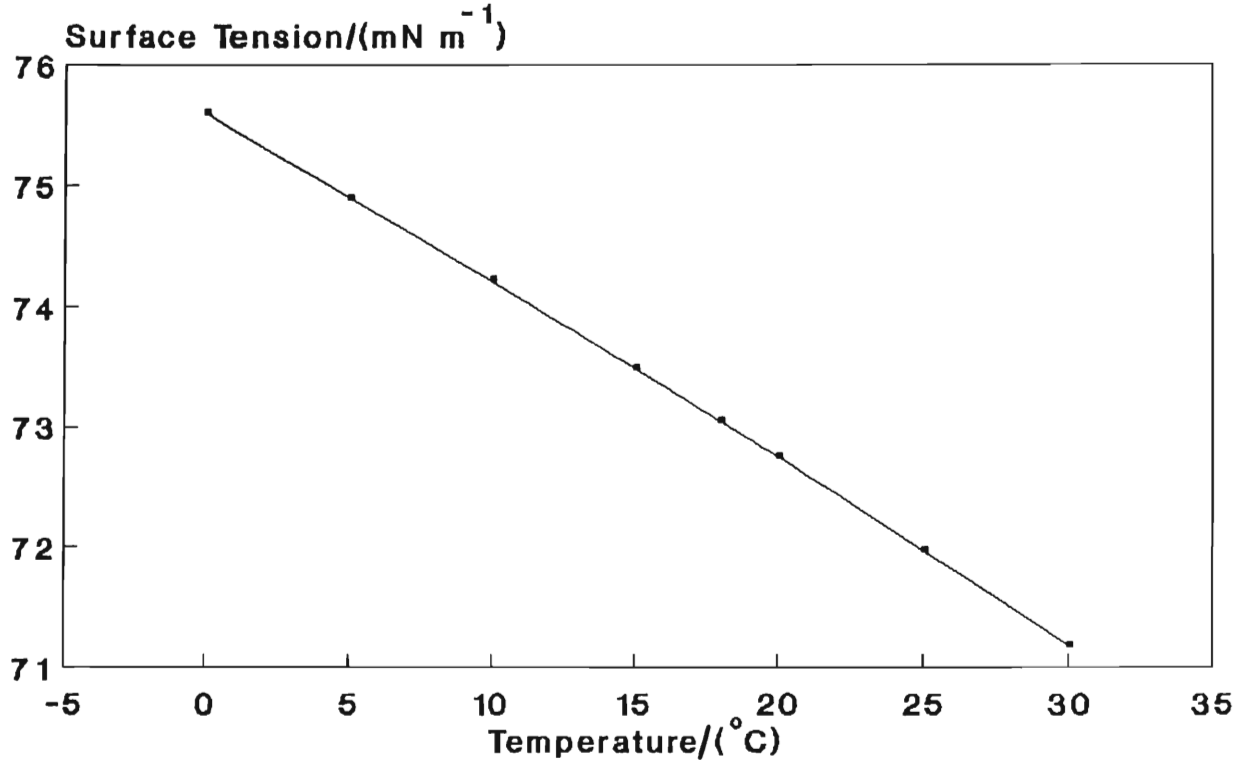

Figure 7. The Change in Surface Tension of Pure Water as a Function of Temperature[62]

Initially all interfacial tension measurements determining the interfacial activity of PICDEA were carried out using solutions prepared from 45% active PICDEA (w/w) (based on ECA 6774 Aktol PIBSA) in diesel oil. Two batches of this type of PICDEA were supplied by AECI. These shall be refered to as Batch A Aktol PICDEA and Batch B Aktol PICDEA. At a later stage PICDEA was prepared in this laboratory (Section 2.2.4.) using starting materials supplied by AECI. This PICDEA (54.7% active (w/w)) contains HVI process oil instead of diesel and was prepared from ADX Adibis PIBSA. It is referred to as Adibis PICDEA. Two batches of Experse-70 were also supplied, one based on Adibis PIBSA the other on Aktol PIBSA.

Surfactant solutions were prepared by weighing the appropriate amount of a particular surfactant-diluent batch and diluting to a desired volume with either diesel (ex. Modderfontein or ex. Umbogintwini) or Batch A or Batch B Shellsol PA. Progressive dilutions were then made to prepare a solution series of decreasing surfactant concentration.

The interfacial tension between a dilute solution (0.0028M) of Batch A Aktol PICDEA in diesel and Milli-Q water was measured at various time intervals. A constant plateau of minimum interfacial tension, which represents the interfacial equilibration time, was reached after approximately 20 hours. This ageing effect on interfacial tension is illustrated in Figure (8). E-70 was tested in a similar fashion, producing an equilibration time of approximately 19 hours. All subsequent readings for all the surfactant systems

studied were taken after 20 hours to allow for interfacial equilibration.

The change in interfacial tension due to a change in surfactant concentration was monitored at the oil/Milli-Q water interface. This effect was studied of the following surfactants:

1. Aktol PICDEA (Batch A and Batch B)
2. Adibis PICDEA
3. Experse-70 (Aktol and Adibis)
4. Dodecenyl succinic anhydride/CDE product (DSA/CDE) (Section 2.2.5)

After each measurement the platinum ring was detached from the torsion balance and washed in a hot solution of chromic acid. (Saturated potassium dichromate (10 ml) carefully mixed with concentrated sulphuric acid (990 ml)). The ring was then rinsed, first with distilled water and then with acetone before drying under a hot air blow dryer.

The strong interfacial activity of PIBSA derivatives caused the interfacial surface excess to vary with the volume above the oil-water interface. Hence a standard volume (20 ml) of surfactant solution was added to the surface of the aqueous phase during subsequent experiments. The highly viscous nature of the oil phase made the estimation of the delivered oil volume difficult, but the error involved in the technique was estimated to be of the order of 1-2% which is acceptable for this work as such a small error in volume will have a negligible effect on the final interfacial tension.

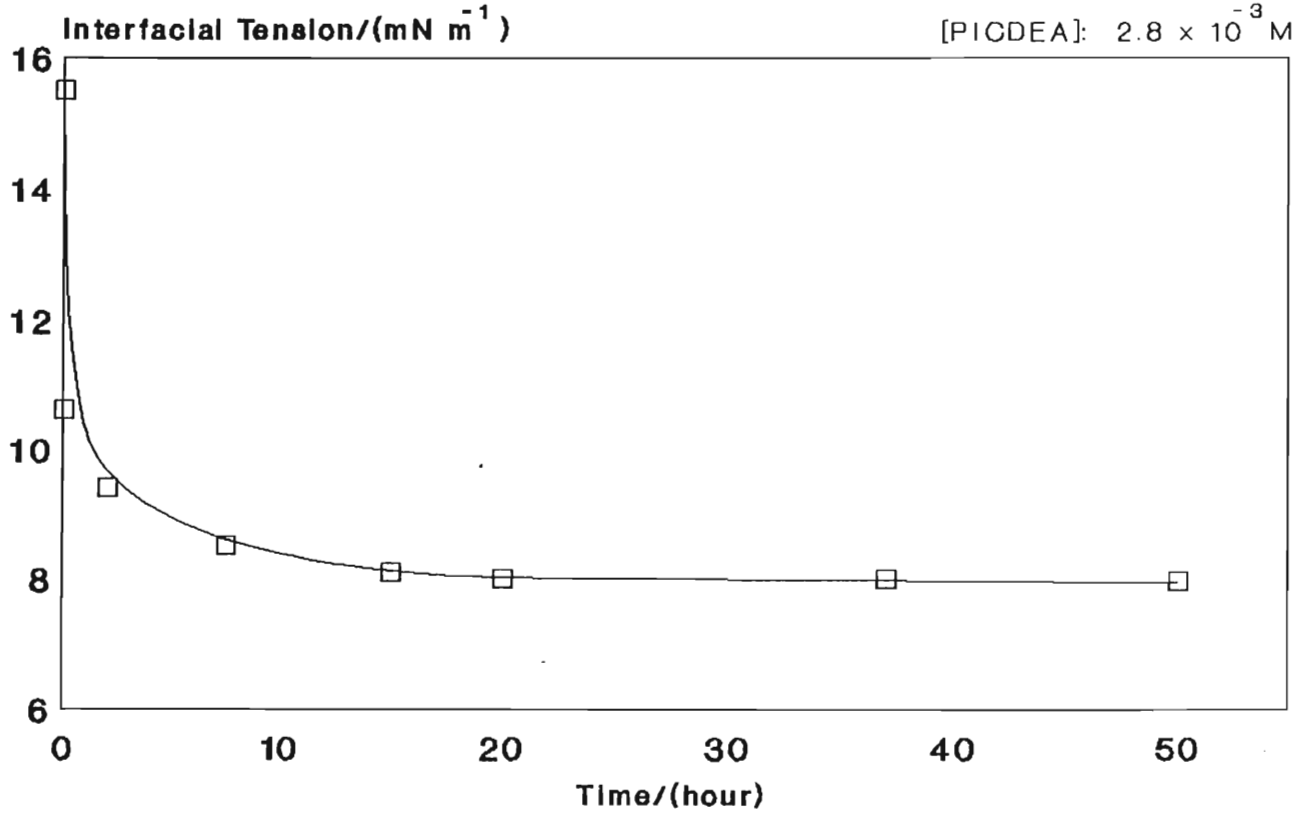

Figure 8. The Change in Interfacial Tension as a Function of Equilibration Time for an Interface Between PICDEA in Diesel and Milli-Q Water

The effect of various nitrate salts on the ability of a particular surfactant to lower the interfacial energy was determined by monitoring the change in interfacial tension as a function of nitrate salt concentration in the aqueous phase. When nitrate salt concentrations were varied, surfactant concentration was maintained at a constant value above the surfactants critical micelle concentration (cmc) thus ensuring that the interface was saturated with surface active molecules. Cmc's were determined from interfacial tension data at the aqueous/oil-surfactant interface in the absence of nitrate salts.

The results of these experiments will be discussed in Sections 3.1.2.2. to 3.1.3.2.

2.2.2. Chromatographic Techniques

If, as discussed in the introduction, a PICDEA - Ca^{2+} complex does exist at the oil water interface, the aim of this work was to characterize it. With this in mind it was essential that a thorough characterization was made of all the components present in the commercially available PICDEA solution. Various chromatographic techniques were used in an attempt to separate and identify these different components. Even though partial separation of PICDEA from its precursors and diluent would seem to be a feasible task, it was rendered difficult by the wide range of hydrocarbon chain lengths which were present in the PICDEA and PIBSA samples.

The following sections (Sections 2.2.2.1. to 2.2.2.3.) will describe thin layer chromatographic procedure, reverse phase liquid chromatography and size exclusion chromatography. It is appropriate to include some of the results at this stage as they help to qualify the logical progression from one chromatographic technique to the next.

2.2.2.1. Thin Layer Chromatography (TLC)

Merck Aluminium foil plates precoated with silica gel (grade 60) without fluorescent indicator (thickness of 0.2 mm) were used for qualitative studies. All samples were prepared by dissolving approximately 0.3g of sample in 20 ml chloroform. Using a Volac 200 µl micropipette, 5 µl samples were spotted onto the plate.

UV light was used to visualize the PIBSA, PICDEA, PIB and diesel components. CDE and its various components were visualized by charring the plate after spraying with a 50% sulphuric acid solution. At a later stage iodine vapour was used to aid visualization as it dissolves in most organic solvents which then appear as brown spots[54]. It was also noted that optimum visualization was obtained when the iodine stained plate was sprayed with 50% sulphuric acid, dried but not charred and then sighted under an ultraviolet lamp.

Figure (9) shows the TLC resolution of the components of Batch A and B Aktol PICDEA and Adibis PICDEA. The standard sample components available were chromatographed alongside the PICDEA samples. The eluent used in this case was 100 % ethyl acetate. R_f values of the components in Figure(9) are given in Table(2).

Figure 9. TLC resolution of the components of Adibis and Aktol PICDEA

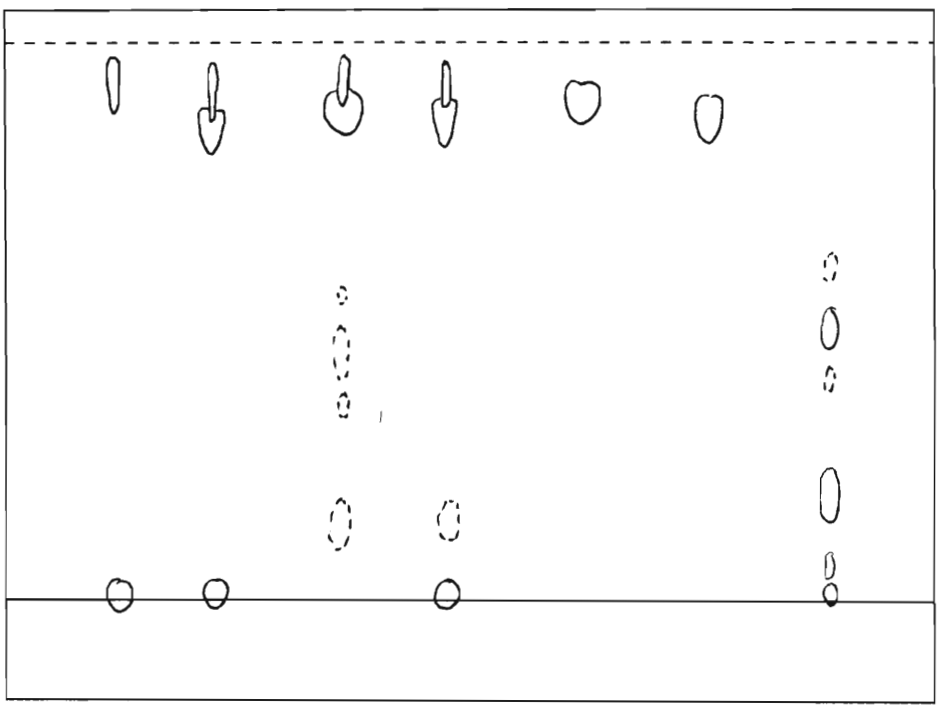

TLC plate: Merck aluminium plate precoated with silica gel (grade 60)

Samples: 5 µl of a 1.5% (w/v) chloroform solution

Table 2. R_f values obtained from TLC of PICDEA components

SAMPLE	COMPONENT R_f VALUES							
DIESEL							0.69	
CDE	0.0	0.04	0.14	0.29	0.45	0.55		
Aktol PIBSA	0.0							0.63-0.83
Aktol PICDEA	0.0		0.11	0.29	0.43	0.53	0.69	0.65- 0.81
Adibis PIBSA	0.0						0.63	
Adibis PICDEA	0.0						0.63	0.65- 0.80
Shellsol PA							0.63	

100 % ethyl acetate did not resolve PIBSA from PICDEA nor did it remove them from the point of application. Many solvent systems were therefore tested in an attempt to elute these components. Referring to the eluotropic series[55] solvent systems were prepared in which PICDEA, its precursors and diluents are completely soluble. It became evident that a solvent system with a high eluent strength was desirable as the polar functional groups of PICDEA and PIBSA are strongly adsorbed by the free silanol polar groups of the silica gel. However, the stronger the eluent strength of the solvent the greater its polarity and hence incompatability with the highly lipophilic PICDEA and PIBSA samples. This made the task of finding a suitable solvent difficult.

Prime examples of the various solvent systems tested are listed in Table (3) together with the R_f values for the different components present in PICDEA.

Table 3. TLC R_f values for the different components of Aktol PICDEA using different eluents.

SOLVENT SYSTEM % v/v	R_f VALUES for components of Aktol PICDEA							
	DIESEL	PROCESS OIL	PIB	PICDEA	CDE R_f Values			
					1	2	3	4
THF 100%	0.83	0.89	0.85-0.96	0.00	0.01	0.30	0.81	0.88
THF/ACN/NH_3 70/25/5	0.82	0.87	0.85-0.97	0.00	0.02	0.50	0.79	0.92
THF/ISO-P 90/10	0.75	0.71	0.76-0.99	0.00	0.01	0.10	0.65	0.81
CH_2Cl_2 100%	0.82	0.78	0.81-0.87	0.00-0.15	/	/	/	/
CH_2Cl_2/A.A 95/5	0.84	/	0.84-0.93	0.00-0.16	0.34	/	/	/
$CHCl_3$ 100%	0.81	/	0.80-0.89	0.00-0.14	0.51	/	/	/
$CHCl_3$/MeOH/Ac 70/15/15	0.87	0.90	0.92-0.99	0.00	0.01	0.30-0.44	0.83	0.75-0.95
TOL/A.A 70/30	0.85	0.80	0.85-0.97	0.00-0.37	0.69	/	/	/
TOL/A.A/ISO-P 55/30/15	0.81	0.78	0.89-0.97	0.03-0.31	0.71	/	/	/

From Table (2) it can be seen that bulk Manro CDE contains 6 different components that are separated from each other using TLC and detectable using the visualisation techniques described above. There are four major amides present in CDE, they are: Lauric diethanolamide, Lauryl diethanol amide, N, N, bis-2-hydroxyethyl lauramide and N,N, bis-2-hydroxyethyl dodecanamide. In addition Manro CDE contains free acids (Appendix II and III), free diethanolamine and free alkali (Appendix III). It can be expected that the more polar components of CDE will have lower R_f values. The component with an R_f value of 0.00 could possibly be free diethanolamine as it is the most polar constituent. The individual components present in CDE have not been characterised in this work, however, it will become evident through the investigation of reverse phase chromatography, size exclusion chromatography and the infra red spectra of the solutes collected (Section 3.2.) that free diethanolamine has an R_f of 0.00. Manro CDE is 84% active (w/w) and therefore it is likely that the larger intense spots detected on a TLC plate will be those of the four major amides listed above. The most intense spots have R_f values of 0.43 and 0.14.

In order to characterize the components separated by TLC, silica was removed from a plate loaded several times with the PICDEA sample by scraping the silica from the appropriate regions. The combined scrapings from two such chromatographic runs were refluxed for 1 hour in dichloromethane (boiling point = 84°C).

The dichloromethane was then rotary evaporated to dryness and infra red spectra were recorded using a liquid cell (NaCl windows; 0.1 mm path length) of a PYE UNICAM SP3-300 Infra Red Spectrophotometer after redissolving the residue in carbon tetrachloride. In some cases the residue was redissolved in chloroform and carefully coated onto a KBr disc under a SPLENDOR 250 W lamp, the heat from which aided the rapid evaporation of the chloroform. Spectra were obtained using a Shimadzu IR-408 Infra Red Spectrophotometer. The infra red spectra of the various components of commercial Aktol PICDEA are illustrated and discussed in Chapter III, Sections 3.2.1. and 3.2.2.

UV spectra were recorded using a quartz cell (1 cm path length) inserted into a VARIAN DMS 300 UV Visible Spectrophotometer. For this purpose residues were dissolved in ethanol or n-heptane. UV spectra are illustrated and discussed in Chapter 3. Section 3.2.1.

Two separate batches of E-70 were compared using TLC. Figure (10) is a representation of the TLC separation of E-70 samples based on Aktol and Adibis PIBSA. The mobile phase was 100 % ethyl acetate. E-70 based on Aktol was found to be contaminated by a solute with an R_f value of 0.139. This component was not present in the Adibis sample. The contaminant was identified as mono-ethanolamine, one of the precursors to E-70. This was achieved by comparing the contaminant's R_f value with that of pure mono-ethanolamine. They were found to be identical.

Figure 10. TLC resolution of the components of Adibis and Aktol Experse-70

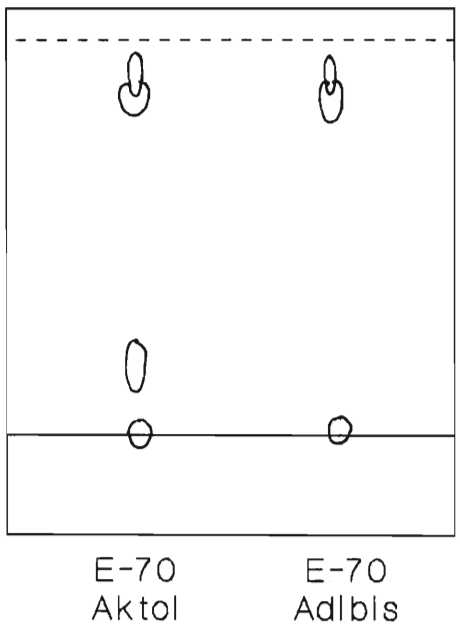

2.2.2.2 Reverse Phase Liquid Chromatography

The strong adsorption of PICDEA and PIBSA molecules to silica gel and the failure to find a solvent system of sufficient eluent strength to elute these polar components from normal phase silica led to the separation attempts using reverse phase liquid column chromatography as described in this section. The polar function of PIBSA surfactants that is strongly adsorbed by silica does not experience any significant adsorption to C18 silica. The most polar components are expected to elute first with diesel, process oils and free PIBSA hydrocarbons having the longest retention times.

A flash chromatographic technique[56] described by W. C. Still et al. was adopted for the purpose of reverse phase liquid chromatography. The apparatus consisted of a glass chromatographic column and an air flow control valve. The flow controller is a simple variable bleed device for precise regulation of the elution rate and is constructed from a glass/teflon needle valve. A small plug of glass wool was placed in the tube connecting the stopcock to the column body. A 1 cm layer of acid washed sand was then added to cover the bottom of the column. 17 cm of dry C18 silica (Bondapak) was poured on top of the sand. The column was gently tapped to pack the gel and another layer of sand was carefully placed on the flat top of the dry gel bed. The column was filled with solvent and pressure applied to rapidly push the air from the silica gel. Figure (11) illustrates the apparatus in detail.

Figure 11. The glass chromatographic column and flow control valve used in reverse phase flash liquid chromatography

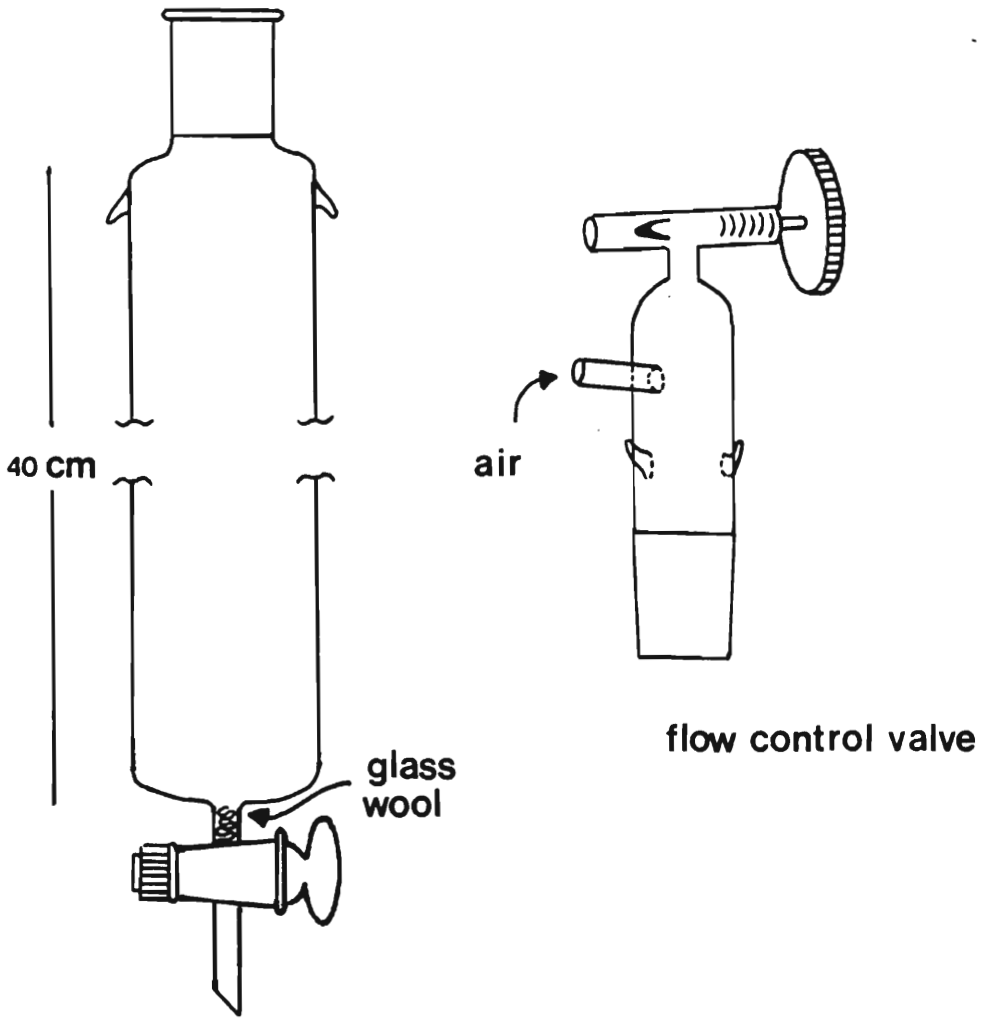

2 ml samples containing 30-40% of 45% active (w/w) Aktol PICDEA (Batch B) in eluent were applied to the top of the adsorbent bed using a Pasteur pipette. By applying pressure the sample was pushed into the gel. The walls of the column were then washed down with a few millilitres of fresh eluent, these washings were also pushed into the gel before refilling the column with eluent. The flow controller was finally secured to the column and adjusted to cause the surface of the solvent to fall at a rate of 4 cm/min. An automatic fraction collector was not used because of the speed of separation. Instead a simple rack holding forty 150 x 14 mm test tubes was manually shifted below the column outlet. In all the systems investigated the first 30 ml of solute free eluent was not collected, all fractions thereafter were 2 ml in volume. Table (4) lists the solvent systems investigated.

Table 4. Solvents used for Reverse Phase Chromatography

SOLVENT	% COMPOSITION
THF	100
THF/ISO-PROPANOL	70/30
$CHCl_3$	100
$CHCl_3$/ACETONE	80/20
$CHCl_3$/ISO-PROPANOL	70/30
CCl_4	100

The order of elution of the sample components was conveniently detected using TLC. TLC identifies those compounds that would not be picked up by a single detection technique such as i.r. or u.v. spectrophotometry. TLC gave a clear visual representation of the co-elution of components and also enabled the identification of components from their known R_f values (see Table (2), Section 2.2.2.1.). The TLC technique adopted is that which is described in Section 2.2.2.1. A mobile phase of 100% ethyl acetate was used throughout.

2.2.2.3 Size Exclusion Chromatography

The role of the solvent is less important in size exclusion chromatography than in other chromatographic techniques[57]. The difficulty in finding a suitable solvent system that could resolve the various components of PICDEA in the chromatographic techniques attempted so far was the main reason which prompted an investigation into size exclusion chromatography.

Sephadex LH-20 (a lipophilic cross-linked dextran gel) has a size exclusion limit of 4000 g mol^{-1}[58]. This means that molecules with a molecular weight greater than 4000 cannot penetrate the gel particles and are therefore eluted without retardation. Since all the components present in commercial PICDEA have molecular weights less than 4000 it is expected that they would be retarded. The extent of retardation will be different for each component depending on both their size and shape.

The gel was prepared by suspending 22 g of Sephadex LH-20 (Bead size 25-100 μm) in 60 ml of tetrahydrofuran (THF) and allowing the gel to swell for 3 hours[58]. Unlike silica gel, LH-20 is a cross-linked dextran gel and thus cannot be dry packed, nor can it be packed under pressure as it is easily compressed[59]. Once swelling was complete, fines and supernatant liquor were decanted and the remaining slurry carefully poured into a glass column with a plug of glass wool and a layer of acid washed sand at the bottom. The gel bed formed as the solvent filtered from the bottom of the column during the sedimentation process, thus improving the homogeneity of the bed.

The experimental apparatus for size exclusion chromatography is illustrated in Figure (12).

LH-20 is the β-hydroxypropyl ether derivative of the hydrophilic dextran gel Sephadex G-25[58]. When chromatography is carried out using organic solvents, eg. 100% chloroform, the remaining free hydroxyl groups of the LH-20 gel retard the migration of solutes containing hydroxyl and carboxyl groups[60,61]. In 1967 Joustra[62] showed that the addition of ethanol or methanol to chloroform eliminates the interaction between these groups and the gel thus making true size exclusion chromatographic fractionation possible. Both pure chloroform and chloroform/ethanol (97:3 % by volume) solvent systems were investigated. The results obtained will be analysed in Chapter 3, Section 3.2.2.

Figure 12. The experimental set up of the chromatographic column used in size exclusion chromatography

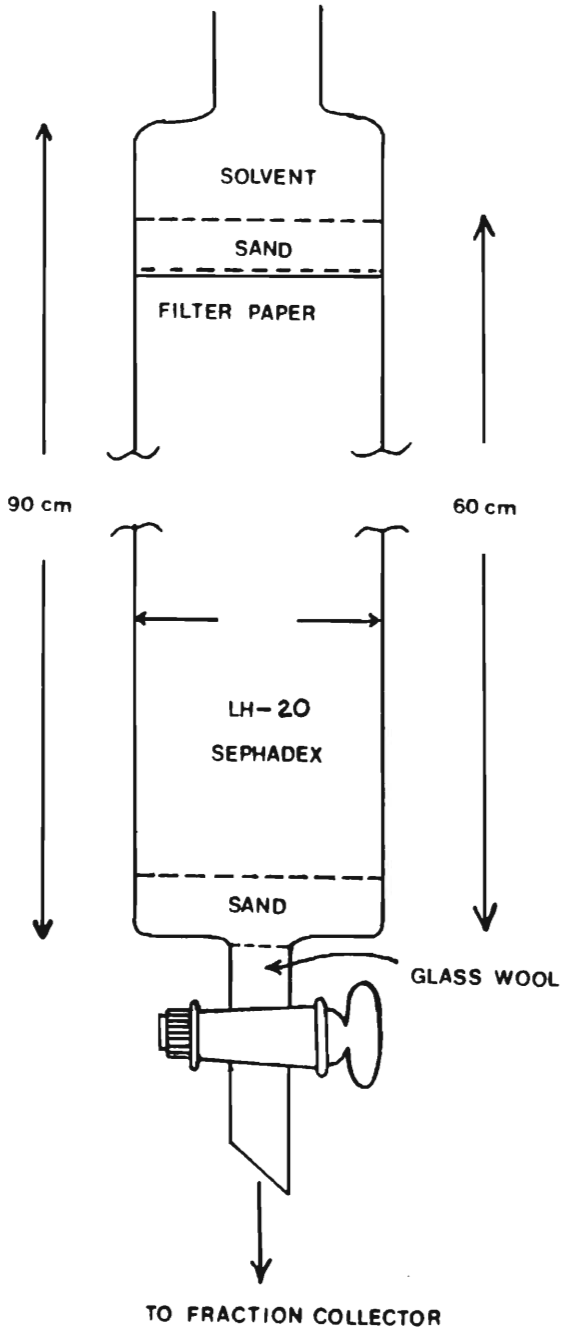

Table (5) describes the samples applied and the elution conditions for each of the solvent systems used.

Table 5. Chromatographic conditions observed in size exclusion chromatography for the various solvent systems used.

SOLVENT SYSTEM	SAMPLE	ELUENT FLOW RATE /ml min^{-1}	FRACTION /ml
$CHCl_3$	Aktol PICDEA	1.15	0.69
$CHCl_3$/EtOH 97:3	Aktol PICDEA	0.63	0.83
THF	Aktol PICDEA	1.16	0.90

In each case the sample solution was 20% rich in solute. Using a pasteur pipette 1 ml of sample solution was pipetted onto the column. The sample was allowed to drain into the gel before additional solvent was applied. The top of the column was protected by a small piece of filter paper which helped to prevent the disturbance of the gel surface when solvent was poured into the column. Fractions were collected using a 2112 REDIRAC fraction collector.

TLC was again used as the detection technique so that the overlapping of solutes could be easily visualised. This was essential as the complete separation of the different components was not expected due to the wide range of molecular weights represented in the surfactant sample. The TLC technique used was that which is described in

Section 2.2.2.1. A mobile phase of 100% EtOAc was used throughout. Once TLC results had been analyzed and solutes identified according to their R_f values, specific fractions were combined and solvents allowed to evaporate. Remaining residues were then redissolved and using the technique described in Section 2.2.2.1., infra red spectra obtained.

2.2.3 Droplet Coalescence Rates

The thermodynamically spontaneous flocculation and coalescence of dispersed phase droplets is an intrinsic characteristic of a surfactant-free emulsion. The surface free energy of a droplet interface can be greatly reduced by the incorporation of a surface active agent. The adsorption of surfactant molecules at an interface forms both mechanical and energy barriers against coalescence. The stronger these barriers against coalescence the more stable the emulsion. The observed destabilization of PICDEA emulsions in the presence of calcium nitrate may be due to the breakdown of mechanical and/or energy barriers due to localised Ca^{2+}-PICDEA interaction or complexation at the interface. It seems reasonable to suppose that this phenomenon may be due to accelerated droplet coalescence and hence a study of the rates of aqueous droplet coalescence suggests itself as a means of monitoring calcium ion effects on emulsion destabilization.

In order to obtain a quantitative evaluation of the effect that Ca^{2+} has on the rate of coalescence and to relate this effect to that of other cations, stability studies were carried out on emulsions of mono-, di- and tri- valent nitrate salts stabilized by PICDEA. The method used is based on the technique described by M. Van Den Tempel in 1957[63] which was subsequently used by P. H. Elworthy et al. in 1970[64] to study the effects of nitrate salts on oil-in-water type emulsions. This method allows for the measurement of coalescence rates in concentrated emulsions. The emulsions prepared in this work are high internal phase emulsions, i.e. they have a

high droplet concentration and can therefore be treated in a similar manner as described by Van Den Tempel. Coalescence rates are determined from droplet size distribution data monitored as a function of time. Section 2.2.3.1. will describe the techniques used in the preparation of emulsions and Section 2.2.3.2. the method used to monitor droplet size distribution.

2.2.3.1. Emulsion Preparation

A series of emulsions, prepared in October 1989, had the following basic volume percentage composition:

Aqueous:	**85%**
Oil (diesel ex. Umbogintwini):	**13%**
Surfactant (PICDEA):	**2%**

The aqueous phase was prepared using Milli-Q water and AR grade nitrate salts, which included $NaNO_3$, $Ca(NO_3)_2.4H_2O$ and $Fe(NO_3)_3.6H_2O$. Nitrate salt concentrations ranged from 0.1 M to 8 M. The oil-surfactant phase was prepared by mixing 70.1 g 45% w/w Aktol PICDEA (Batch B) and diesel in a 250 ml volumetric flask. Combining 15% v/v of this approximately 0.11 M PICDEA in diesel solution with 85% v/v of the aqueous nitrate solution resulted in emulsions being prepared with an overall PICDEA content of 2% v/v. Although the exact ammount of PICDEA cannot be determined accurately, the use of a single stock solution of PICDEA in diesel ensured that each emulsion contained equivalent amounts of PICDEA.

A Heidolph overhead stirrer connected to a variable D.C. supply was used for emulsification. The aqueous phase was slowly added to the oil phase during the first minute whilst the mixture was stirred at a slow speed. The speed was then increased to maximum (No. 10, unknown rpm) and left until the mixture emulsified. The point at which emulsification occurs was clearly visible; the mixture suddenly turned into a highly viscous creamy coloured gel. Emulsification was then terminated approximately 1 minute after the emulsion first appeared simply by switching off the overhead stirrer. These emulsions were stored in 100 ml screw top glass jars in a water bath at 24 ^{o}C. Table (6) lists the cation concentrations used for each of the nitrate salts and the times taken for emulsification to occur. It is apparent that high nitrate concentrations aid in emulsification which is in agreement with the observed reduction in interfacial tension (i.e. surface free energy) as electrolyte concentration is increased (see Chapter 3, Section 3.1.3.2.).

Table 6. Emulsification Times

Na^+ / mol dm^{-3}	Time /min	Ca^{2+} / mol dm^{-3}	Time /min	Fe^{3+} / mol dm^{-3}	Time /min
8.0	20.0	melt	3.0	4.0	19.0
6.0	21.0	6.4	15.0	2.0	24.0
4.0	29.0	5.6	14.0	0.8	23.0
2.0	35.0	4.0	17.0	0.4	25.0
0.8	40.5	2.0	21.0	0.1	26.0
0.4	46.5	0.8	29.0		
		0.4	31.0		
		0.1	30.0		

To determine the effect of increasing the emulsification time beyond the minimum time required to form the emulsion, a series of 2 M calcium nitrate emulsions were prepared. The emulsification time was extended by an additional 5 minutes for each of the emulsions in this series.

A sodium nitrate melt emulsion could not be prepared because of its high melting point, i.e. 306.8°C. The ferric nitrate melt, 8M, 6M and 4M emulsions all crystallized within one week of preparation and an emulsion free of nitrate salt would not form even after emulsification in excess of 1 hour 30 minutes. This precluded these samples from further investigation.

2.2.3.2. The Emulsion Droplet Distribution Analysis Technique

Emulsions were observed after suitable time intervals using an optical microscope. A drop of emulsion was mounted on a glass slide and allowed to spread under a cover slip. The microscope was then focused near the edge of the slowly expanding emulsion drop where the thickness was no more than 2 or 3 droplets. Images were recorded photographically, enlarged and individually analysed to determine droplet size distributions. This section is divided into three sub-sections: the first describes the optical equipment and its set up procedure, the second describes the photographic development and the last describes droplet size analysis.

2.2.3.2.1. The Microscope

The optical equipment consisted of a Nikon BIOPHOT microscope, an Achromat substage condenser, a Nikon Plan 4x projective lense and two Nikon objective lenses: Plan 40x and Plan 20x lenses corrected for chromatic aberration[65].

The following microscope settings were used to ensure that the final projected image would be clearly resolved, of sharp contrast and be projected from a focal plane with the minimum possible depth of focus:

1. The field diaphragm was centered and adjusted so that its image was about the same size as that of the field of view. This aided in creating a sharp image.

2. A bright field was chosen whereby the sample is illuminated by a solid cone of uninterrupted light. This was achieved simply by setting the Achromat phase contraster to zero. Better contrast is achieved using the phase contraster, especially when illuminating samples containing materials of different refractive indices[66], as is the case with a water-in-oil emulsion. However, when using the phase contraster the projected droplet image acquires a 'halo' which makes measurement of droplet diameters almost (and often completely) impossible even though the overall image has better phase contrast.

3. The correct setting of the substage achromat condenser was vitally important. If incorrectly set it causes a reduction in resolution and increases the depth of field. The Numerical Aperture (N.A.) of the illuminating system is adjusted by the substage condenser aperture diaphragm which itself has a N.A. of 0.90. An optimum setting for the aperture ensures that 60-70% of the back focal of the objective is illuminated[67]. This setting ensures that the apical angle of the illuminating cone of light corresponds to the N.A. of the objective lense being used. In this way the optimum N.A. of the objective lense is realised. If the apical angle is increased, dispersed light from the objective will introduce glare or haziness in the image. If the cone is too small, the N.A. of the objective is not fully used thus reducing resolution and increasing the depth of field. The substage condenser aperture was readjusted each time the objective was changed.

4. The two objective lenses used have different N.A.'s and consequently their focal planes have different depths of focus[68], these are indicated in Table (7).

Table 7. Objective Lenses

Objective Lense	Numerical Aperture	Approx. depth of field
Plan 40 x mag.	0.65	1 µm
Plan 20 x mag.	0.4	5 - 10 µm

5. The brightness of the image was reduced slightly by the simultaneous use of a blue and a grey filter built into the illumination system of the microscope and also by adjusting the rheostat control.

2.2.3.2.2. Photomicrographic Development

The BIOPHOT Nikon microscope was fitted with a Nikon FX 35mm camera. The sample image was projected via a Nikon Plan CF 4x projective lense onto a black and white 35 mm Ilford Pan F film (50 ASA). 50 ASA (American Standards Association) refers to the speed of the film, which in this case is very slow. A slow speed film sharply records details and maximises contrast so that enlargements retain the clarity of the original image[68].

Ilford Pan F film is panchromatic, i.e. it is sensitive to all visible wavelengths, however, it is particularly sensitive to blue, hence the choice of a blue filter to reduce the brightness of the illuminating source. A shutter speed of 0.10 seconds was kept constant by altering the brightness of illumination via the rheostat control. This fixed shutter speed ensured a consistent film exposure time which in turn meant that photomicrographic exposure times would be identical for each frame on one particular film. This saved time and minimised wastage of photographic materials.

Negatives and photomicrographs were developed using the following procedure:
Throughout the entire procedure the only light source in the darkroom was a Philips green PF711 lamp suitable for working with panchromatic film. Negatives were developed for 5 mins 30 secs in 500 mls Rodinal film developer (dilution: Rodinal:water::1:50) contained in a Paterson's developing tank. When the developer was poured out of the tank the film was immediately washed under running water for 30 seconds. The film was then fixed using Acufix (dilution: Acufix:water::1:30) for 5 minutes. For optimum permanence, film and papers were fixed for twice the clearance time suggested by Patersons. The film was finally removed from the tank, washed in a bath of clean water for several minutes and then rinsed in water containing a few drops of an anti-static wetting agent to prevent droplet formation so that there would be no marking of the film when it was hung up to dry.

Using an Osram IIa enlarger, photographic paper was exposed with light shone through the negative image. The paper used was Agfa Brovira speed B310 PE glossy grade 4, which gives an image tone of neutral to cold black. Enhanced picture sharpness was achieved by shutting down the aperture to f.11 thus dimming the image and increasing exposure times. Typical exposure times ranged between 10 and 16 seconds. Paper was then developed for 1 minute in Neutol NE developer (dilution: Neutol:water::1:9). Development was terminated by passing the paper through an acetic acid stop bath before fixing in Acufix for several minutes.

2.2.3.2.3. Droplet Size Distribution Analysis

To determine the rate of coalescence it is necessary to monitor the rate of disappearance of droplets per unit volume of emulsion, ie. the change in concentration of aqueous droplets with time[63,64]. Ideally, Laser Diffraction or Coulter Counter techniques should have been used as they determine droplet concentrations directly. Unfortunately, this equipment was not available either in this laboratory or at AECI, Modderfontein.

The determination of droplet concentration from two dimensional photomicrographic images represented a problem. Within a specified area of a photomicrograph, representing 6400 μm^2 in the sample, droplet diameters were measured and arranged into intervals. A histogram could then be constructed showing the percentage of

emulsion droplets per unit area which fall within each size interval. However, this distribution represents only those droplets in a two dimensional plane through the sample centered around the focal plane. As shown in Table (7), depth of field for the objective lenses used is of the order of 1-10 μm. An emulsion is a three dimensional system containing droplets much larger than this (ie. >1-10 μm) that are also centered above and below the focal plane. Hence, a measured diameter is not necessarily the true droplet diameter. Figure (13) illustrates this point, depicting a droplet larger than the depth of field, centered below the focal plane.

Figure 13. The droplet diameter

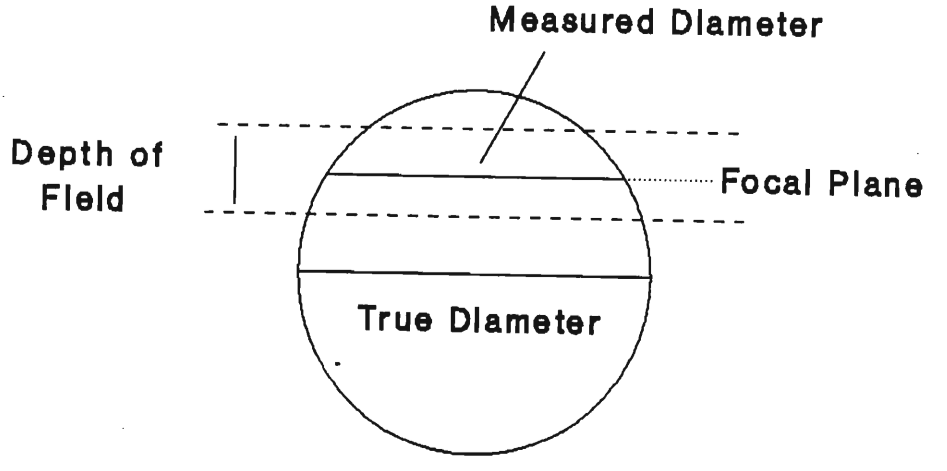

In February 1990 a paper was published by Jokela et al.[69] who believe that they are the first to use a computerized microscope image analysis technique to study emulsion stabilities. Their paper is of particular interest as they report the successful application of a conversion factor to the two dimensional image in order

to obtain droplet concentrations of each range of droplet sizes present in an emulsion sample.

The derivation of this conversion factor is based on their observation that the size of a particle is largely responsible for the maximum distance, D_o, above and below the focal plane within the limits of which the particle can be detected.

Jokela et al. defined the following parameters:

D_f = the recorded diameter in focus.
D_o = the effective observation depth dependent on the particle size.

By plotting D_o vs D_f a linear relationship was observed. The proportionality constant (determined from the slope) for a water in crude oil emulsion was shown to be 1.25. This analysis applied to particles whose centers are located in the same plane. In real emulsions however, the particle centers are located above and below the focal plane as illustrated in Figure (13). Because particles are observed within approximately one diameter of the plane of focus, D_o for real emulsions is twice that of two dimensional systems ie. $D_o = 2.5D_f$.

Concentrations can then be calculated by dividing the number of particles in a particular size range by the effective observed volume relevant to that size. The volume being the product of the measuring frame area (in this work 6400 μm^2) and the value D_o for the particular size range.

2.2.4. Preparation of Adibis PICDEA

Batch A and Batch B Aktol PICDEA exhibit different adsorption characteristics at the oil-water interface (Chapter 3, Section 3.1.2.2.). The presence of unreacted precursors, such as unreacted CDE, is seen to have a detrimental effect on the interfacial properties of the surfactant system. With this in mind a new batch of Adibis based PICDEA was prepared in this laboratory. The aim of this preparation was to minimize the amount of unreacted CDE in the final product. The method described here, using ADX Adibis PIBSA (M.wt = 950 g/mol), is an adaptation of the GTC method which uses 60 % active ECA Aktol PIBSA (M.wt = 1000 g/mol) and assumes that CDE is 100 % active.

Two batches of PICDEA were prepared, one using a test sample of Manro CDE and the other using a sample of the bulk Manro CDE supplied to AECI.

400.6 g of 50 % Adibis PIBSA w/w in HVI process oil was mixed with 72.0 g Manro CDE. According to the specifications provided by Manro, their CDE is 84 % active (Appendix III) and has an average molecular weight of 287 g/mol (Appendix II). These quantities therefore represent equimolar amounts of the reactants. The mixture was heated and kept between 88°C and 93°C for 2 hours. I.R. spectra were taken at various time intervals to monitor the extent of esterification. Figure (14) shows the infra red spectra obtained after the full 2 hour reaction period for the two batches of PICDEA prepared from sample and bulk CDE. In both spectra the peak at 1740 cm^{-1} shows the presence of an ester.

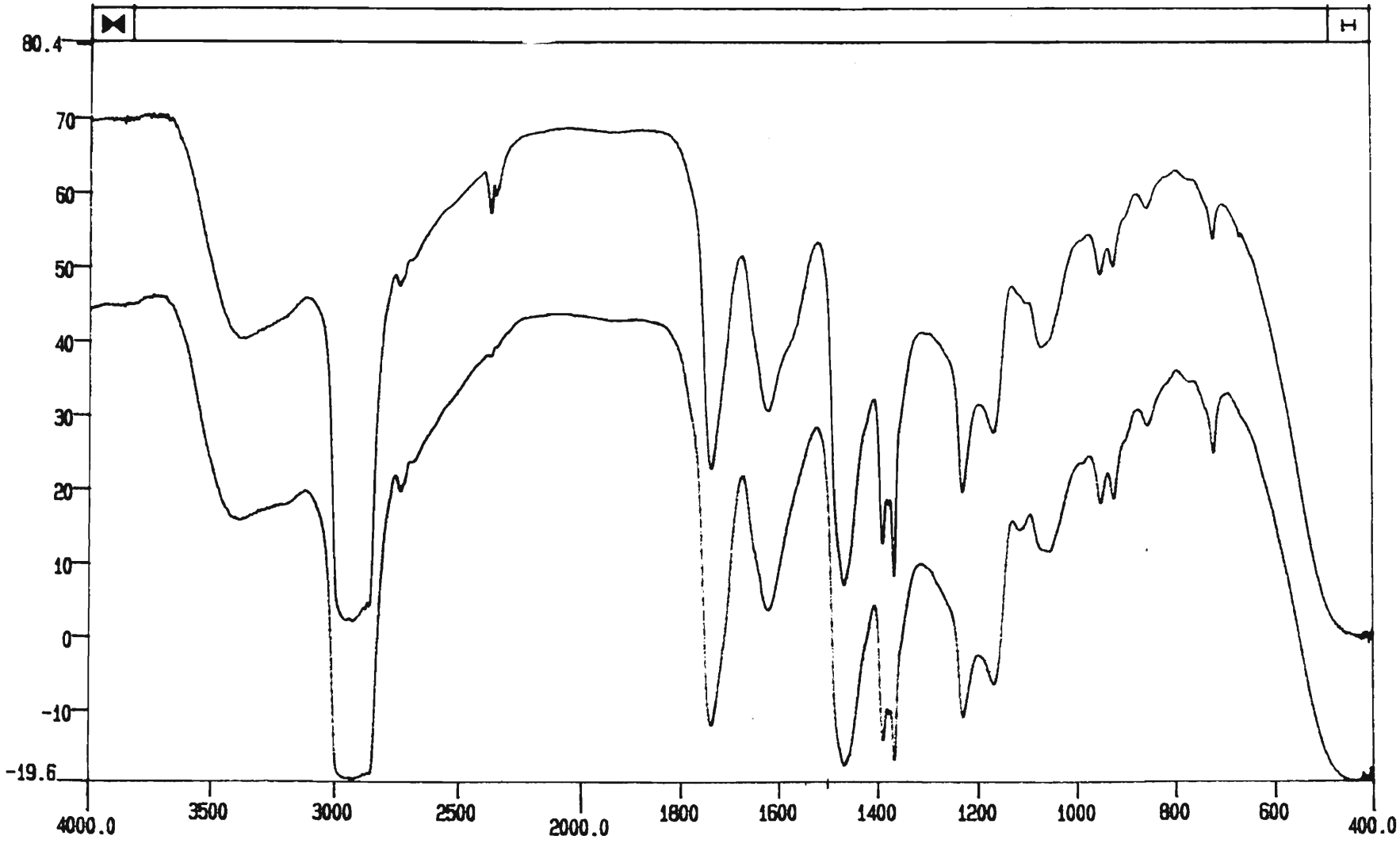

Figure 14. Infra red spectra of Adibis PICDEA; the esterification product of Adibis ADX 101 PIBSA and 1. sample Manro CDE and 2. bulk Manro CDE

Assuming that the esterification reaction goes to completion then the final product is 54.7% w/w PICDEA. The PICDEA prepared from bulk CDE absorbs at a frequency of 1540 cm^{-1}. This is due to the N-H bending vibration of the free amine, diethanolamine. This peak is absent in PICDEA prepared from the initial sample of Manro CDE, suggesting that this batch of CDE is free of unreacted diethanolamine. Bampfield[70] pointed out that short to medium chain length alcohols tend to break down explosive emulsions. Diethanolamine is a short chain alcohol and could, therefore, contribute to the destabilisation of emulsion droplets. The Adibis PICDEA used in the interfacial tension investigation described in Section 3.1.2.5. was that based on sample CDE, thus eliminating the effect of diethanolamine on interfacial tension. The 45% Aktol PICDEA in diesel supplied by AECI was prepared from bulk CDE and therefore contains diethanolamine. This becomes evident in the investigation of chromatographic techniques described in Section 3.2.

2.2.5. Preparation of the esterification product of Dodecenyl succinic anhydride and Coco-diethanolamide

With the aim of determining the interfacial adsorption characteristics of short chain surfactants with the same polar functional groups as PICDEA, the esterification product of dodecenyl succinic anhydride (DSA) and CDE was prepared. Equimolar amounts of DSA and CDE were mixed (ie. 51.02 g 98 % DSA and 64.22 g 84% CDE) and then heated to between 80°C and 90°C for 2 hours 30 minutes. An opaque, yellow, highly viscous substance was produced. The esterification product was identified on examination of the I.R. spectrum shown in Figure (15). As in the preparation and identification of PICDEA, the peak at 1740 cm^{-1} indicates that esterification has occurred. Figure (16) details the molecular structure of the product.

Figure 16. The molecular structure of the esterification product of CDE and DSA

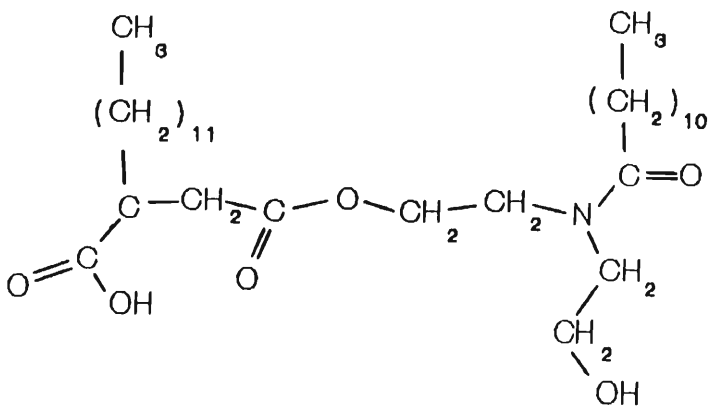

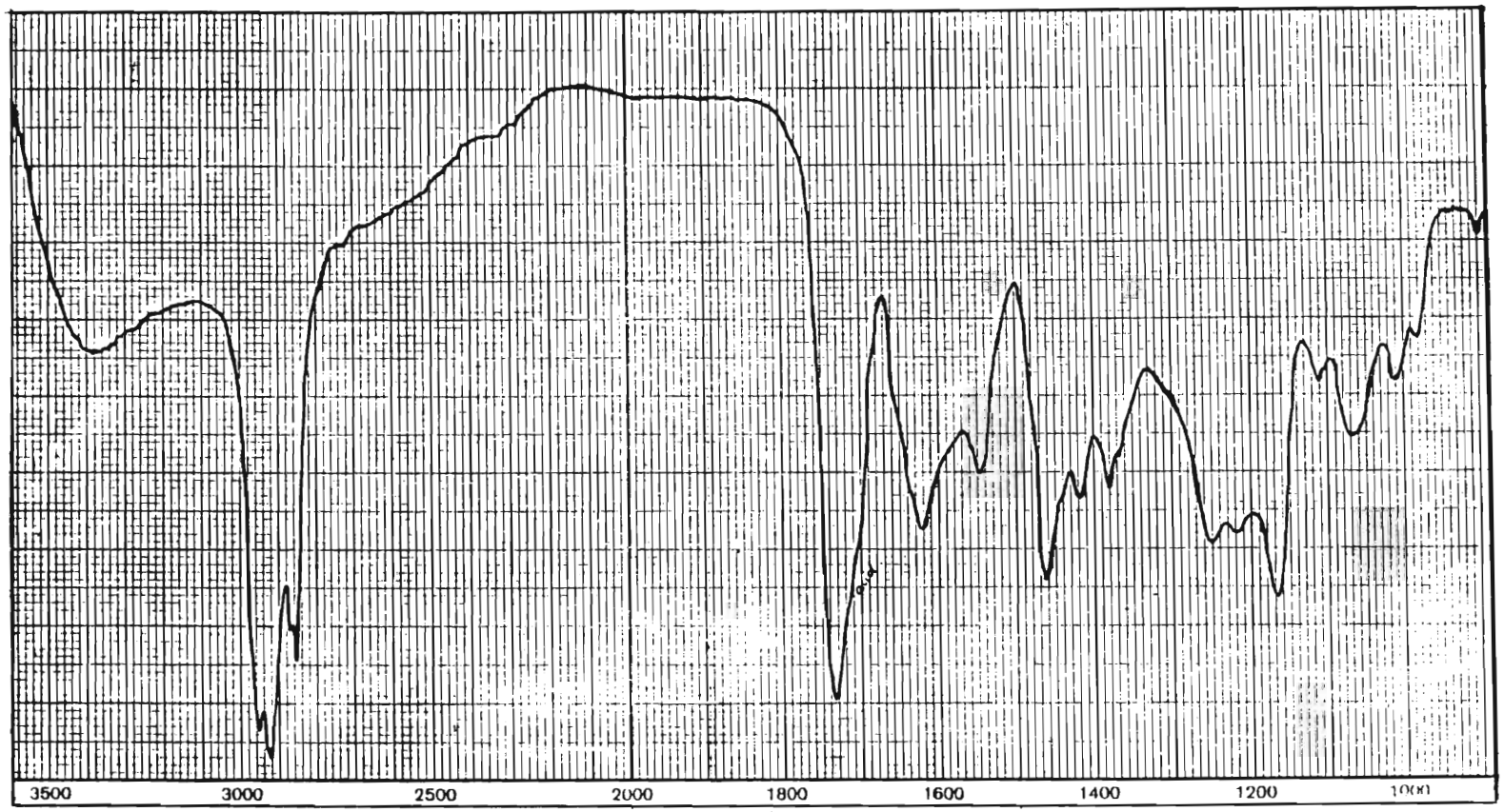

Figure 15. Infra red spectrum of the esterification product of DSA and CDE

CHAPTER III

RESULTS AND DISCUSSION

3.1. Interpretation of Interfacial Tension Data

The interfacial tension existing between two liquid phases is of considerable importance to the theory of emulsion stability. When two immiscible liquids are emulsified there is a vast increase in interfacial area between the dispersed and continuous phases. Considering the size of this interfacial area one can appreciate the importance of the physical properties and interfacial free energies associated with this interfacial region. It is known that a large positive interfacial tension is a common characteristic of an unstable emulsion[71,72] and in order to increase the stability it is neccessary to reduce the interfacial tension by the inclusion of a surface active agent.

In the sections that follow it will become evident that the measurement of interfacial tension is a valuable technique for emulsion studies because it provides useful information about the behaviour of surfactant molecules at an interface e.g. the surfactant surface excess concentration, the molecular area of a surfactant molecule at the interface and the effect of an electrolyte on the nature and interfacial orientation of surfactant molecules.

3.1.1. The Gibbs Adsorption Isotherm

The amount of a surfactant adsorbed at an interface is an important parameter and of particular importance is the relationship between the extent of surfactant adsorption and surface tension. This can be examined by means of a surface tension isotherm, i.e. the variation in surface tension at constant temperature as a function of concentration of the surface active agent in the bulk phase. In 1876 Gibbs[11] used a thermodynamic argument to describe the consequences of the accumulation of surface active molecules at a surface or interface. Gibbs defined a quantity Γ, called the surface excess. This is the excess concentration of the adsorbed species in the surface expressed in units of concentration per unit area.

The Gibbs Adsorption Isotherm can be expressed as follows:

$$-d\gamma = \sum_i \Gamma_i d\mu_i \qquad (5)$$

where Γ_i = the concentration of the surfactant species i per unit area at the interface

μ_i = the chemical potential of species i

γ = the surface tension

Using this expression the Gibbs Equation is derived for a two component system:

$$\Gamma_2 = -\frac{c}{RT}\left(\frac{d\gamma}{dc}\right)_T \qquad (6)$$

where Γ_2 = the surface excess concentration of surfactant in the interphase in units of moles per unit area

c = concentration of surfactant which is substituted for the activity in dilute solutions

γ = surface tension

R = gas constant: 8,314 J mol^{-1} K^{-1}

T = temperature (K)

The Gibbs Equation may also be used to predict the behaviour of interfacially active materials at an oil-water interface. For a three component system however, the Gibbs Equation no longer has a simple form. For a system composed of two immiscible liquids and a solute distributed between them the equation has the form:

$$-d\gamma = [\Gamma_3 - \Gamma_2 \frac{x_3^\beta}{x_2^\beta} - \Gamma_1 \frac{x_3^\alpha}{x_1^\alpha}]\, d\mu_3 \qquad (7)$$

where Γ_1 and Γ_2 are the concentrations of liquids 1 and 2 in the interphase

Γ_3 is the concentration of the solute in the interphase

α refers to the phase mainly of component 1

β refers to the phase mainly of component 2

x = mole fraction of component i (i = 1,2 or 3)

μ_3 = the chemical potential of the solute

In a system investigated by Aveyard and Briscoe[73] it was possible for the authors to put $x_3^{\alpha} = 0$ (ie. the surfactant is not distributed between the two liquid phases) and since $x_3^{\beta} \sim 3 \times 10^{-3}$ was the most concentrated surfactant solution investigated they were able to rewrite Equation (6) as follows:

$$\Gamma_3 = -\frac{x_3}{RT}\left(\frac{d\gamma}{dx_3}\right) \qquad (8)$$

Because $x_3^{\alpha} = 0$, it follows that x_3^{β} represents the total concentration of surfactant. Thus:

$$\Gamma_3 = -\frac{c}{RT}\left(\frac{d\gamma}{dc}\right) \qquad (9)$$

This is the same as the Gibbs Equation for a two component system (Equation (2)).

In the interfacial systems investigated in this work the PIBSA derived surfactants are not distributed between the two bulk phases ie. $x_3^{\alpha} = 0$,(where α refers to the aqueous phase) and the most concentrated solutions used to investigate adsorption behaviour are less than 3×10^{-3} M. Since $x_3^{\alpha} = 0$, x_3^{β} equals the total concentration of surfactant, c, and thus if c is less than 3×10^{-3} M then x_3^{β} is also less than 3×10^{-3} units. Hence, in the sections which follow, Equation (5) is used for the determination of the surfactant surface excess concentration at the oil-water interface.

The Gibbs Equation also permits the calculation of the area, A, occupied by a surfactant molecule at the interface using the following relation:

$$A = \frac{1}{N_A . \Gamma} \qquad (10)$$

where N_A = Avogadro Constant: 6.022×10^{23} mol^{-1}

Γ = surface excess calculated using Equation (2)

Figure (17) is an archetypal plot of interfacial tension (γ) versus the natural log of surfactant concentration (ln c). The linear gradient between points A and B is strongly negative indicating a positive constant surface excess.

Figure 17. Archetypal plot of interfacial tension as a function of ln (surfactant concentration)

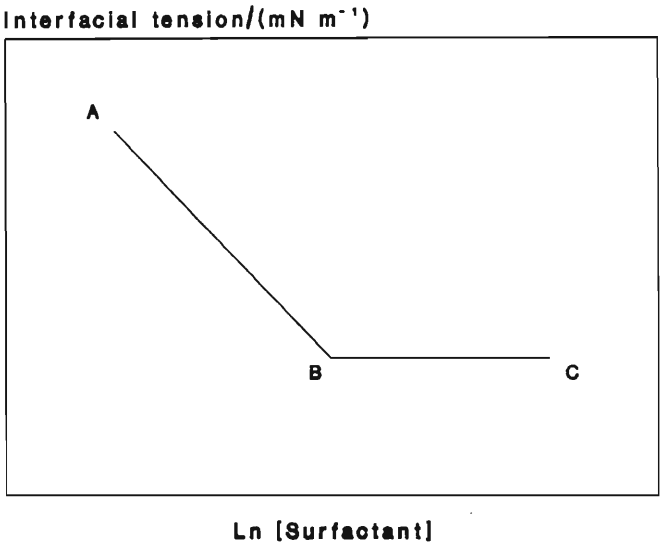

The Gibbs Equation assumes that the linear portion BC, of the plot at concentrations greater than the critical micelle concentration (cmc) represents an interface saturated by a monolayer of surfactant molecules.[1] It should be noted that the concentration scale in Figure (17) refers to the total concentration of surfactant whereas in the Gibbs Equation the surface excess concentration is that of a monolayer of surfactant molecules. The surface excess concentration remains constant above the cmc because maximum adsorption has been attained, and consequently γ is also constant above the cmc.

[1] cmc is the concentration at which micelles (aggregates) of surfactant molecules begin to form in one of the bulk phases.

3.1.2. Interfacial Tension at the Oil-Surfactant/ Milli-Q Water Interface.

The amphiphilic structure of PIBSA derived surfactants (Chapter I, Section 1.3.) results in their accumulation at the organic-aqueous interface. This has the favourable effect of lowering the free energy of the interface. This effect can be quantified by monitoring changes in interfacial tension with surfactant concentration.

3.1.2.1. The Thermodynamic Relationship Between Interfacial Tension and Interfacial Free Energy

Interfacial tension is shown to be equivalent to interfacial free energy using the following argument:

Since the surface tension for most liquids decreases with increasing temperature[74], it follows that there would be an adsorption of heat when the surface is expanded. This point was made by Kelvin[75] using a classical thermodynamic cyclic process producing the following relation:

$$l_s = -T\left(\frac{d\gamma}{dT}\right) \qquad (11)$$

where l_s = the heat adsorbed per unit increase of surface at constant temperature. l_s is always positive by virtue of the decrease in surface tension with temperature.

γ = surface tension

T = absolute temperature

If a unit increase in surface area results in an increase in surface energy, u, then

$$l_s = u - \gamma \tag{12}$$

substituting Equation (11) into Equation (12)

$$u = \gamma - T\left(\frac{d\gamma}{dT}\right) \tag{13}$$

From which it follows that γ is the surface free energy of the surface film. Similarly interfacial tension is the interfacial free energy of an interface.

The units of surface free energy are:

$$F_s(10^{-3} Jm^{-2}) \equiv \gamma(Nm^{-1}) \tag{14}$$

where F_s = the free energy per unit area of the surface.

Thus in order to determine the change in interfacial free energy at an aqueous/organic-surfactant interface one needs simply to determine the change in interfacial tension.

3.1.2.2. Aktol PICDEA in Diesel over Milli-Q Water

The effect of the concentration of Aktol PICDEA (Batch A and Batch B) on the interfacial free energy of the diesel/Milli-Q water interface is illustrated in Figure (18), a plot of γ (mN m^{-1}) versus the natural log of PICDEA concentration (ln c).

The shape of this plot is typical of that produced by most amphiphilic surfactants. In 1937 McBain, Ford and Wilson[76], classified the three main types of surface tension curves and these are shown in Figure (19). Type I curves, showing decreasing surface tension, are typical of fatty acid solutions. Type II curves in which there is a slight but definite increase in surface tension are found in solutions of strong electrolytes. Of particular interest to this work is the type III curve, caused by the inclusion of amphiphilic surfactants. An important feature of the type III curve is the extremely low interfacial tensions attained at relatively high surfactant concentrations. It would appear that this curve represents a failure of the Gibbs Equation. The curve which is expected theoretically is illustrated in Figure (20) together with an experimental type III curve. The experimental curve shows a decrease in interfacial tension to a minimum followed by an increase in tension before reaching a constant plateau region. According to

the Gibbs Equation, the positive slope suggests that the system has changed from positive adsorption to negative adsorption. However, experiments with solutions in this concentration range indicate that adsorption remains positive[77].

Bulkeley and Bitner[78] and Reichenberg [79] showed that the minimum is probably due to impurities in the chemical compounds examined. This was verified by Brady[80] and Williams et al.[81] who showed that it was possible to remove the minimum by successive purification processes. Furthermore, Miles and Shedlovsky[82] were able to produce a minimum by the addition of small amounts of a third surface active component. Becher[83] suggests that this minimum is possibly the result of a complex interaction which occurs when more than one surface active species is present. Such impurities may include unreacted precursors, contaminants and even dust particles. The theoretical curve in Figure (20) is realised when pure surfactant systems are used.

Figure 18. Interfacial tension-concentration curve for Batch A and Batch B Aktol PICDEA in diesel over Milli-Q water

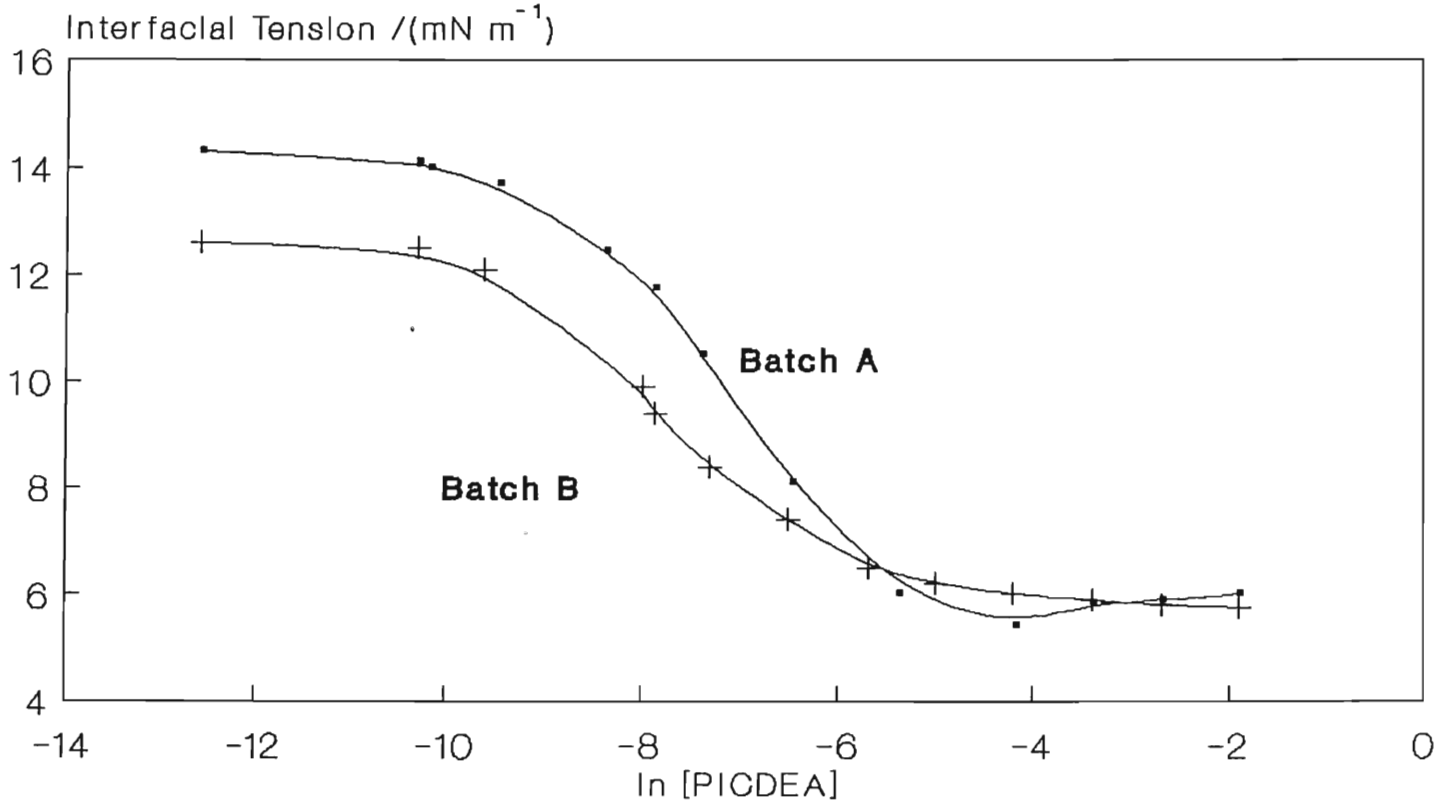

Equilibration Time = 20 hrs.
Temperature = 23 °C ± 0.5 °C

Figure 19. Schematic representation of the principle types of surface tension concentration curves, after McBain, Ford and Wilson[76]

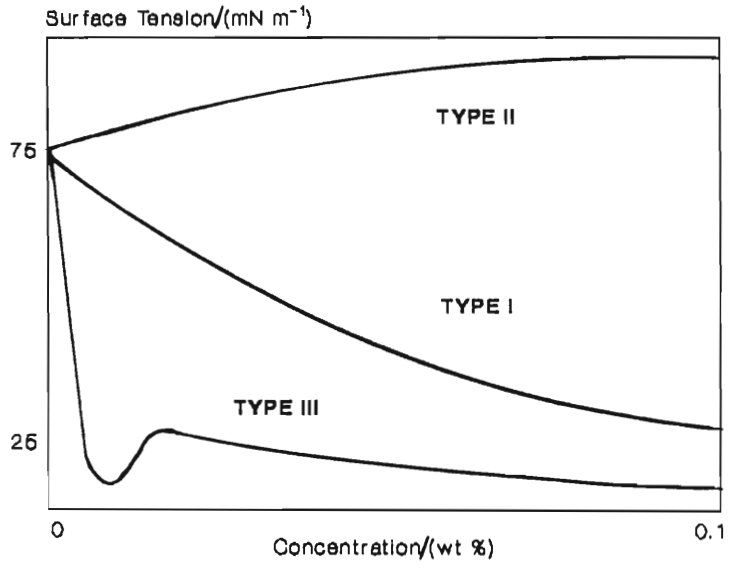

Figure 20. Surface tension-concentration curves for Type III compounds. ——— experimental ------ theoretical

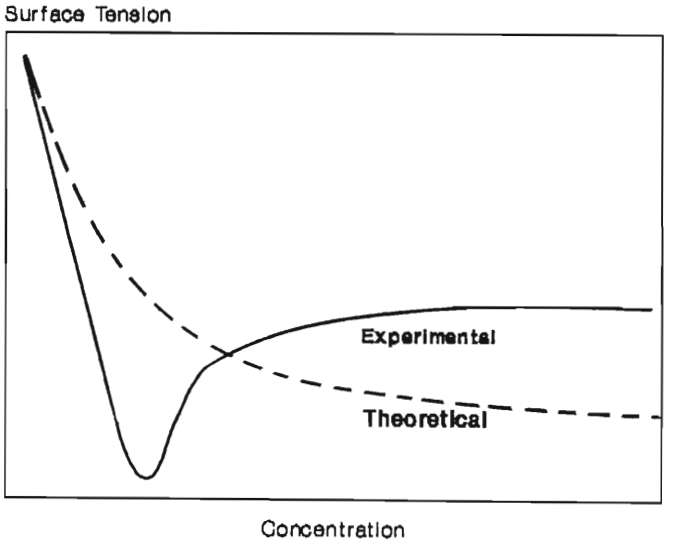

Referring once again to Figure (18), the observed minimum in the interfacial tension-concentration curve of PICDEA Batch A, may indeed be the result of one or more surface active impurities affecting the interfacial adsorption of PICDEA. Note that this minimum does not occur in the case of PICDEA Batch B. Comparison of TLC separations of the components present in each of the PICDEA samples (refer to Chapter II, Section 2.2.2.1.) and examination of the respective solute R_f values showed that a significant amount of unreacted CDE (precursor to PICDEA) was present in Batch A, whereas only traces were found in Batch B. CDE, an amphiphilic surface active agent would be adsorbed at the diesel/water interface together with PICDEA molecules. This would account for the minimum in the γ vs ln c curve observed for Batch A. Evidently the concentration of CDE in Batch B PICDEA is not enough to produce a minimum.

By application of the Gibbs Equation (Equation 6) the surface excess, Γ, and the average area occupied by a single surfactant molecule, A, at the interface were determined. This data is displayed in Table (8).

Table 8. Aktol PICDEA: Surface Excess, Γ, and Molecular Area, A.

Aktol PICDEA	Γ/ (mol m^{-2})	A/ ($Å^2$ molecule^{-1})
Batch A	1.02×10^{-6}	163.5
Batch B	7.36×10^{-7}	225.7

From the data in Table (8) the following conclusions can

be drawn: Batch A PICDEA molecules pack closer together at the interface than do Batch B molecules, which can be deduced from the larger surface excess and smaller molecular area of Batch A PICDEA molecules at the interface. However, the presence of a higher concentration of CDE in Batch A PICDEA could account for this difference.

CDE is a smaller molecule than PICDEA in both molecular weight and volume, hence its adsorption at the interface would result in the observed increase in Γ and decrease in A for Batch A PICDEA. This argument does of course assume that CDE will be adsorbed at the interface and not "blocked" in some way by the bulky, amphiphilic PICDEA molecules. In view of the following statement made by Langmuir[47] it is thought that CDE is adsorbed at the interface: "The work required to bring one mole of $-CH_2-$ from the interior of the bulk phase to the interphase is 2.615×10^3 J." This suggests that short chain surfactants such as CDE (Appendix II) are in fact preferentially adsorbed at the interface.

The data obtained from the curve for Batch B PICDEA (Figure (18)) which contains only a trace of CDE (refer to Chapter II, Section 2.2.2.1.) is thought to be a more accurate representation of the true adsorptive behaviour of PICDEA at the diesel/Milli-Q water interface. Unfortunately even a trace of CDE can be expected to increase the observed surface excess of PICDEA due to its preferential adsorption at the interface. It is therefore expected that the area occupied by a single PICDEA molecule at the diesel/water interface will be slightly greater than 225.7 $Å^2$ $molecule^{-1}$.

The effect of interference from CDE on the stability of an emulsion has not been quantified in this work, however from an understanding of basic emulsion theory it is expected that its presence may aid in emulsion destabilisation: Bampfield[70] has suggested that short-to-medium chain length alcohols and certain water soluble amphiphiles break down explosive emulsions. CDE is a water soluble amphiphile.

Further consideration of the curves in Figure (18) provides the following information: By extrapolation of the linear negative gradient towards higher concentration, the point where the extrapolated line crosses the minimum constant interfacial tension corresponds to the cmc of the surfactant (assuming that the interface is saturated when a monolayer of surface active molecules has been adsorbed[84]). The cmc for Batch A PICDEA is equal to 3.7×10^{-3} M, and for Batch B PICDEA is 4.1×10^{-3} M. The slight difference in values may be due to the presence of CDE in Batch A PICDEA but otherwise they are very similar.

At low surfactant concentrations, and to a lesser extent at high concentrations, Batch B PICDEA is more efficient at lowering interfacial free energy. This is probably because there is less interference from CDE in Batch B than in Batch A PICDEA. Equally, the preferential adsorption of CDE at low concentrations of Batch A is probably the cause of the observed higher interfacial free energy since CDE is not as strong an amphiphilic surfactant as PICDEA.

3.1.2.3. DSA/CDE in Diesel over Milli-Q Water.

The esterification product of DSA and CDE was prepared in this laboratory using the technique described in Chapter II, Section 2.2.5. Unlike PICDEA, DSA/CDE has a 12-C (twelve carbon) unbranched chain introduced by dodecenyl succinic anhydride (DSA) instead of the long bulky hydrocarbon chain in PICDEA (ranging from 20-C to 60-C) originating from the PIBSA precursor. The interfacial tension-concentration curve illustrated in Figure (21), provides some interesting information concerning the interfacial adsorption characteristics of a short chain length, double hydrocarbon surfactant with a polar head group identical to that of PICDEA.

Using the Gibbs Equation, Γ and A were calculated from the slope of the linear portion of the curve in Figure (21). These values are compared in Table (9) with those obtained for Aktol PICDEA Batch B previously shown in Table (8).

Included in Table (9) are the cmc's determined for each surfactant from the relevant γ vs ln c curves.

Table 9. A Comparison of Γ, A and CMC for DSA/CDE and Aktol PICDEA

Surfactant	Γ /(mol m^{-2})	A /($Å^2$ $molecule^{-1}$)	cmc /(mol dm^{-3})
DSA/CDE	1.6×10^{-6}	103.8	1.63×10^{-3}
Aktol PICDEA Batch B	7.35×10^{-7}	225.9	4.1×10^{-3}

Figure 21. Interfacial tension-concentration curve for DSA/CDE in diesel over Milli-Q water

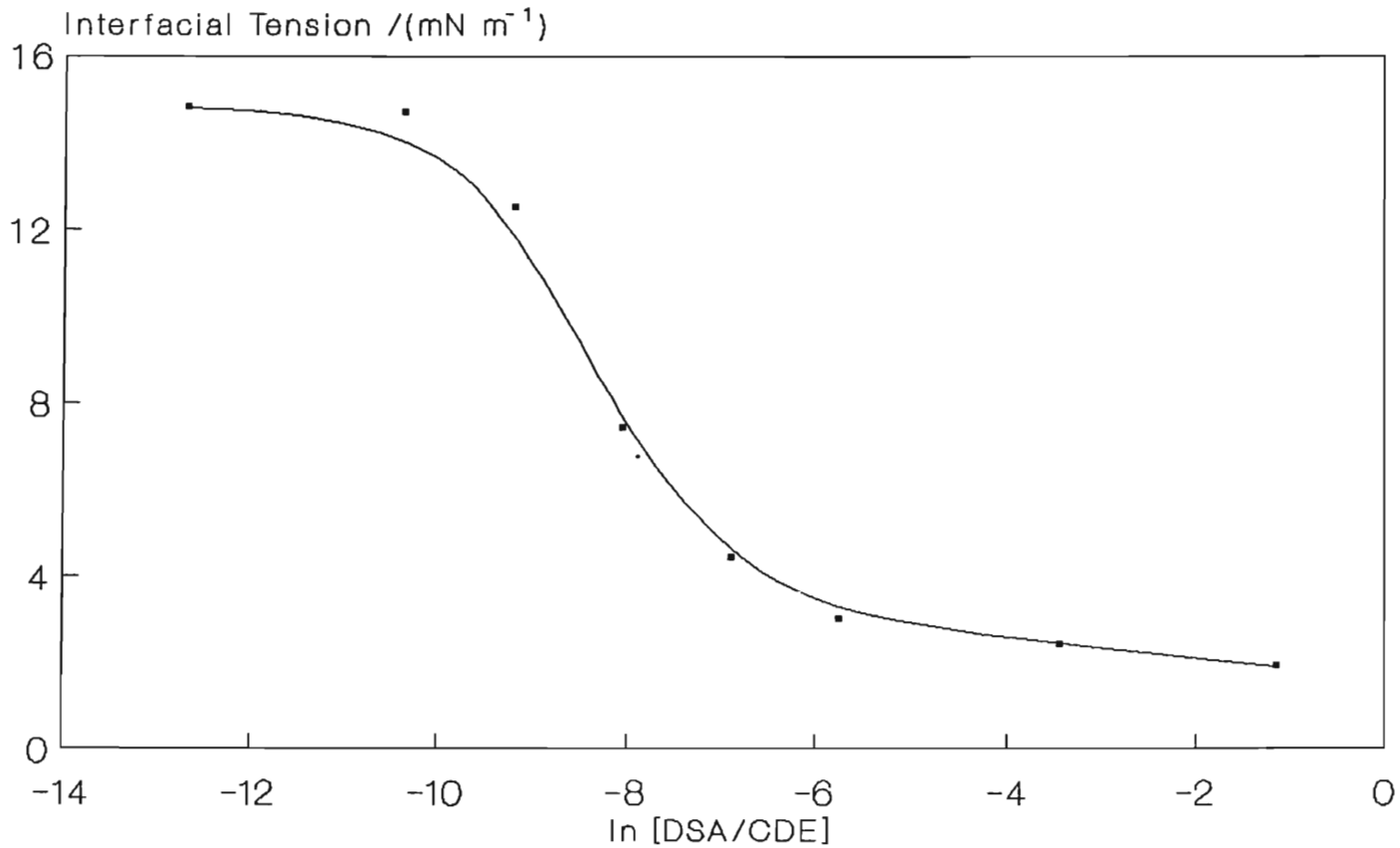

DSA/CDE: Dodecenyl succinic anhydride/ Coco-diethanolamide Product

Although both DSA/CDE and PICDEA possess the same polar functions, a DSA/CDE molecule occupies less than half the area of a PICDEA molecule at the interface. This must be a direct effect of the shorter, less bulky hydrocarbon chain in the DSA/CDE molecule. Figure (22) is a ball and stick representation of the DSA/CDE product modelled and minimized using the Alchemy minimization software package. Figure (22b) views Figure (22a) along the axis of the polar functional group, i.e. the molecule is rotated through 90^{o} around the axis A-B. This view shows the offset of the two hydrocarbon chains by ~ 80^{o} achieved in the minimization of Van der Waals energy of interaction between the hydrogens of adjacent hydrocarbon chains.

The Alchemy minimizer performs a conjugate minimization on a force field equation which is dependent on the positions of the atoms of the molecule. The potential energy, E, of a molecule is the sum of the following terms:

$$E = E_{str} + E_{ang} + E_{tor} + E_{vdw} + E_{oop} \qquad (15)$$

where str = bond stretching
ang = angle bending
tor = torsional strain
vdw = van der Waals interactions
oop = out-of-plane bending

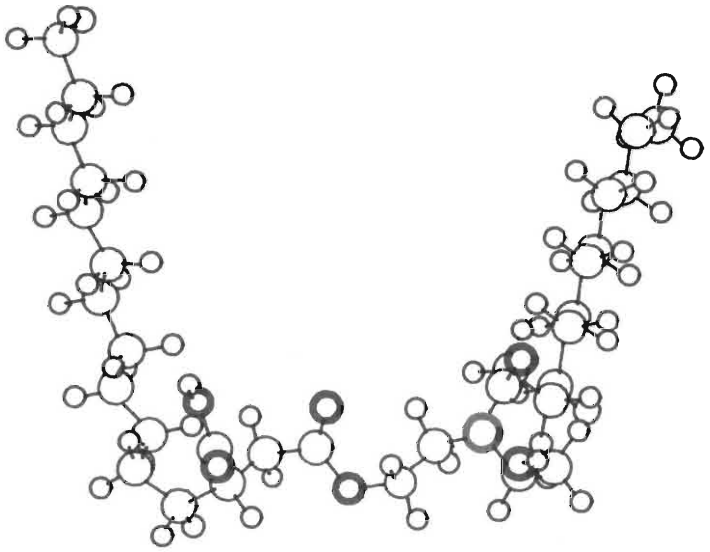

Figure 22(a)

Figure 22(b)

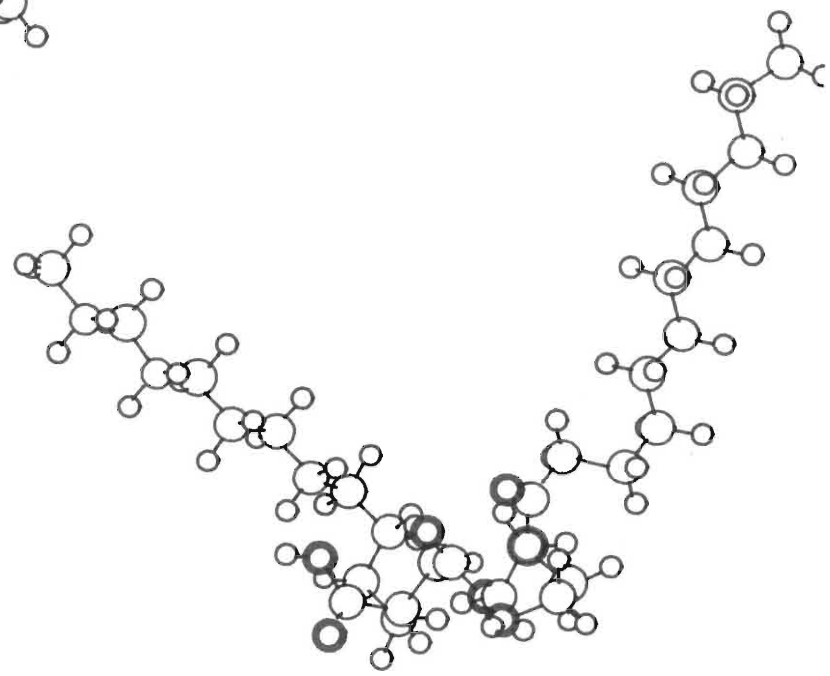

Figure 22. A ball and stick representation of the DSA/CDE product modelled and minimised using the Alchemy minimisation software package

The values for each of these contributing energy terms for both DSA/CDE and PICDEA are compared in Table (10). Unfortunately the minimization program can only minimize molecules with less than 170 atoms so the PIB hydrocarbon chain in PICDEA was cut down to a 13-C chain.

Table 10. Energies obtained using the Alchemy Minimization Program for DSA/CDE and PICDEA

Energy term	DSA/CDE/ (k cal mol^{-1})	PICDEA/ (k cal mol^{-1})
E	-16.9	6.0
E_{str}	0.2	0
E_{ang}	2.9	0.5
E_{tor}	4.1	5.5
E_{vdw}	-24.2	0
E_{oop}	0	0

The lower interaction energies, especially E_{vdw}, associated with DSA/CDE indicate that DSA/CDE molecules can be more closely packed at the interface than PICDEA molecules which is indeed what was observed experimentally. Figure (23) is a ball and stick representation of PICDEA.

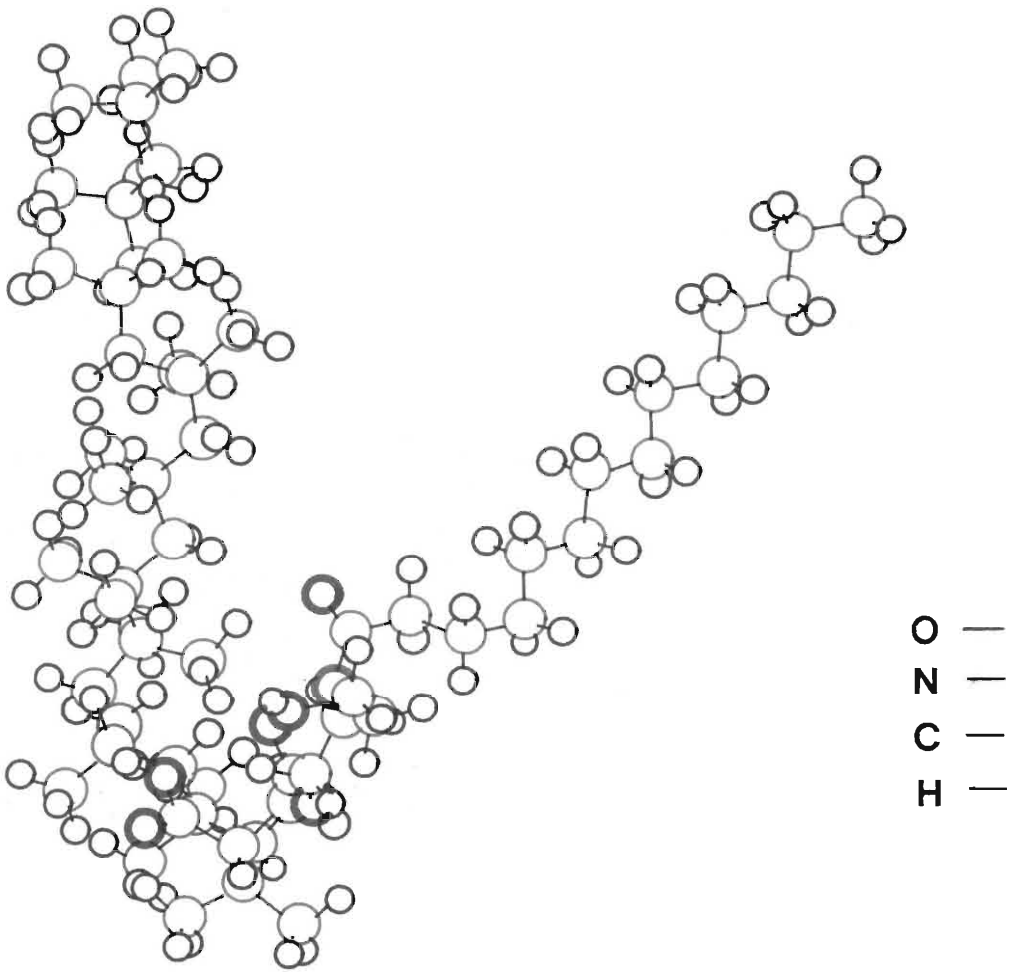

Figure 23. A ball and stick representation of PICDEA modelled and minimized using the Alchemy minimisation software package

It is important to note that the Alchemy minimization package does not take into account the effect of neighbouring molecules or the forces of adsorption at an organic-aqueous interface on the orientation or potential energy of the molecule. Nor does it consider the interaction of the organic diluent molecular structure with the hydrocarbon chains of the surfactant molecule. It is none the less interesting to compare the contributing energy factors of PICDEA and its short hydrocarbon analogue, DSA/CDE. Such a comparison suggests that the bulky PIBSA hydrocarbon structure of PICDEA is largely responsible for the observed differences in interfacial packing. According to Derivichian[85] it is the Van der Waals forces between the hydrocarbon chains which are responsible for the regular arrangement of emulsifier molecules in mixed adsorbed monolayers. Not only do the bulky hydrocarbon chains of adjacent PICDEA molecules possess large van der Waals energies with respect to each other, but they are also probably less compatible with the unbranched, shorter hydrocarbons of the diesel diluent than the uniform unbranched 12-C chain of DSA/CDE. The surprisingly low cmc obtained for DSA/CDE suggests that the shorter hydrocarbon surfactant forms micelles more easily. Perhaps the uniformity of the DSA/CDE molecules (i.e. the hydrocarbon chain originating from the DSA precursor does not range in length as does the PIB hydrocarbon of PICDEA), in addition to the shorter chain length, may also aid in micelle formation.

3.1.2.4. Aktol E-70 and Adibis E-70 in Diesel over Milli-Q Water

The interfacial tension-concentration curves for Adibis and Aktol based E-70 are plotted in Figure (24). Although the gradients of these plots are very similar, the determination of Γ and A using the Gibbs Equation enables small differences in interfacial adsorption to be detected. Γ and A for both E-70 samples are shown in Table (11).

Table 11. Aktol and Adibis E-70: Surface Excess, Γ, and Interfacial Molecular Area, A.

Experse-70	Γ /(mol m^{-2})	A /($Å^2$ $molecule^{-1}$)
Adibis	1.24×10^{-6}	133.9
Aktol	1.29×10^{-6}	129.2

E-70 molecules based on Aktol PIBSA apparently occupy a slightly smaller area at the interface than do Adibis based E-70 molecules. As in the case of Aktol PICDEA (Batch A and Batch B) this could be caused by the presence of an unreacted surface active precursor. As was illustrated in Figure (10) (Chapter II, Section 2.2.2.1.), the TLC separation of Adibis and Aktol E-70 components shows that Aktol E-70 does indeed contain small amounts of excess mono-ethanolamide (a precursor to E-70) which was not detected in Adibis E-70.

Figure 24. Interfacial tension-concentration curve for Aktol and Adibis E-70 in diesel over Milli-Q water

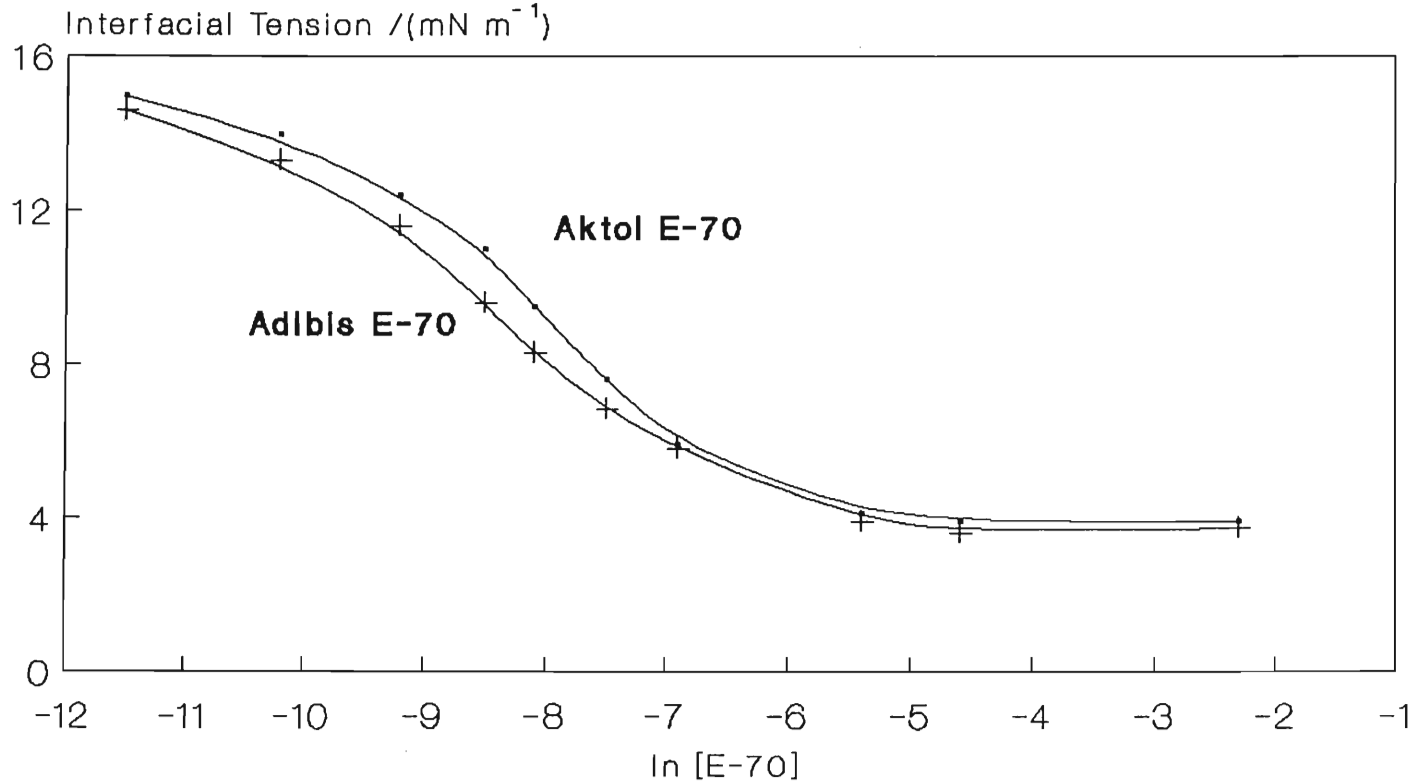

Adibis E-70: E-70 prepared from Adibis ADX 101 PIBSA
Aktol E-70: E-70 prepared from Aktol ECA 6774 PIBSA
Equilibration Time = 20 hrs
Temperature = 22°C ±0.5°C

However, unlike Batch A and B Aktol PICDEA, there are two other factors which must be considered before conclusions can be made as to the adverse effect of mono-diethanolamide on interfacial tension.

First, there is only a 3.5 % difference in the determined interfacial areas per E-70 molecule from each sample. Considering the gradient of the linear portion of the Adibis E-70 curve in Figure (24), an increase in gradient of 2.5 % causes a drop in the calculated area per molecule from 133.9 $Å^2$ to 130.5 $Å^2$. A 2.5 % change in gradient results when there is a 1.5 % error in the measurement of interfacial tension. Such a deviation falls within the limit of the error of the experimental technique. Thus the limits of uncertainty for the two determined areas overlap and consequently it is quite possible that experimental error alone is responsible for the apparent differences between the adsorption of Adibis and Aktol E-70.

The second point to consider is that these two E-70 samples are based on PIBSA from different suppliers, ie. Adibis PIBSA is supplied by BP and Aktol PIBSA by Exon (refer to Chapter I, Section 1.3.). The major difference is their molecular weights: Adibis PIBSA = 950 g mol^{-1} and Aktol PIBSA = 1400 g mol^{-1}, i.e. Aktol PIBSA has a longer average hydrocarbon chain length. Consequently, based on the conclusions drawn from the previous section (Section 3.1.2.3.), one would expect the bulkier Aktol based E-70 molecule to occupy a greater interfacial area than the smaller Adibis E-70 molecule. However this is not the case; Adibis and Aktol E-70 molecules occupy very similar areas at the interface. This observation suggests the

following: If the chain length does not effect the packing of molecules (as shown in the comparison of Aktol and Adibis E-70) then perhaps it is the increased volume or "bulkiness" of the hydrocarbon chain that increases the interfacial molecular area of a molecule at the interface (as was observed in the comparison of DSA/CDE and PICDEA).

Further inspection of the curves in Figure (24) shows quite clearly that Adibis E-70 is more efficient at reducing interfacial free energy than Aktol E-70. This may be caused by the different hydrocarbon chain lengths, Adibis E-70 possessing a shorter hydrocarbon chain may require less energy to migrate to the interface[47]. The interfacial free energy of each specific organic-aqueous interface is minimized by a particular surfactant with an optimum HLB value. Positive or negative deviations from this optimum value will cause an increase in interfacial free energy. Adibis and Aktol E-70 have different HLB values because of their different hydrocarbon chain lengths. Since Aktol E-70 is more lipophilic it has a lower HLB value than Adibis E-70. According to HLB theory the difference in HLB values will result in different interfacial tensions[86]. In other words, hydrocarbon chain length does affect the ability of an E-70 molecule to lower interfacial free energy, even though chain length has little, if any, effect on the packing at the interface.

These observations prompted a similar study on Adibis and Aktol PICDEA which is discussed in the following section.

3.1.2.5. Aktol and Adibis PICDEA in Shellsol PA Mineral Oil over Milli-Q Water

Figure (25) is the interfacial tension-concentration curve for Adibis based PICDEA in Batch B Shellsol PA mineral oil. 54.7 % w/w Adibis PICDEA was prepared in this laboratory using the technique described in Chapter II, Section 2.2.6. Figure (26) is a similar curve for Batch A Aktol based PICDEA in Batch A Shellsol PA mineral oil. Aktol and Adibis interfacial tension data have been plotted separately to prevent the reader from comparing the interfacial tension data directly. Differences between Batch A and Batch B Shellsol PA made a direct comparison impossible. These differences were detected by comparing the surface tensions and also interfacial tensions of the two oils over Milli-Q water. This data is displayed in Table (12). Interfacial tension measurements were taken after 30 second and 20 hour equilibration times.

Table 12. Surface, γ, and Interfacial Tensions, γ_o, of Batch A and B Shellsol PA Mineral Oil.

Shellsol PA	γ /(mN m^{-1})	γ_o /(mN m^{-1}) 30 sec.	γ_o /(mN m^{-1}) 20 hrs.
Batch A	29.0	28.6	10.3
Batch B	28.9	23.2	9.8

Figure 25. Interfacial tension-concentration curve for Adibis PICDEA in Shellsol PA over Milli-Q water

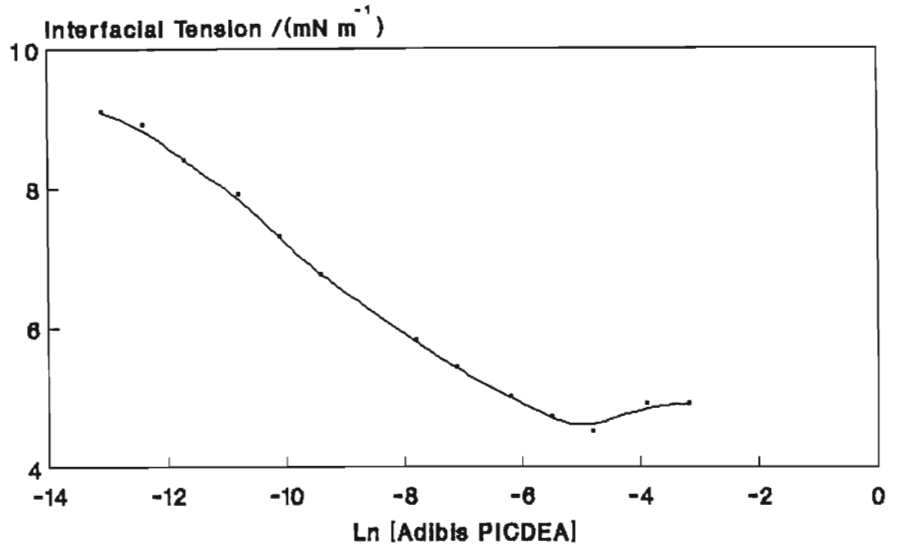

Adibis PICDEA: PICDEA prepared from Adibis PIBSA

Figure 26. Interfacial tension-concentration curve for Aktol PICDEA in Shellsol PA over Milli-Q water

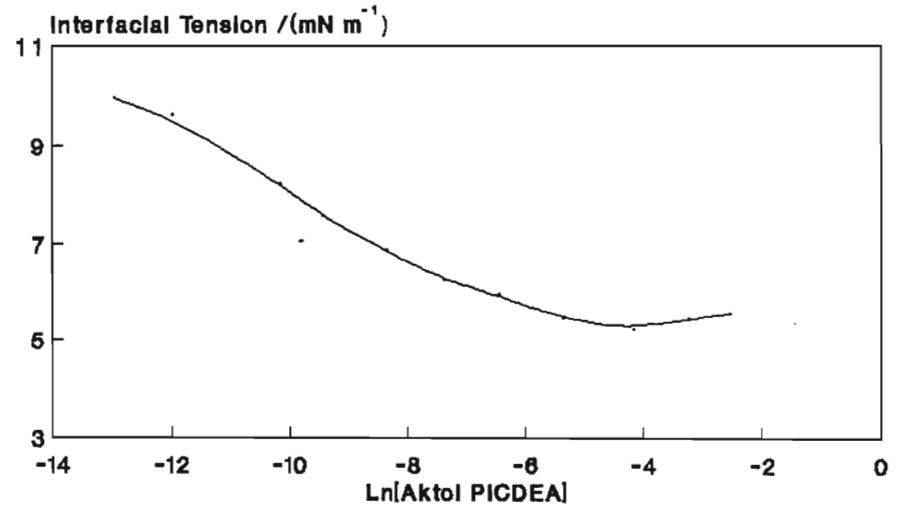

Aktol PICDEA: PICDEA prepared from Aktol PIBSA

Equilibration Time - 20 hrs.
Temperature - 22°C ±0.5°C

Although the surface tensions of these two oil samples are approximately equal, the differences in the interfacial tension data at the interface with Milli-Q water show that the two samples differ in composition. Apparently both samples contain surface active species which result in the reduction in interfacial tension as the equilibration time is extended. If Shellsol PA mineral oil were a "pure oil" containing only non polar hydrocarbons, then the interfacial tension with Milli-Q water would lie between the surface tension of pure water (~72.6 mN m^{-1}) and that of Shellsol PA (~29.0 mN m^{-1}). However, γ_o for both samples is far smaller than the surface tension of the oil, thus showing that the oil samples must contain surface active additives or contaminants. Furthermore, it appears that Batch B Shellsol PA contains a higher proportion of this unknown surfactant than Batch A and consequently a direct comparison of the effect of Aktol and Adibis PICDEA on this oil-water interface is not possible.

Determination of the change in surfactant pressure at the interface can be used to eliminate the effective contribution of the surface active oil components on the reduction in interfacial tension at the surfactant-oil/water interface. This technique enables a direct comparison of Aktol and Adibis PICDEA. Interfacial pressure is defined as follows:

$$\Pi_s = \gamma_o + \gamma_{os} \qquad (16)$$

where Π_s = the surface or interfacial pressure of an adsorbed surfactant

γ_o = surface or interfacial tension in the absence of surfactant

γ_{os} = surface or interfacial tension at an interface containing adsorbed surfactant molecules

The interfacial pressure-concentration curves are plotted in Figure (27). Adibis PICDEA has a greater interfacial pressure than Aktol PICDEA at concentrations less than 1.7×10^{-2} M, whereas above this concentration their pressures are identical. This suggests that shorter hydrocarbon chain Adibis PICDEA molecules are more efficient at lowering the interfacial free energy. This observation is in agreement with the conclusions made in a similar analysis of Aktol and Adibis E-70 in Section 3.1.2.4. This does not, however, imply that interfacial tension will continue to decrease as carbon chain length decreases. According to HLB theory an optimum chain length must exist which will produce an interface of minimum interfacial free energy. The HLB of an average Adibis PICDEA molecule will be closer to the optimum HLB than an average Aktol PICDEA molecule.

As already mentioned, the strong interfacial ageing of the "pure" Shellsol PA/water interface is proof that certain surface active species are present in the oil samples. Consequently, experimentally determined values of Γ and A, do not represent the true adsorptive behaviour of PICDEA but rather the combined effect of the surfactants in Shellsol PA and PICDEA molecules.

Figure 27. Interfacial pressure-concentration curve for Adibis and Aktol PICDEA at the Shellsol PA - Milli-Q water interface

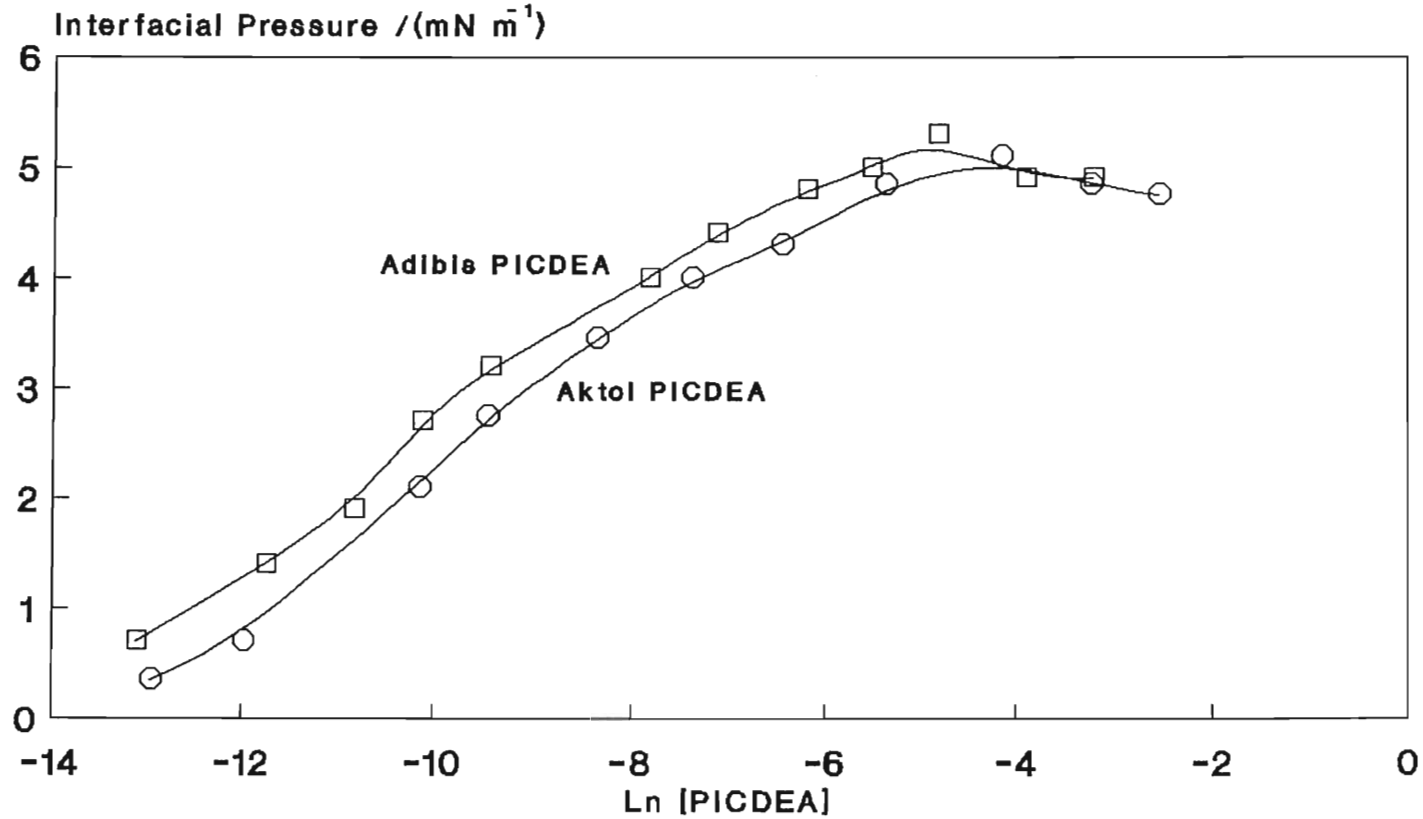

Adibis PICDEA: PICDEA prepared from Adibis PIBSA

Aktol PICDEA: PICDEA prepared from Aktol PIBSA

By applying the Gibbs Equation, values for Γ and A have been determined and are displayed in Table (13).

Table 13. Aktol and Adibis PICDEA: Surface Excess, Γ, and Interfacial Molecular Area, A.

PICDEA	Γ /(mol dm^{-3})	A /($Å^2$ $molecule^{-1}$)
ADIBIS	2.78×10^{-7}	597.9
AKTOL	2.80×10^{-7}	592.2

The exceptionally high values obtained for both Γ and A suggest that there is considerable interference from surface active impurities present in the oil phase. The similarity between these values once again confirms that hydrocarbon chain length has little effect on the packing of PIBSA derived surfactants at the organic-aqueous interface. However, the similarity of these values, and the fact that once the interface is saturated ($>1.7 \times 10^{-2}$ M) both Aktol and Adibis PICDEA have identical interfacial pressures, suggests that perhaps there is no difference in the effects of the two on the interface. Referring to Figure (9) (Chapter II, Section 2.2.2.1.) which shows the comparative TLC resolution of the components of Aktol PICDEA (Batch A) and Adibis PICDEA, it is clear from the presence of excess CDE in Aktol PICDEA that the esterification reaction between CDE and PIBSA did not go to completion. Consequently, there would be a lower percentage of PICDEA in the sample than that quoted by the supplier (assuming that equimolar amounts of the reactants were initially reacted). If this is the case then the calculated concentration of

Aktol PICDEA per unit weight of sample in Shellsol PA mineral oil would be greater than the actual PICDEA concentration. The Aktol PICDEA interfacial pressure-concentration curve should then be shifted to lower concentrations ie. towards the Adibis PICDEA curve. However, in order to superimpose the curves the %w/w of Aktol PICDEA supplied by AECI would have to be as low as ~26 %, i.e. 43 % less than the quoted percentage activity, which is totally unacceptable and unlikely. Assuming that the original sample does contain more than 26 % PICDEA, then the experimental results indicate that at concentrations less than 1.7×10^{-2} M, PICDEA molecules based on the shorter hydrocarbon Adibis PIBSA are more efficient at lowering the interfacial free energy of the Shellsol PA/Milli-Q water interface than those based on the longer Aktol PIBSA molecule.

3.1.2.6. A Comparison of Surfactant Interfacial Pressures

At this stage it is convenient to compare the interfacial pressures of the surfactants discussed in the previous four sections. These surfactants include: Aktol PICDEA Batch A and B; Aktol E-70; Adibis E-70 and DSA/CDE all at the diesel-water interface, and also Aktol PICDEA Batch A and Adibis PICDEA at the Shellsol PA-water interface.

Surfactant interfacial pressure, Π_s, which was defined in Section 3.1.2.4. by Equation (16), is plotted as a function of the natural log of surfactant concentration in Figure (28), for each of the above mentioned surfactants.

Figure 28. Interfacial pressure-concentration curves for Aktol PICDEA (Batch A and B), Adibis and Aktol E-70 and DSA/CDE product

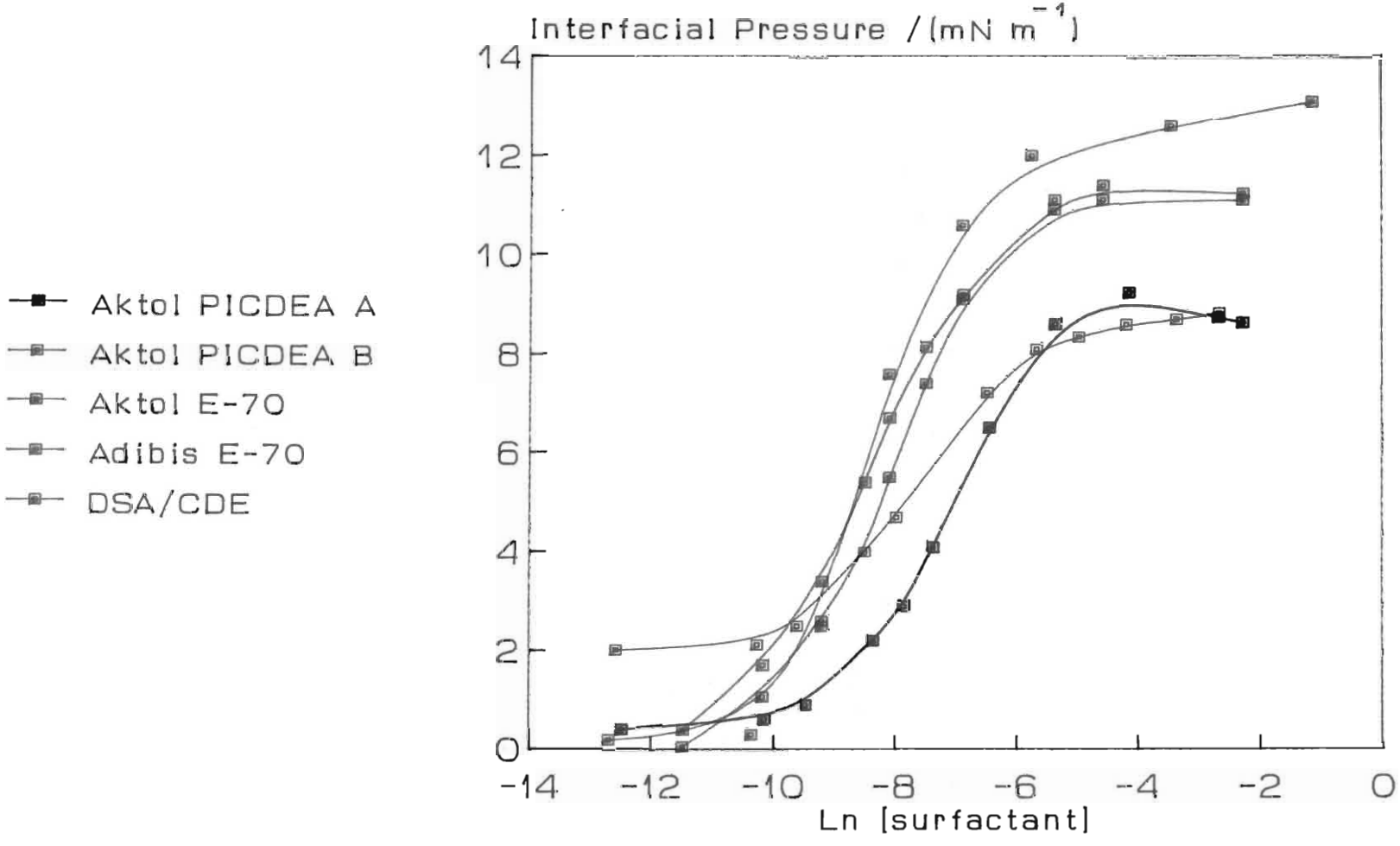

The interfacial tension values γ_o for the pure oil-water interfaces which were used for the determination of interfacial pressures are listed below in Table (14).

Table 14. Interfacial Tension at the Surfactant Free Oil - Water Interface after 20 hours Equilibration.

Surfactant System	Oil Phase	γ_o /(mN m^{-1}) 20hrs
Aktol PICDEA A	Diesel (a)	14.6
Aktol PICDEA B	Diesel (a)	
DSA/CDE	Diesel (b)	15.0
Aktol E-70	Diesel (b)	
Adibis E-70	Diesel (b)	

(a): ex. Modderfontein, AECI

(b): ex. Umbogintwini, AECI

Adibis and Aktol PICDEA in Shellsol PA have not been included as plots of their interfacial pressures have already been shown in Figure (27).

The effect of hydrocarbon chain length on interfacial free energy is clearly seen in Figure (28). At concentrations greater than ~2 x 10^{-4} M the DSA/CDE product has the highest interfacial pressure indicating that the PICDEA type surfactants with a shorter hydrocarbon chain are more surface active and hence more efficient at lowering interfacial free energy at the aqueous-organic interface. It is interesting to note

that at low concentrations the converse is true, i.e. DSA/CDE exhibits one of the lowest interfacial pressures. This is possibly due to the fact that it occupies a far smaller surface area at the interface than the other surfactant molecules (refer to Table (9), Section 3.1.2.2.) and will therefore need a higher surface excess concentration to achieve a significant interfacial pressure.

Adibis E-70 has a greater interfacial pressure than Aktol E-70 at all concentrations, this was thoroughly discussed in terms of the reduction in interfacial tension in Section 3.1.2.3. Figure (28) shows that at high concentrations, Aktol E-70 has a greater interfacial pressure than Aktol PICDEA. The polar function of the E-70 molecule is much smaller than that of PICDEA (refer to Figure (4), Chapter I) which would account for the smaller interfacial area occupied by an E-70 molecule. The molecular interfacial area for Aktol E-70 is 129.2 $Å^2$ $molecule^{-1}$ whereas Aktol PICDEA occupies an interfacial area of 225.9 $Å^2$ $molecule^{-1}$.

Furthermore, the single hydrocarbon structure of the E-70 molecule will probably enable a closer packing at the interface than the double hydrocarbon structure of the PICDEA molecule. The corresponding higher interfacial surface excess of E-70 would therefore result in the higher interfacial pressure observed in Figure (28).

3.1.3. The Aqueous Nitrate / Oil-Surfactant Interface

Introduction of an electrolyte into an aqueous/oil-amphiphilic surfactant system causes a drastic reduction in interfacial free energy. Harkins and Zollman[14] illustrated this point in 1926 in their investigation of the paraffin/water interface. The paraffin/water interfacial tension is 40.6 mN m^{-1} at 20 ^{o}C, this was reduced to 31.05 mN m^{-1} when the organic phase was made 0.001 N in oleic acid. The addition of an equivalent amount of sodium hydroxide to the aqueous phase neutralized the interface thereby reducing the interfacial tension to 7.2 mN m^{-1} forming the soap, sodium oleate. Harkins and Zollman suggest that the energy of chemical union between the base and the acid may be used directly in the formation of the surface. Further addition of sodium chloride (0.001 N) to the aqueous phase caused a large reduction in interfacial tension to 0.01 mN m^{-1}.

Thus the interfacial tension is affected by the electrical charges at the interface and these charges undoubtedly play an important role in the emulsification process and the long term stability of the emulsion.

The following sections (Sections 3.1.3.1 and 3.1.3.2.) will discuss the effects of various nitrate salts on the absorptive behaviour of PIBSA derived surfactants and their ability to lower interfacial free energy.

3.1.3.1. The Effect of pH on the Interfacial Tension of the Aqueous Nitrate/Organic-PIBSA Surfactant Interface

Interfacial tensions of 0.018 M Adibis PICDEA and Adibis E-70 in n-hexane (HPLC grade) were measured as a function of aqueous phase pH. Aqueous phases were prepared from a 1 M sodium nitrate solution with subsequent adjustment of pH by the addition of small volumes of 1 M nitric acid and 1 M sodium hydroxide ensuring a constant ionic strength in all samples[87]. Aqueous phase pH values were determined before contact with the organic phase.

n-Hexane was used as the surfactant diluent instead of diesel or Shellsol PA mineral oil because relatively high interfacial tension measurements were required to reduce the experimental error. Experimental error was reduced because larger differences were obtained between extreme high and low values and hence the effect of pH on interfacial tension was clearly defined. Figure (29) is a plot of interfacial tension versus aqueous sodium nitrate pH for both Adibis PICDEA and E-70 systems.

3.1.3.1.1. Protonation of PICDEA at low pH values

As the pH value of the aqueous phase is lowered from approximately 4, the interfacial tension suddenly drops from 3.5 mN m^{-1} to 0.6 mN m^{-1}. This is caused by the protonation of the amide to give a positively charged species of higher surface activity than the neutral PICDEA molecule i.e.

$$H^+ + -N\!\!\begin{array}{l}\diagup\\\diagdown\end{array} \rightleftharpoons -\overset{|}{\underset{|}{N}}H^+$$

Figure 29. Interfacial tension at the n-hexane-PICDEA and E-70/ aqueous sodium nitrate interface as a function of aqueous phase pH

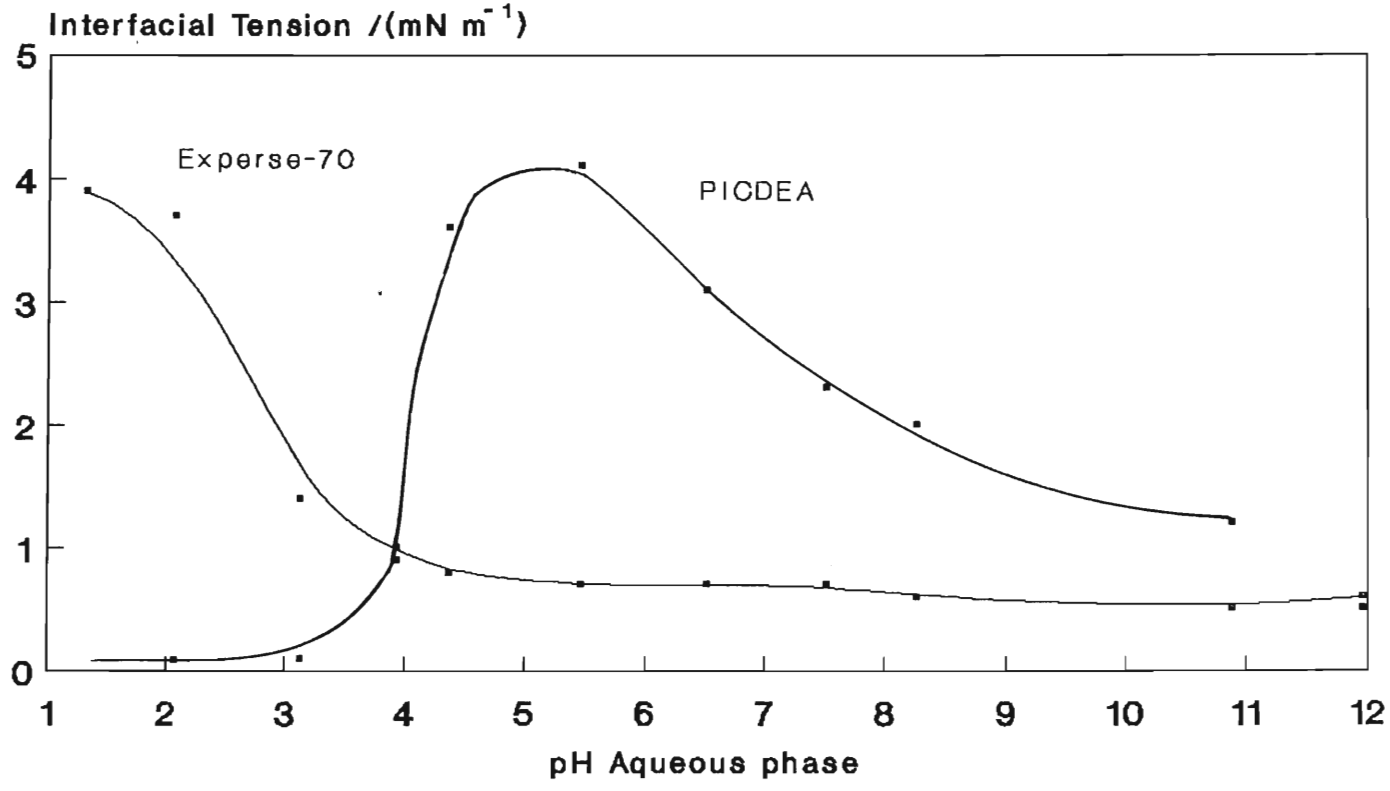

0.018 M PICDEA
1 M sodium nitrate aqueous phase.
Equilibration Time = 10 mins.

The charged species is strongly adsorbed at the interface causing interfacial tension to drop. Further reduction is achieved when nitrate anions in the aqueous phase below the interface behave as counterions and are attracted to this positively charged interface. Such a neutralizing "interaction" lowers the electrostatic free energy of the interface causing the overall interfacial free energy to drop as observed experimentally at low pH.

E-70, on the other hand, is not protonated at low pH values. Interfacial tension is at a maximum at low pH because the uncharged E-70 molecule is less surface active.

3.1.3.1.2. Deprotonation of PICDEA and E-70 with increasing pH

As pH is raised the interfacial tension decreases (Figure (29)). This decrease is caused by the deprotonation of the carboxyl group of the PICDEA molecule producing an anion of higher surface activity than PICDEA itself. Similarly the deprotonation of the E-70 hydroxyl group produces a more surface active anionic species. These two deprotonation reactions are summarised below:

$$\text{PICDEA -COOH} \rightleftharpoons H^+ + \text{PICDEA-COO}^-$$

$$\text{E-70 -OH} \rightleftharpoons H^+ + \text{E-70-O}^-$$

If the negative gradient of the plot of γ versus $[NaNO_3]$ is extrapolated to low pH values a point can be identified where the extrapolated line crosses the horizontal line representing the maximum value of

interfacial tension achieved over the pH range studied. For PICDEA this maximum pH value is 4.65. Deprotonation of the carboxyl group of PICDEA is expected at pH values higher than 4.65 whilst protonation of the amide occurs at values below 4.65. Therefore, at a pH of 4.65 a neutral species is expected to be present at the interface. Furthermore, it appears that the protonated form of PICDEA is more surface active than the deprotonated form since the interfacial tension at low pH is lower than that at high pH (Figure (29)).

For E-70 the maximum interfacial tension was measured at pH 1.3. E-70 will exist in the neutral state at an interface with an acidic aqueous phase of pH less than 1.3. An increase in pH causes the hydroxyl group to dissociate resulting in the production of a highly surface active anionic species.

The effect of pH on the nature of adsorbed PICDEA and E-70 molecules will frequently be referred to in the following three sections (Sections 3.1.3.2.1 to 3.1.3.2.3.) which discuss the effects of various nitrate salts on interfacial tension.

3.1.3.2. The Effect of Sodium, Calcium and Ferric Nitrate Salt Concentration on the Interfacial Tension of the PIBSA Surfactant-Diesel/Milli-Q Water Interface

A comparative study of PICDEA and E-70 surfactant systems was performed. Section 3.1.3.2.1. analyses the interfacial tension data for Aktol PICDEA in a diesel-aqueous nitrate interface and Section 3.1.3.2.2. gives a comparative discussion of the results obtained for Aktol E-70 in a diesel/aqueous nitrate interface. In both PICDEA and E-70 systems the surfactant concentration was kept constant above the cmc at 0.018 M to ensure a well populated, if not saturated, interface.

3.1.3.2.1. Interfacial tension at the Aktol PICDEA-diesel/aqueous nitrate interface

Interfacial tension data showing the effects of sodium and calcium nitrate salt concentration on the PICDEA-diesel/aqueous interface are displayed in Figure (30), a plot of interfacial tension versus the natural log of salt concentration. Figure (31) is a similar plot showing the effects of ferric nitrate concentration on interfacial tension.

Over the range of nitrate salt concentrations used, sodium and calcium nitrate aqueous phases ranged in pH from 4.8 to 6.0, whereas ferric nitrate solutions ranged from 1.0 to 2.0. It is therefore possible to predict the nature of the surfactant at the various nitrate salt interfaces by referring to Figure (29) (Section 3.1.3.1).

Figure 30. Interfacial tension-concentration curves for the aqueous sodium and calcium nitrate/PICDEA in diesel interface

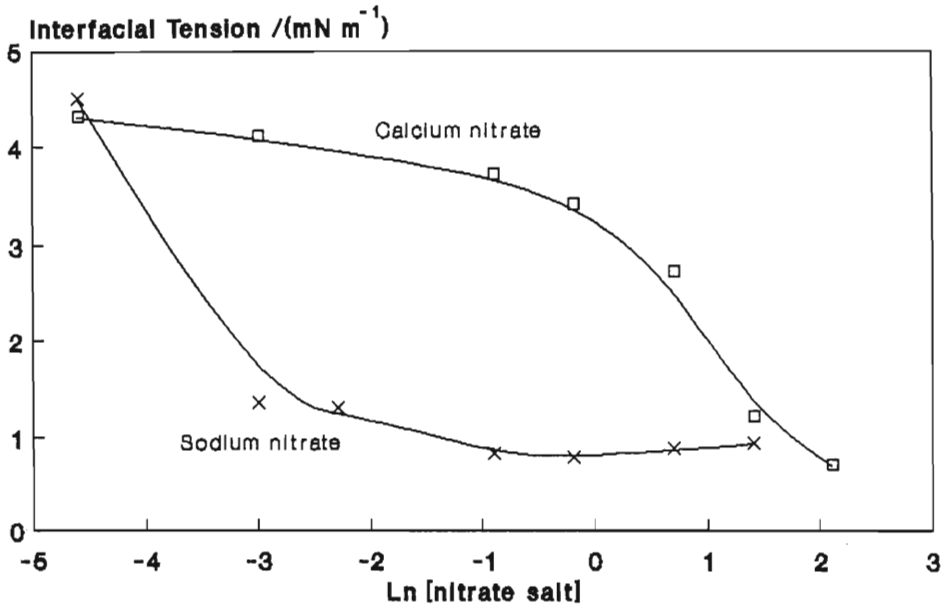

Figure31. Interfacial tension-concentration curve for the aqueous ferric nitrate /PICDEA in diesel interface

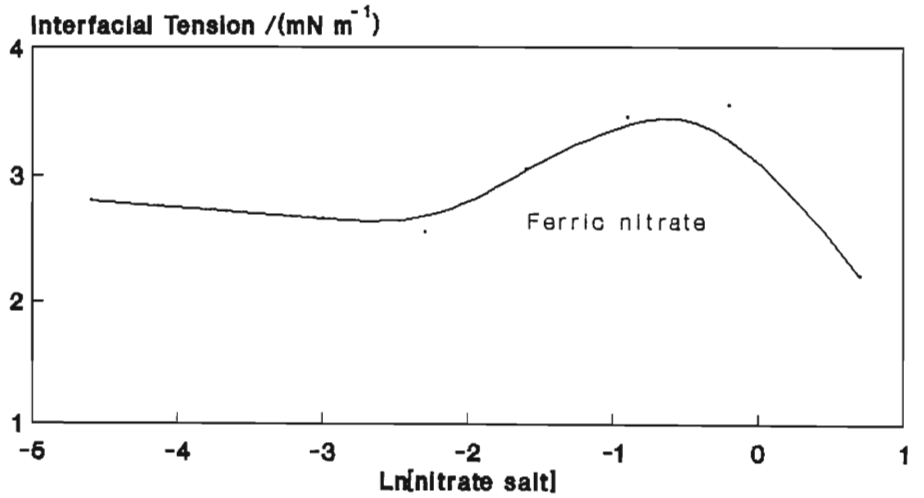

[PICDEA] constant at 0.018 M
PICDEA-diesel/MIIII-Q water interfacial tension = 6.0 mN m^{-1}.

At interfaces with sodium and calcium nitrate solutions PICDEA is partially deprotonated and hence both neutral PICDEA and the anionic species are expected. A nett negatively charged interface will therefore be produced. At the interface with ferric nitrate solutions PICDEA will exist in the protonated form resulting in a positively charged interface.

For all three nitrate salt interfaces the following general trend was observed: The interface experiences an overall reduction in interfacial free energy as nitrate concentration is increased. This is due to the build up of counterions in the aqueous phase below the interface causing a reduction in the electrostatic free energy of the interface which in turn results in the observed reduction in interfacial tension.

Evidence of the counterion effect at low nitrate concentrations is clearly observed in Figure (30). The negatively charged interface attracts sodium or calcium cations and the reduction in interfacial free energy is dependent on the ionic strength of the cation in the aqueous phase. Interfacial free energy decreases with increasing cation charge because the ionic strength of a 0.011 M calcium nitrate solution is greater than that of a sodium nitrate solution of the same concentration.

As nitrate salt concentration increases the extent by which interfacial free energy is reduced is no longer a function of ionic strength alone. An increase in sodium nitrate concentration causes a sudden drop in interfacial tension. Over the same concentration range calcium nitrate causes only a gradual decrease in interfacial

tension and only at much higher concentrations (>1 M) does it drop substantially.

The sodium cation, being mono-valent, attracts individual anionic PICDEA molecules at the interface. The divalent calcium cation, on the other hand, attracts two adjacent PICDEA anions resulting in an unfavourable orientation of bulky hydrocarbons above the interface. This would cause an increase in the energies of interaction in the interfacial region and may account for the observed gradual decrease in interfacial tension for calcium nitrate solutions. At higher concentrations the accumulation of calcium ions at the interface eventually reduces the electrostatic free energy to such an extent that it causes the overall interfacial free energy to drop. Furthermore, as Ca^{2+} concentration increases, eventually there will be one Ca^{2+} per PICDEA molecule at the interface and the unfavourable orientation between adjacent PICDEA hydrocarbons will disappear.

Apparently the interaction between individual PICDEA molecules and sodium cations does not cause this energetically unfavourable hydrocarbon orientation above the interface. In the presence of sodium counterions PICDEA is able to pack closely in the interface because of the low energies of interaction between adjacent hydrocarbons.

An increase in ferric nitrate concentration produces an interesting plot as shown in Figure (31). After an initial drop the interfacial tension increases by ~ 1 mN m^{-1} between concentrations of 0.1 M and 0.8 M before finally decreasing at higher concentrations. At the

interface with ferric nitrate solutions PICDEA exists in the protonated state and hence a positively charged interface is produced. The counterion in this system will therefore be the nitrate anion, NO_3^-. Perhaps the size of the nitrate anion, which is 5 times larger than a calcium or sodium cation, may account for the observed increase in interfacial free energy. This may be explained in terms of the conflicting forces of attraction and repulsion which exist in the interfacial region. Attractive forces occur between counterions and the positively charged interface, and forces of repulsion are expected to exist between the large nitrate anions in the counterion layer below the interface. As the nitrate concentration builds up so a point is reached when the forces of repulsion exceed the magnitude of the attractive forces and cause the observed increase in interfacial free energy. However, if this were the case then why at higher concentrations (>0.6 M) does the interfacial tension decrease? A point may be reached when the build up of negative charge below the interface is a favourable property for this particular interfacial system.

Figure (32) shows the change in interfacial tension with nitrate salt concentration at the PICDEA-diesel/aqueous nitrate interface after only 10 minutes of interfacial equilibration. The observed effects of the different nitrate salts on interfacial free energy after such a short equilibration time are thought to be representative of the forces existing at the interface during the emulsification process. From basic emulsion theory[10,15] it is known that the lower the interfacial tension between two immiscible liquids the shorter the

emulsification time necessary to produce the emulsion. This is indeed the case as illustrated in Figure (33) which is a plot of emulsification time versus nitrate salt concentration for a series of emulsions prepared in this laboratory using PICDEA, diesel and aqueous nitrate salt solutions. The data displayed in this graph was obtained directly from Table (6) (Chapter II, Section 2.2.3.1.). Comparison of Figures (32) and (33) suggests a relationship between the type of nitrate salt, nitrate salt concentration, emulsification time and interfacial tension.

Although PICDEA concentration is once again constant at 0.018 M, after only 10 minutes of interfacial ageing the interface has adsorbed only a small percentage of its total PICDEA adsorption capacity (refer to Figure (8), Chapter II, Section 2.2.1.). This relatively weakly populated interface is less likely to experience the highly energetic interaction between adjacent PICDEA molecules when divalent calcium cations are present at the interface because the molecules are not tightly packed. Sodium and calcium nitrate solutions lower interfacial tension according to their ionic strengths i.e. at any particular nitrate concentration calcium causes a greater reduction in interfacial tension than sodium. The sudden drop in interfacial tension at a completely equilibrated interface (i.e. 20 hours) as shown in Figure (30) is not observed in this system. Apparently only 10 minutes of interfacial contact is insufficient time for the interface to benefit energetically from the favourable interaction between sodium ions and individual PICDEA anions.

Figure 32. Interfacial tension as a function of nitrate salt concentration for aqueous sodium, calcium and ferric nitrate/PICDEA in diesel interfaces after a 10 minute equilibration period

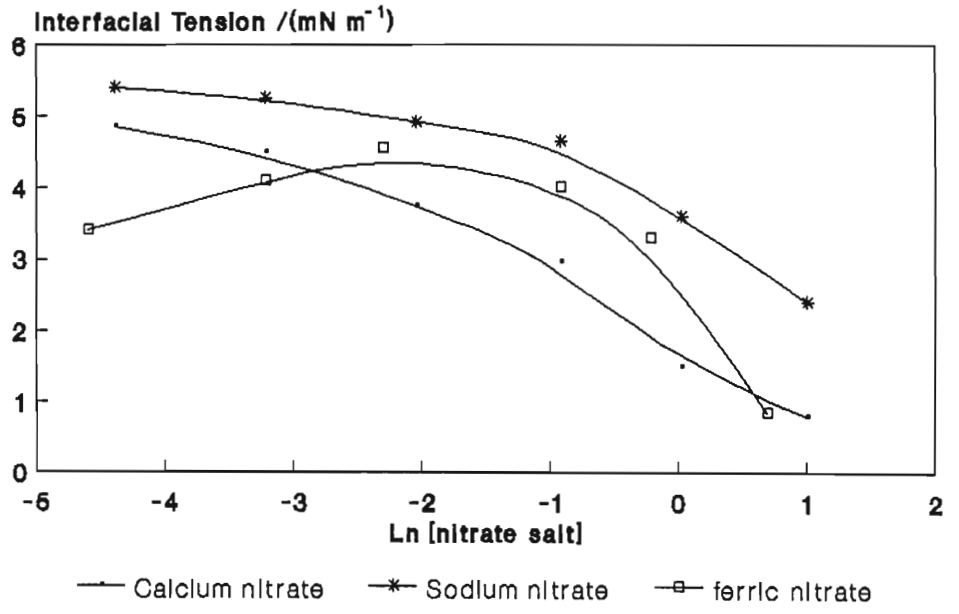

[PICDEA] constant at 0.018 M
Equilibration Time = 10 min.

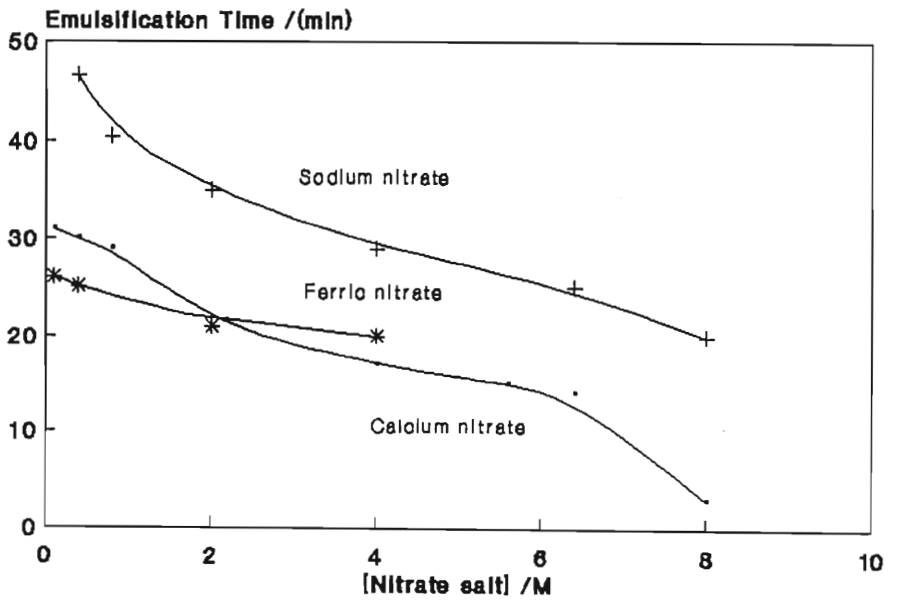

Figure 33. Emulsification time needed to produce an emulsion stabilised with Aktol PICDEA (Batch B) as a function of nitrate salt concentration

As in the previous equilibrated system the interfacial free energy at an interface with a ferric nitrate aqueous phase increases with nitrate concentration. This observation is reflected in the change in emulsification time as ferric nitrate concentration is increased (Figure (33)). Although emulsification time does not increase in a manner proportional to the increase in interfacial tension, there is a far slower reduction in emulsification time in comparison with the times recorded for similar concentrations of sodium and calcium emulsion systems.

The observed increase in interfacial free energy as ferric nitrate concentration increases at an interface which has equilibrated for only 10 minutes (Figure (32)) tends to support the explanation given for the similar observation at the equilibrated interface (Figure (30)). Even though the interface has equilibrated for only 10 minutes and has not yet attained a point of saturated PICDEA adsorption, the accumulation of nitrate anions below the interface causes an increase in interfacial free energy. This suggests that unlike the calcium nitrate system, at an interface with ferric nitrate solution it is not the highly energetic interaction between neighbouring PICDEA hydrocarbons that is responsible for the observed increase in interfacial free energy. The increase in free energy must therefore be related in some way to the nature of the nitrate anion.

3.1.3.2.2. The Effect of Calcium Nitrate on the Surface Pressure and Adsorption of PICDEA at the Diesel-Water Interface

To determine the effect of calcium nitrate on the interfacial pressure of PICDEA at the diesel/ Milli-Q water interface, the following interfacial systems were examined:

1. Aktol PICDEA (Batch A) in diesel over Milli-Q water
2. Diesel over Milli-Q water
3. Aktol PICDEA (Batch A) in diesel over 2.92 M calcium nitrate aqueous phase
4. Diesel over a 2.92 M calcium nitrate aqueous phase

(Diesel: ex. Modderfontein, AECI)

To facilitate in the analysis of these four systems and also to add clarity to the subsequent discussion several symbols are defined as follows:

γ_A = PICDEA-diesel/Milli-Q water interfacial tension

γ_B = PICDEA-diesel/calcium nitrate in Milli-Q water interfacial tension

γ_{Ca} = Diesel/calcium nitrate in Milli-Q water interfacial tension

γ_o = Diesel/Milli-Q water interfacial tension

$\Pi_{Ca} = \gamma_o - \gamma_{Ca}$ = interfacial pressure of calcium nitrate at the diesel-water interface

$\Pi_{PICDEA}^{A} = \gamma_o - \gamma_A$ = interfacial pressure of PICDEA at the diesel-water interface

$\Pi_{PICDEA}^{B} = \gamma_{Ca} - \gamma_B$ = Interfacial pressure of PICDEA at the diesel-calcium nitrate interface

Interfacial tension data and the calculated values for interfacial pressures are tabulated in Tables (14a) and (14b). All interfacial tension measurements were taken after a 20 hour equilibration time and at a temperature of 22 ± 0.5 °C.

Table 14a. Calcium Nitrate Surface Pressure at the Diesel/Water Interface

Parameter	mN m^{-1}
γ_o	14.6
γ_{Ca}	10.1
Π_{Ca}	4.5

Table 14b. Interfacial Tension and Interfacial Pressure Data

[PICDEA]/ mol.dm^{-3}	ln[PICDEA]	γ_A /mN m^{-1}	Π_{PICDEA}^{A} /mN m^{-1}	γ_B /mN m^{-1}	Π_{PICDEA}^{B} /mN m^{-1}
$1.5x10^{-2}$	-4.17	5.4	9.2	1.9	8.1
$4.6x10^{-3}$	-5.38	6.0	8.6	2.5	7.5
$1.5x10^{-3}$	-6.49	8.1	6.5	3.0	7.0
$6.2x10^{-4}$	-7.39	10.5	4.1	3.4	6.6
$3.8x10^{-4}$	-7.87	11.7	2.9	4.4	5.6
$2.3x10^{-4}$	-8.37	12.5	2.1	5.6	4.5
$7.7x10^{-5}$	-9.47	13.7	0.9	7.0	3.0

Figure (34) shows two plots of the interfacial pressure of PICDEA, as a function of the natural log of PICDEA concentration at; a) the diesel/Milli-Q water interface, $\Pi_{PICDEA}{}^{A}$, and at b) the diesel/aqueous calcium nitrate interface, $\Pi_{PICDEA}{}^{B}$.

Differences between the rate of change of Π_{PICDEA} with concentration for the two systems A and B, which are depicted in Figure (34), indicate that a cation-surfactant interaction of some type does occur at the interface. At high concentrations of PICDEA (≥cmc) $\Pi_{PICDEA}{}^{B}$ (in the presence of calcium nitrate) is weaker than $\Pi_{PICDEA}{}^{A}$ (in the absence of the electrolyte). This observed reduction in Π_{PICDEA} may be due to an energetically unfavourable interaction of adjacent PICDEA hydrocarbon chains immediately above the interface caused by the attraction of free carboxyl groups of two adjacent PICDEA molecules to a single divalent calcium cation in the aqueous phase. Such an attraction would result in the inefficient packing of PICDEA hydrocarbon chains above the interface causing the observed increase in interfacial free energy and hence the decrease in Π_{PICDEA}. This is in agreement with the conclusions drawn from the observations made in Section 3.1.3.2.1.

At low concentrations of PICDEA (<cmc) this unfavourable orientation effect is apparently absent, in fact Π_{PICDEA} is enhanced in the presence of calcium nitrate. PICDEA and calcium nitrate appear to be more efficient at reducing interfacial free energy when both are present at an interface than would be expected by the simple summation of their separate surface pressures.

Figure 34. Interfacial pressure-concentration curves for Aktol PICDEA (Batch A) over:

A: MIIII-Q water B: 2.92M calcium nitrate aqueous phase

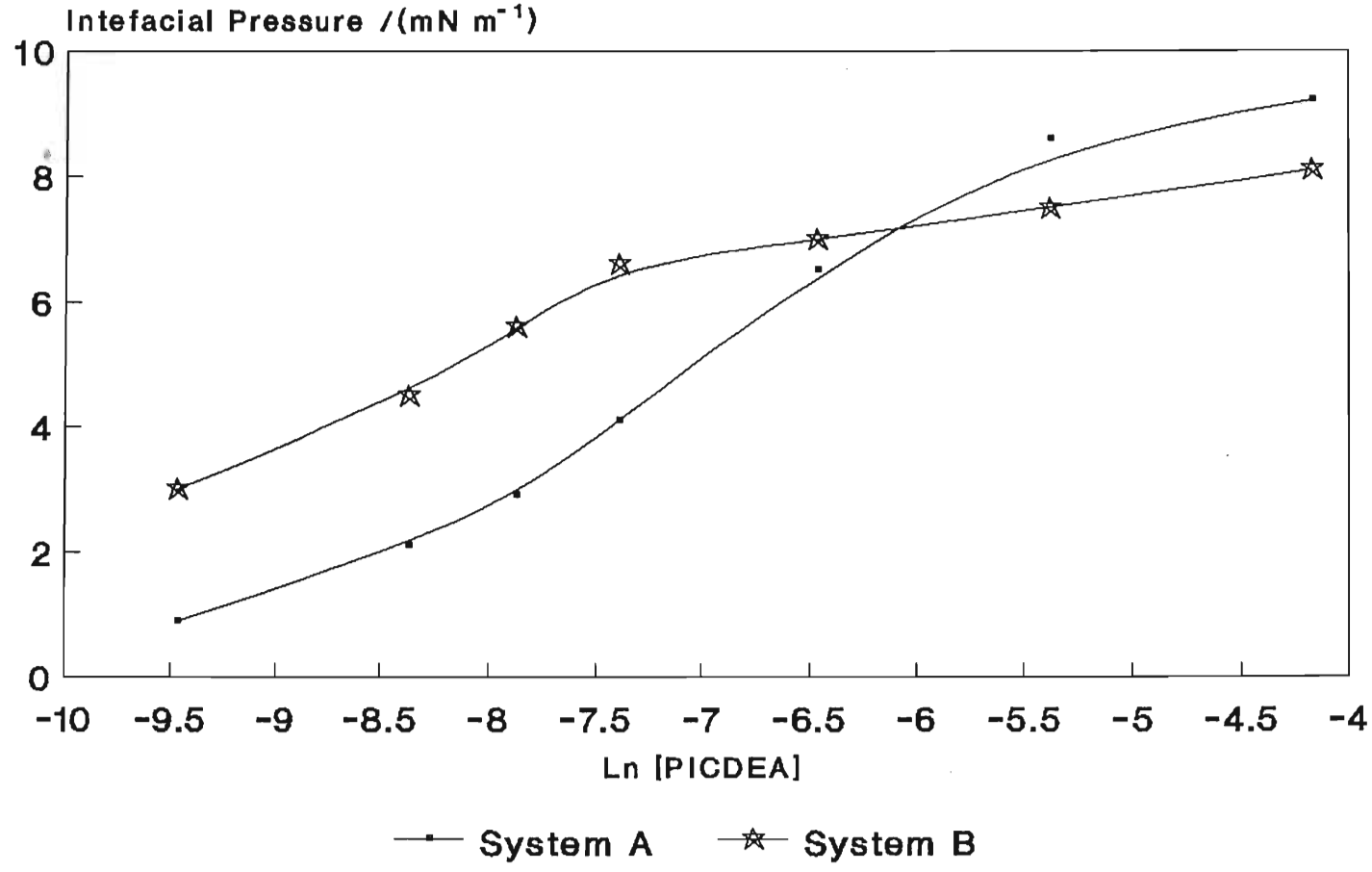

This effect can be illustrated as follows: Consider the system comprising 7.7 x 10^{-5} M PICDEA in diesel in contact with aqueous calcium nitrate. The expected total interfacial pressure of PICDEA and calcium nitrate can be determined by the following addition:

$$\Pi_{Ca,PICDEA}^{*} = \Pi_{Ca} + \Pi_{PICDEA}^{A} = 4.5 + 0.9$$
$$= \underline{5.4 \text{ mN m}^{-1}}$$

where * denotes the expected value

Therefore the expected interfacial tension would be:

$$\gamma_B^{*} = \gamma_o - \Pi_{Ca,PICDEA}^{*} = 14.6 - 5.4$$
$$= \underline{9.2 \text{ mN m}^{-1}}$$

However the experimentally determined interfacial tension for this system, γ_B, equals 7.0 mN m^{-1}

$$\text{i.e. } \gamma_B^{*} > \gamma_B$$

and therefore $\Pi_{PICDEA}^{B*} < \Pi_{PICDEA}^{B}$

$$\text{i.e. } \Pi_{PICDEA}^{B*} = \gamma_{Ca} - \gamma_B^{*} = 10.1 - 9.2$$
$$= \underline{0.9 \text{ mN m}^{-1}}$$

and $\Pi_{PICDEA}^{B} = \underline{3.0 \text{ mN m}^{-1}}$

This greater than expected reduction in γ_B is most likely due to the effect of Ca^{2+} at the interface. Ca^{2+} neutralizes the partially dissociated carboxylic acid groups of PICDEA thus reducing the electrostatic free energy of the interface which would account for the observed reduction in interfacial free energy.

3.1.3.2.3. Interfacial Tension at the Aktol E-70 Diesel/Aqueous Nitrate Interface

The interfacial tension curves showing the effects of sodium, calcium and ferric nitrate salt concentration on the E-70 diesel/aqueous interface are shown in Figure (35). For all three systems interfacial free energy drops as nitrate salt concentration increases. Sodium and calcium nitrate solutions lower interfacial tension according to their ionic strengths. Ferric nitrate solutions which have higher ionic strengths may be expected to give even lower interfacial tensions. However, the low pH of the ferric nitrate aqueous solutions ensures that the E-70 molecules adsorbed at the interface remain predominantly in the neutral state which is less surface active and hence higher interfacial tensions were observed.

The curves in Figure (35) do not, however, suggest the existence of any undesirable cation-surfactant interactions. The single hydrocarbon structure of the E-70 molecule enables closer packing at the interface than the double hydrocarbon structure of the PICDEA molecule. When two adjacent deprotonated E-70 molecules are attracted to a Ca^{2+} cation there is apparently no significant increase in the interaction energies between the hydrocarbons above the interface. Consequently, interfacial tension decreases with calcium nitrate concentration at a similar rate as that observed for sodium nitrate.

When three E-70 molecules are attracted to a single Fe^{3+} cation it might be expected that an increase in the

Figure 35. Interfacial tension at the E-70 - diesel/aqueous sodium, calcium and ferric nitrate interfaces as a function of nitrate salt concentration

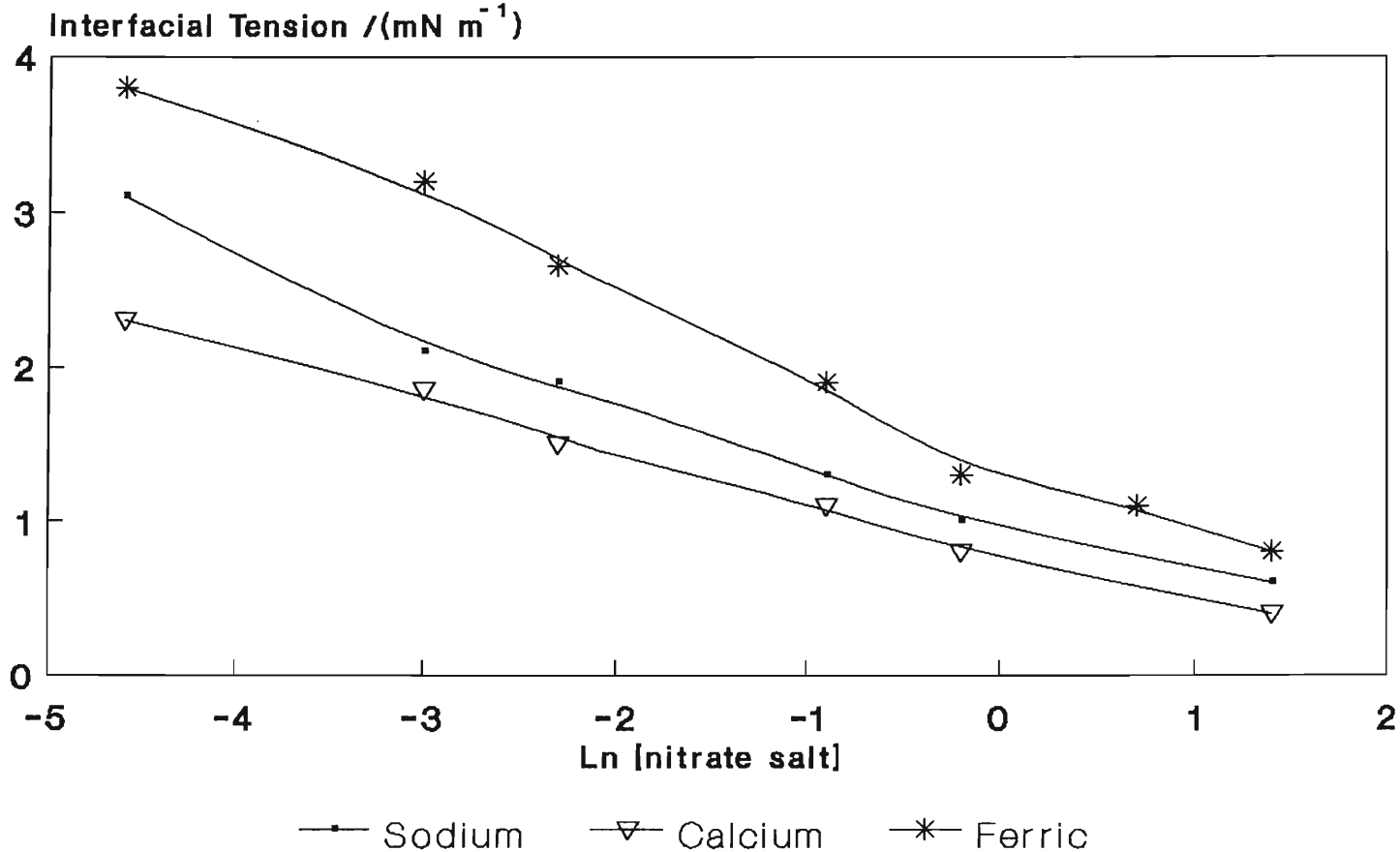

[E-70] constant at 0.018 M
Equilibration Time = 20 hrs.

energies of interaction between adjacent hydrocarbons would occur. However, the majority of adsorbed E-70 molecules are in the neutral state so that if such an interaction is energetically unfavourable it would have little effect on the overall reduction in interfacial free energy.

Figure (36) is a pictorial representation of PICDEA and E-70 molecules at the various aqueous nitrate interfaces showing the expected orientation of hydrocarbons above the interfaces described in the previous three sections.

PICDEA

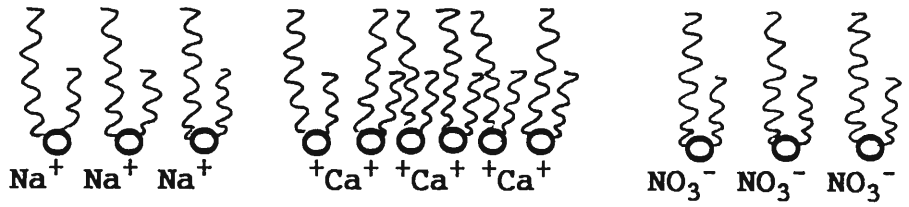

E-70

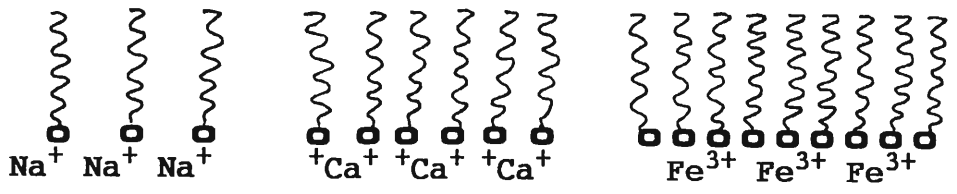

Figure 36. A pictorial representation of PICDEA and E-70 at the various aqueous nitrate interfaces

3.1.3.3. Surfactant-cation Complexation

It remains unclear whether or not nitrate cations form complexes with deprotonated PICDEA molecules at the oil/water interface. It is, however, relevant at this stage to discuss the implications of such a complexation on the interfacial activity of PICDEA and the stabilizing properties of the interfacial film.

According to HLB theory[88] a surfactant with an HLB value greater than approximately 9 is suitable for the formation of oil-in-water emulsions. HLB values of less than 7 are necessary for the production of water-in-oil emulsions. The scale in Figure (37) shows the HLB range required for various systems. The original method for determining HLB numbers was devised by Griffin[89] in 1949 and involves a long experimental procedure. A rough approximation can be obtained, however, by the water solubility of the surfactant[90]. Table (15) shows how Griffin classified surfactants according to their solubility in water. Both 45% Aktol PICDEA in diesel and 54.7% Adibis PICDEA in process oil are completely immiscible in water and therefore according to Griffin's descriptions in Table (15) will have very low HLB values.

Figure 37. The HLB scale[88]

Range	Application
3-6	W/O Emulsifier
7-9	Wetting Agent
8-13	O/W Emulsifier
13-15	Detergent
15-18	Solubilizer

Table 15. Approximation of HLB by water solubility[90]

Behaviour when added to water	HLB Range
No dispersibility in water	1-4
Poor dispersion	3-6
Milky dispersion after vigorous agitation	6-8
Stable milky dispersion (upper end almost translucent)	8-10
From translucent to clear dispersion	10-13
Clear solution	13+

Davies[91] showed how an approximation of HLB is possible from the summation of structural factors. Davies resolved the structure of a surfactant into component groups, each of which makes a contribution to the HLB number. Table (16) shows the group numbers obtained from several known structures of defined HLB.

The HLB number can be calculated by substituting the group numbers into the relation:

$$HLB = 7 + \Sigma(\textit{hydrophilic group number}) - \Sigma(\textit{lipophilic group number}) \quad (17)$$

Table 16. HLB group numbers[91]

Group	factor
$-SO_4Na$	38.7
-COOK	21.1
-COONa	19.1
-N (tertiary amine)	9.4
Ester (Sorbitan ring)	6.8
Ester (free)	2.4
-COOH	2.1
-OH (free)	1.9
-O-	1.3
-OH (sorbitan ring)	0.5
CH-	-0.475
$-CH_2-$	-0.475
$-CH_3$	-0.475
=CH-	-0.475

The HLB number for PICDEA has not been determined experimentally because of the presence of contaminants such as surface active precursors and diluent hydrocarbons. However, using Equation (17) and the relevant values listed in Table (16), the HLB number can be approximated. For a PICDEA molecule with a molecular weight of 1240 g mol^{-1} (i.e. x = 14 in Figure (1), Chapter I, Section 1.4) the HLB number is approximately -7.6. This extremely low value is due to the long PIB and COCO hydrocarbon chains.

From Table (16) Davies indicates that a -COO-Na group will increase a surfactants HLB by a factor of 19.1 as opposed to a factor of 2.1 for a free -COOH group. It is reasonable to assume that a similar effect would occur if a complexation occurred between the divalent calcium cation and the carboxyl groups of two adjacent PICDEA molecules. A PICDEA-Na complex will have an HLB value of approximately 9.4, which, according to the scale in Figure (37), falls within the range of HLB values required for the stabilisation of oil-in-water emulsions. Such a complexation would, therefore, be expected to result in the destabilisation of a water-in-oil emulsion. This is possibly a result of a weakening of the interfacial film (i.e. due to the weakening of mechanical and/or energy barriers) brought about by a change in surfactant adsorption properties.

In practise, however, the addition of sodium nitrate to the aqueous phase of an explosive emulsion does not cause an acceleration in emulsion breakdown as is observed in the presence of calcium nitrate. If complexation does occur this suggests that calcium preferentially binds

with PICDEA at the droplet interface. If a PICDEA-Ca-PICDEA ligand complexation does occur, then both the surfactant-cation orientational effect discussed in Sections 3.1.3.1.1 and 3.1.3.1.2, and the positive shift in HLB, i.e. the change in the adsorptive properties of PICDEA, will contribute to the destabilisation of the water-in-oil structure of an explosive emulsion.

There have been a number of publications[92,93,94,95] which have investigated the preferential binding of the Ca^{2+} cation to phospholipid cell membranes. A bilayer membrane consists of two monolayers of amphiphilic phospholipid molecules with their hydrophobic tails back to back forming a lipophilic core. The outer surfaces of the membrane are hydrophilic in nature.

Insight into Ca^{2+} binding to PICDEA hydrophilic groups can be gained by looking at comparable phospholipid/cation binding studies. It is possible that the observed effects of divalent cations on the properties of phospholipid vesicle membranes can be compared with the effect of various cations on the stabilising properties of the PICDEA interfacial "membrane".

Ca^{2+} has long been known to bind with phosphatidylserine[96,97] (phosphatidylserine is one of many phospholipids which make up cell membranes). McLaughlin[94] used phosphorus-31 and carbon-13 NMR to identify the divalent cation binding sites at the surface of a phosphatidylserine membrane. The paramagnetic divalent cobalt cation was used as a "probe" for determining the cation binding sites. Three binding

sites were identified; the phosphodiester group, the carboxyl group and the amino group. According to McLaughlin the carboxyl group is the preferred site for calcium cation binding.

Papahadjopoulos et al[98] observed that the presence of Ca^{2+} results in increased vesicle permeability, aggregation and fusion of vesicles. The hydrocarbon chains of the lipid bilayers undergo an isothermic phase change from a fluid to a crystalline state. Ca^{2+} induced phase changes may be responsible for altering the energetics of the system by providing an unstable transition state of relatively low free energy of activation, thus increasing the probability of membrane fusion.

Lis et al.[99] observed a decrease in the binding affinity of Ca^{2+} for various phosphatidylcholine bilayers with an increasing degree of membrane fluidization. This offers the possibility that the rigidity[30] of the PICDEA stabilised interface may aid chelation with Ca^{2+} and that the mobility associated with other PIBSA surfactants may decrease the adverse effects of Ca^{2+}.

3.2. Chromatographic Techniques

3.2.1. Reverse Phase Silica Chromatography

In the attempt to find a suitable solvent system for reverse phase chromatography, the flash chromatographic technique[56] described in Chapter I, Section 2.2.2.2 was adopted. 30-40% (v/v) solutions of 45% active (w/w) Aktol PICDEA in diesel were prepared using the various solvent systems listed in Table (4) (Chapter I, Section 2.2.2.2). TLC was used to identify the solute components eluted in each of the 2 ml fractions collected.

The first mobile phase investigated was 100% chloroform (HPLC grade). A total of 66 fractions were collected, the last of which contained the final traces of solute detectable by TLC. Developed TLC plates showed that fractions 29 to 66 contained PICDEA and probably PIBSA (R_f = 0.00), fractions 41 onwards contained PIB (R_f = 0.65 - 0.83) and components of CDE (R_f = 0.11 and 0.30). From fractions 45 onwards CDE (R_f = 0.45) began to elute and finally at fraction 47 diesel appeared. The remaining CDE components were not detected possibly because they were eluted over many fractions. This would result in excessive dilution of the components which would prevent their detection via TLC analysis.

An infra red spectrum of the first 11 fractions containing solute, i.e. fractions 29 to 39, is shown in Figure (38). Table (17) is a list of the characteristic adsorption peaks in Figure (38).

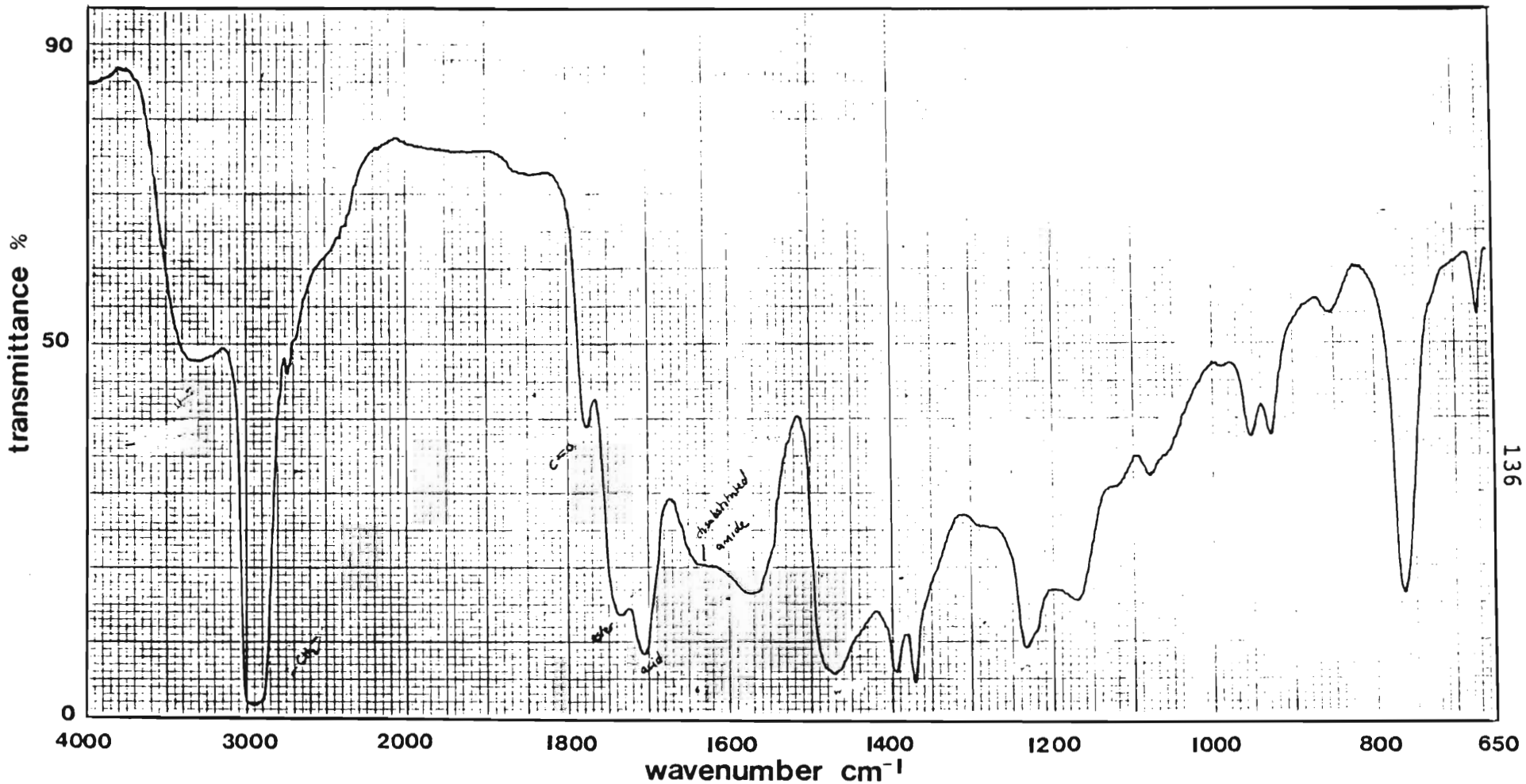

Figure 38. Infra red spectrum of the components of Aktol PICDEA in diesel eluted in fractions 29 to 39 from a reverse phase liquid chromatographic column using chloroform as the mobile phase

Table 17. Infra red adsorption peaks characteristic of the solutes eluted from commercial Aktol based PICDEA in fractions 29 to 39 collected from a reverse phase C18 chromatographic column. Mobile phase: 100% chloroform

Wavenumber /cm^{-1}	
2950	C-H stretching
1780	anhydride carbonyl
1735	ester carbonyl
1710	acid carbonyl
1640	tertiary amide
1570	free amine, N-H
1250-1150	C→O→C stretching in an anhydride or ester
1050-1080	C→N stretching of CDE
3350	N-H and O-H stretching

Taking into account the relative intensities of the adsorption peaks in Figure (38) one can conclude from this table that the following components are present in fractions 29 to 39: PICDEA, PIBSA, free amines and probably free fatty acids present in commercial CDE (refer to Appendix II) and traces of CDE.

A reduction in the diesel alkane adsorption peaks can be seen when this spectrum in Figure (38) is compared with that of 45% Aktol PICDEA in diesel shown in Figure (39). The alkane peaks were identified from the infra red spectrum of pure diesel (ex. AECI, Modderfontein) shown in Figure (40).

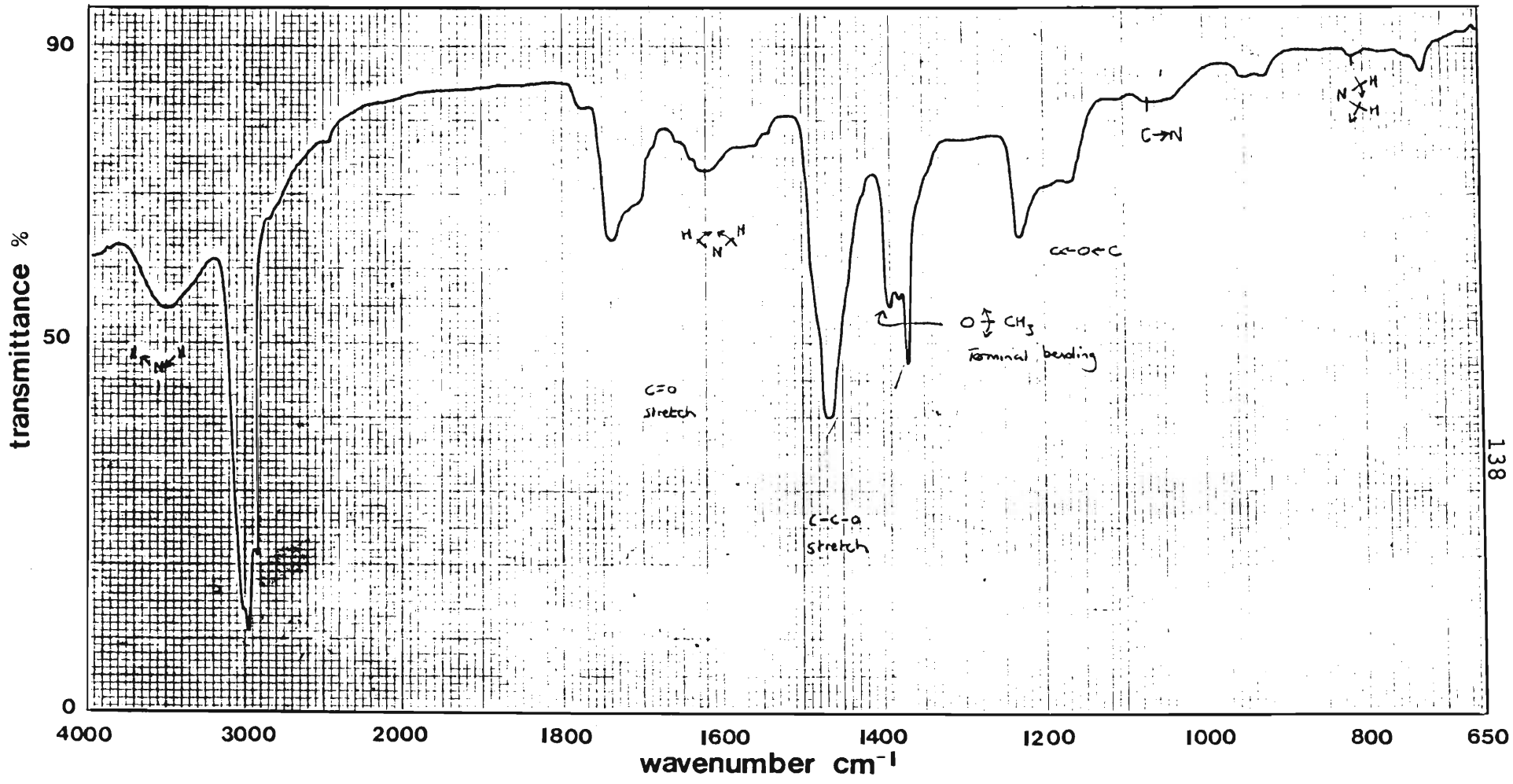

Figure 39. Infra red spectrum of unpurified 45% active (w/w) Aktol PICDEA in diesel

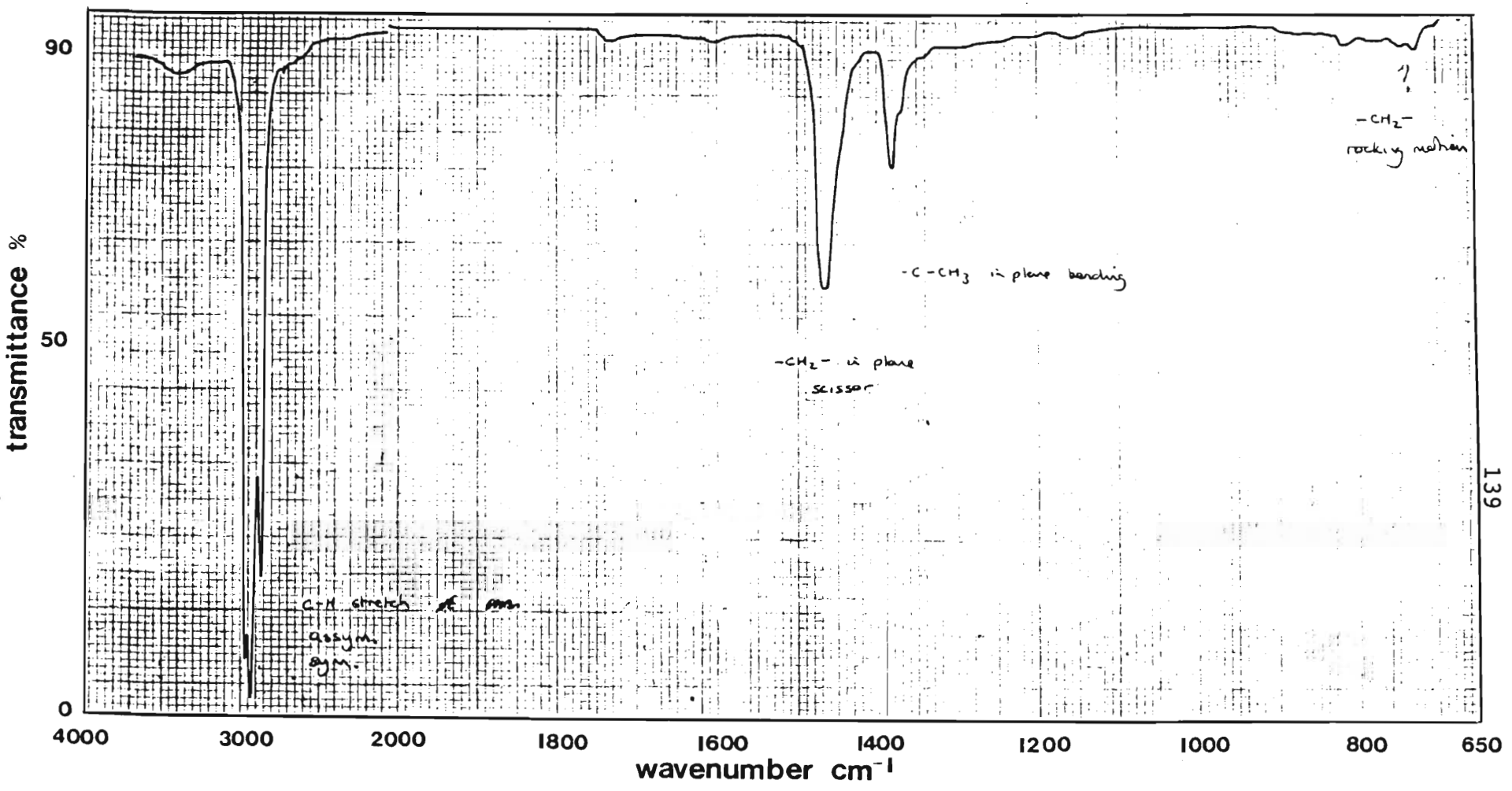

Figure 40. Infra red spectrum of diesel (ex. AECI, Modderfontein)

The uv spectrum in Figure (41) verifies the absence of diesel in fractions 29 to 39. The uv spectrum of pure diesel in Figure (42) has a single adsorption peak at 227.1 nm. Comparing this with the uv spectrum of 45% Aktol PICDEA in diesel (Figure (43)) which has adsorption peaks at 202.4 nm and 226.1 nm, it can be seen that diesel is absent in the first 11 fractions.

The strength of the acid carbonyl peak in the infra red spectrum in Figure (38) suggests that some of the PIBSA may be present in the dicarboxylic form. The infra red spectrum of Manro CDE is shown in Figure (44). There are two characteristic peaks; the first at 1640 cm^{-1} is due to the amide carbonyl and the second (between 1050 and 1080 cm^{-1}) is due to C→N stretching. The latter appears in the spectrum shown in Figure (38) confirming the presence of CDE in the fractions 29 to 39.

The order of elution was as expected, i.e. the more polar constituents eluting before the non-polar diesel and PIB hydrocarbons. Unfortunately not all of the PICDEA and PIBSA is eluted in the first 11 fractions. The uv spectrum, shown in Figure (45), of the solutes in fractions 47 to 55 shows the presence of both diesel and surfactant components. The wide range in PIB hydrocarbon chain lengths in commercial Aktol PICDEA is largely responsible for the spreading of the solute over almost 30 of the 2 ml fractions. One can predict from the nature of the interaction between the non-polar gel structure and the surfactant molecules that the shorter chain PICDEA and PIBSA molecules will elute first.

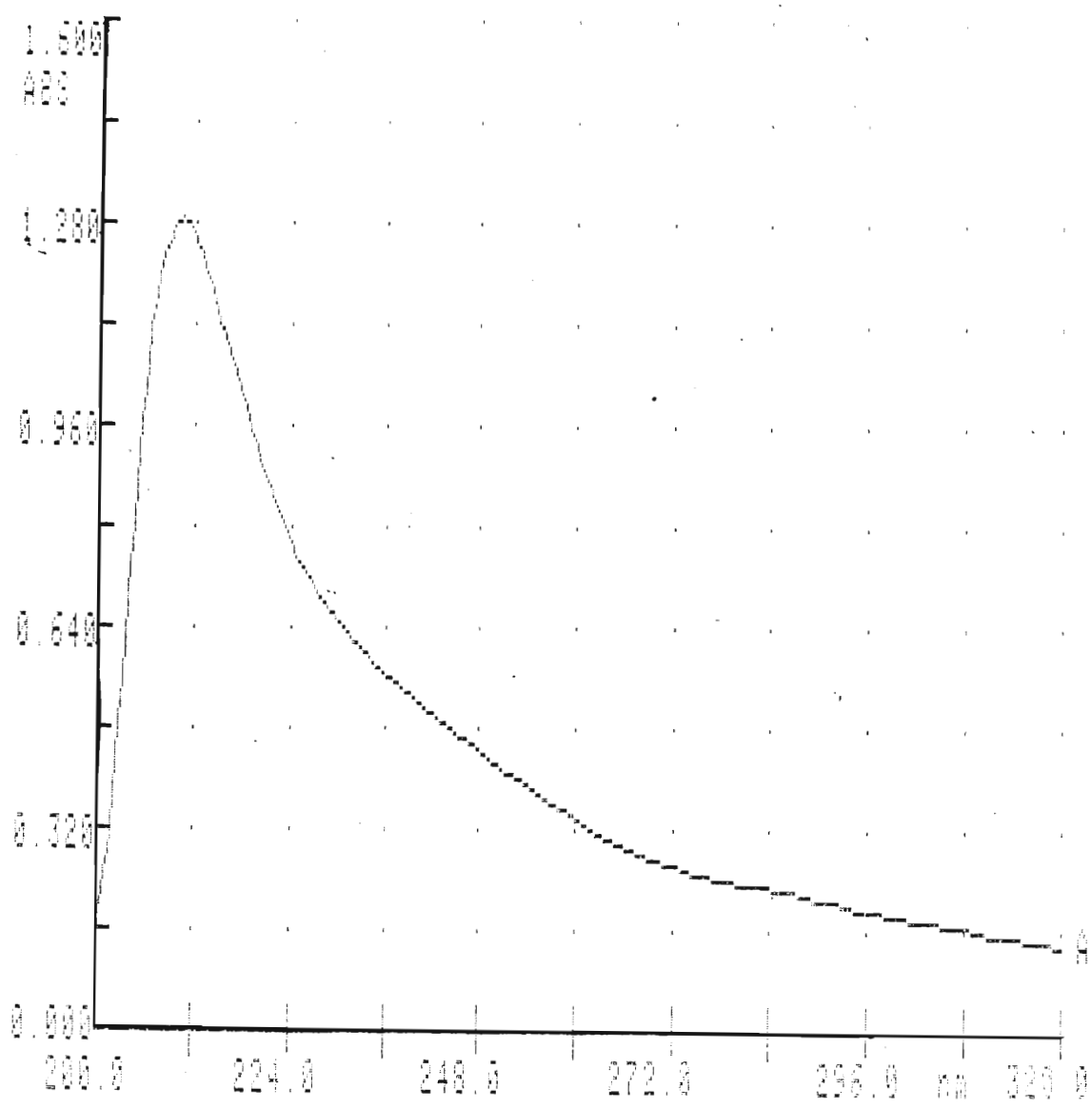

Figure 41. Ultra violet absorption spectrum of the components of Aktol PICDEA collected in fractions 29 to 39 from a reverse phase liquid chromatographic column using chloroform as the mobile phase

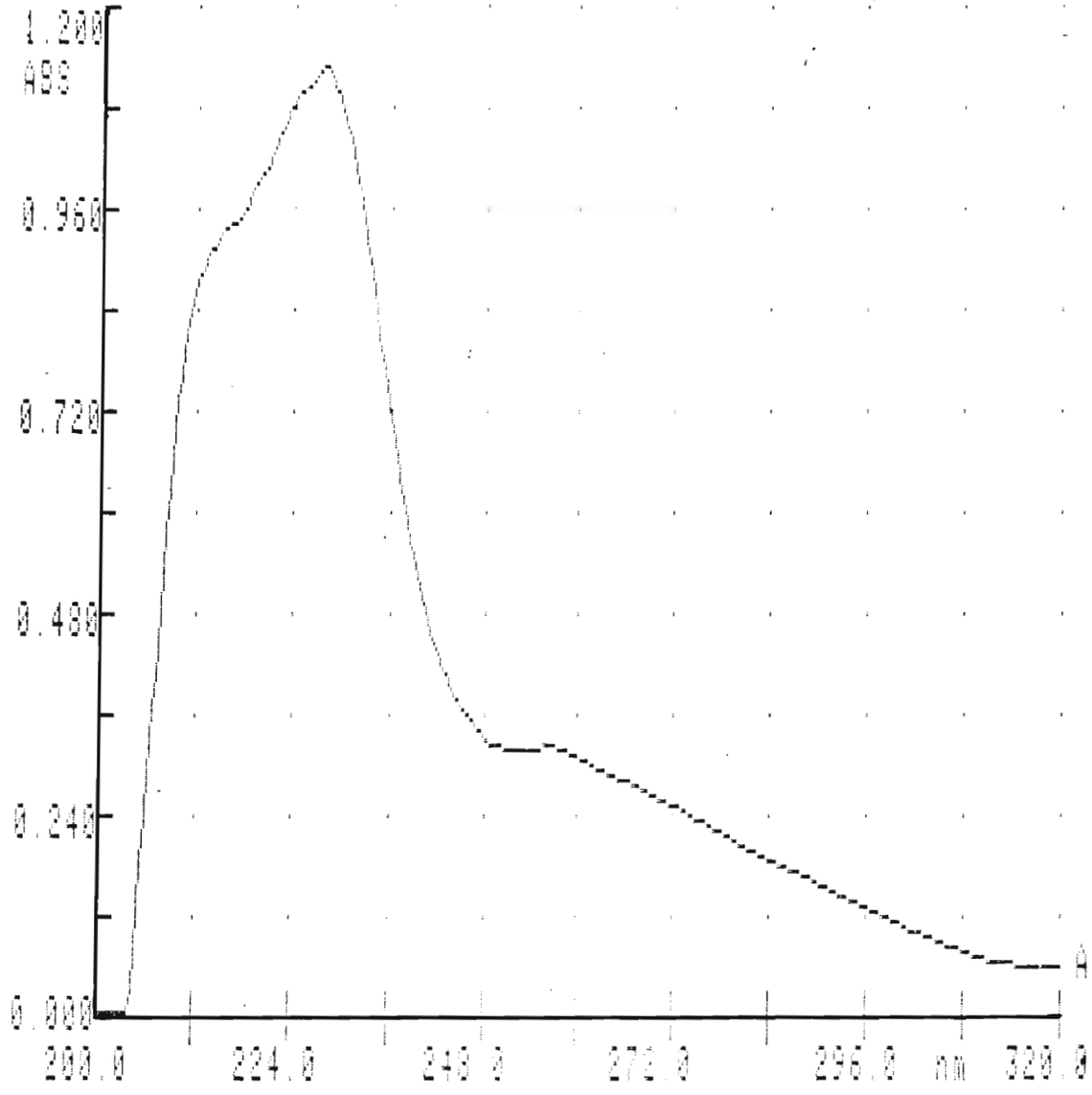

Figure 42. Ultra violet absorption spectrum of diesel (ex. AECI, Modderfontein)

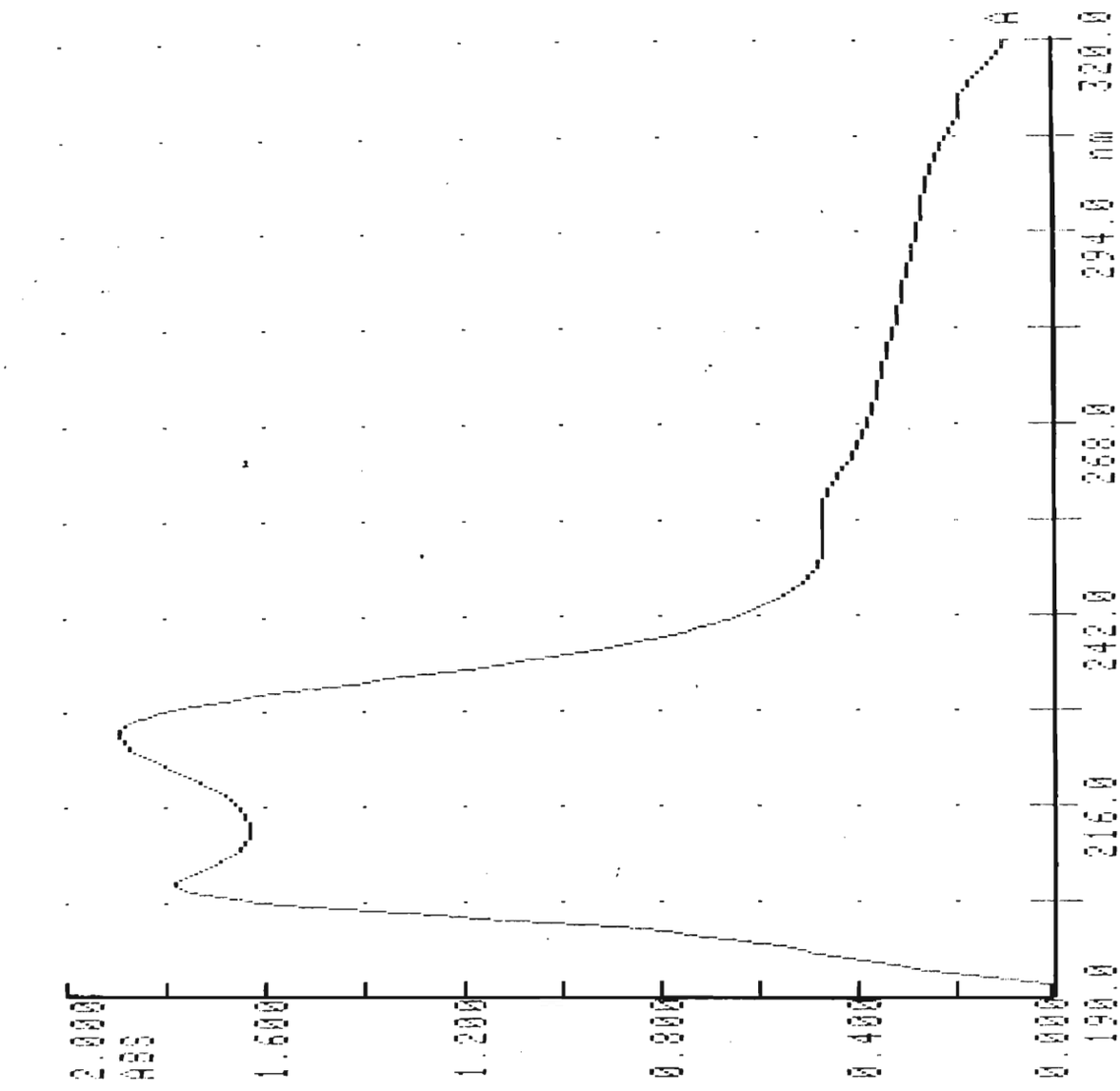

Figure 43. Ultra violet absorption spectrum of unpurified 45% Aktol PICDEA in diesel

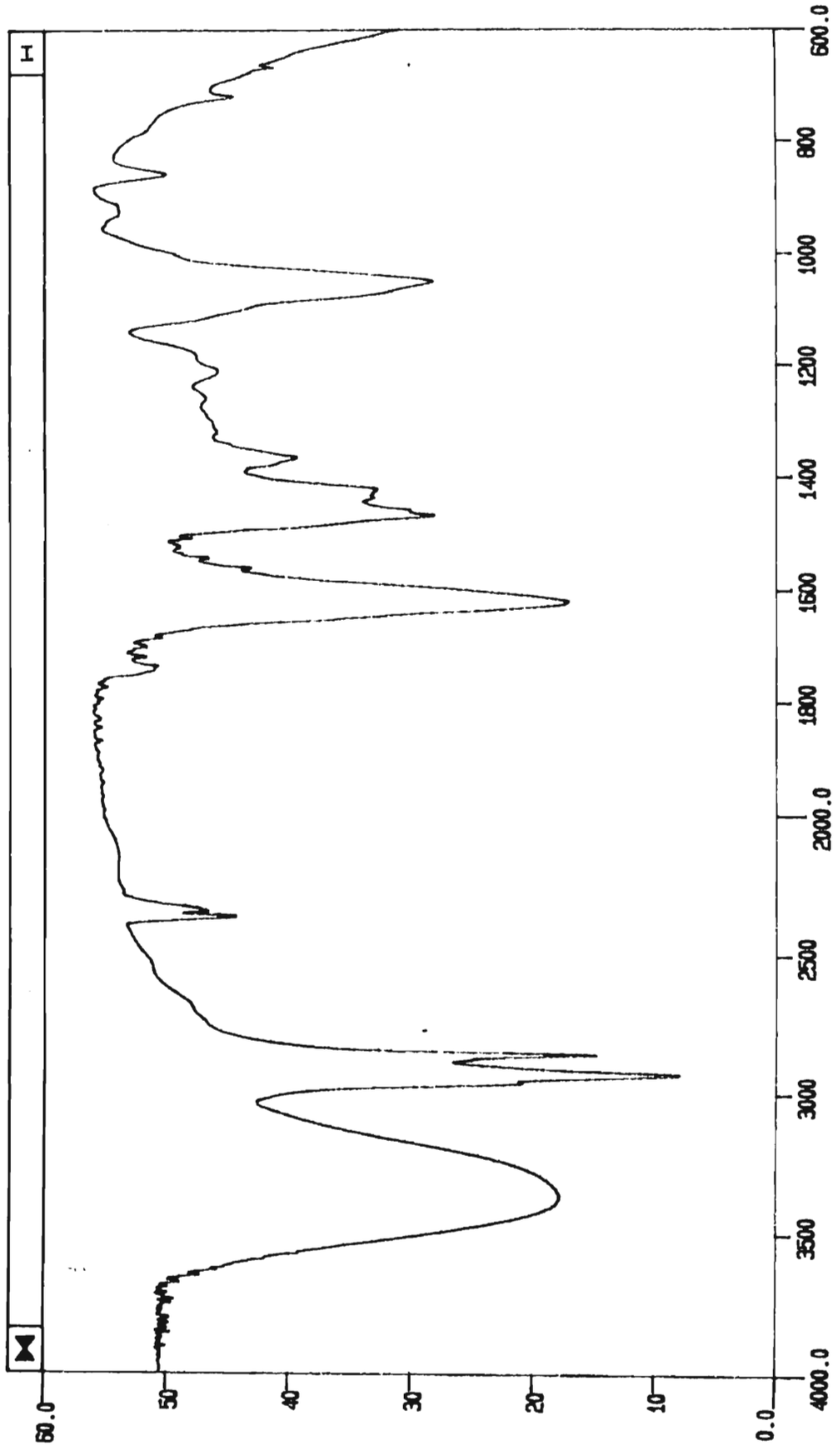

Figure 44. Infra red spectrum of Manro coco-diethanolamide (CDE)

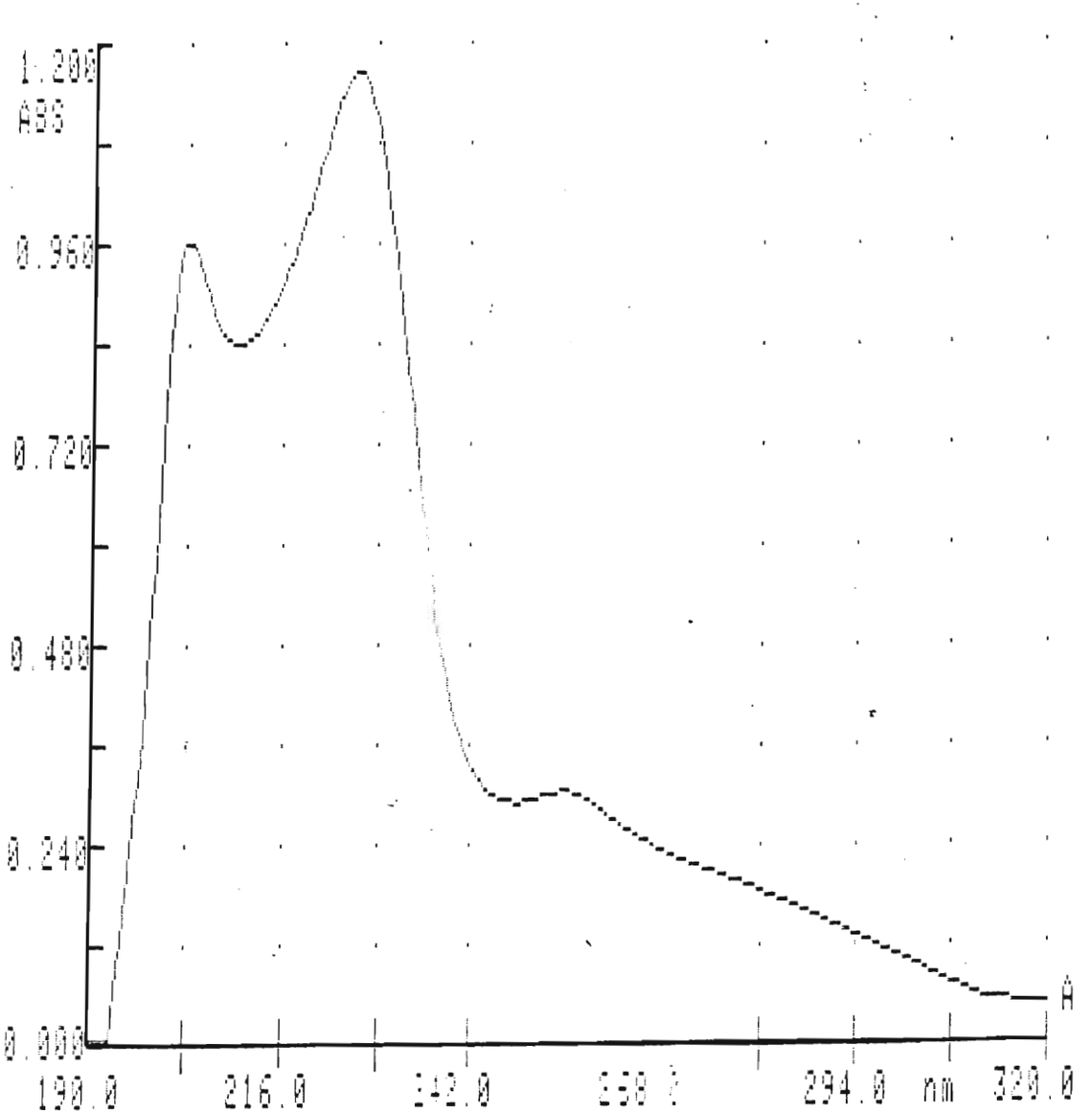

Figure 45. Ultra violet absorption spectrum of the components of Aktol PICDEA eluted in fractions 47 to 55 from a reverse phase liquid chromatographic column using chloroform as the mobile phase

Long hydrocarbon chain molecules which are more lipophilic in character will be retarded to a greater extent by the C18 gel than the shorter chain molecules. Hence, the first fractions collected were free of diesel and PIB hydrocarbons and do not contain PICDEA and PIBSA molecules with PIB hydrocarbon chains covering the whole range of chain lengths present in the commercial sample, i.e. the solute collected is not a true representation of the surfactant present in the commercial product.

In an attempt to improve the separation of the polar components from the free hydrocarbons the polarity of the solvent was increased by the addition of acetone. The solvent system used was 80% chloroform/20% acetone.

From the analysis of TLC plates the only difference observed was the earlier elution of CDE components (R_f = 0.11, 0.35 and 0.54) before PIB and diesel components. Otherwise there was no improvement in the separation of polar and non-polar constituents.

A solvent system of THF gave a poorer separation but eluted the components sooner than the chloroform systems. Addition of 30% iso-propanol to THF caused less spreading of the sample components and fewer fractions were collected, i.e. 59 fractions. Mobile phases of 70% chloroform/30% iso-propanol and 100% carbon tetrachloride did not result in any significant improvements in the separation of the sample components over and above that achieved using 100% chloroform.

The limited separation achieved using reverse phase liquid chromatography can be attributed largely to the wide range in PIB hydrocarbon chain lengths which exist in commercial Aktol PICDEA.

3.2.2. Size Exclusion Chromatography

The molecular weight of Aktol based PICDEA is on average 1700 g mol^{-1} (Chapter I, Section 1.4.). For a PICDEA molecule with the minimum 20 carbon PIB moiety the molecular weight would be approximately 1000 g mol^{-1}. PIBSA has a minimum weight of ~550 g mol^{-1} and an average of~950 gmol^{-1}. Diesel hydrocarbons weigh in the region of 300 g mol^{-1} and CDE components range from 105 g mol^{-1} for free diethanolamine to 370 g mol^{-1} for CDE based on linoleic acid (Appendix II).

Considering this wide range in molecular weights it is feasible that separation of the components of Aktol PICDEA in diesel may be achieved using size exclusion chromatography. The order of elution is expected to follow the decrease in molecular weight of the sample components, i.e. PICDEA > PIBSA ≥ PIB > Diesel ≥ CDE. In a true size exclusion separation pure PICDEA will be eluted from the column before any of the other components are detected.

Sephadex LH-20 (the dextran gel used in this investigation) has an exclusion limit of 4000 g mol^{-1}. Therefore all of the components of the Aktol PICDEA sample will be retarded by the gel with the extent of retardation being dependent on the molecular size of the

individual components.

The first solvent system investigated was 100% THF (UV grade). Figure (46) is a bar type graph showing the fractions over which each sample component was eluted. TLC was used to detect the various solutes present in each fraction as described in Chapter I, Section 2.2.2.1. The results obtained from such an analysis were used to construct the graph in Figure (46). It can be seen that solutes were eluted over a wide range of fractions with very poor resolution. According to the TLC results, i.e. Figure (46), a solute with an R_f value of 0.00 was eluted first. If size exclusion is operative this solute is expected to be pure PICDEA. This is probably followed by PIBSA which cannot be detected by TLC because it also has an R_f value of 0.00. The first traces of solute were detected in fraction 20, which is equivalent to an elution volume of 23.5 ml (fraction volume = 1.18 ml). CDE and diesel components were not retarded effectively and appeared in fractions 26 and 35 respectively.

A solvent system of 100% chloroform gave no improvement in the separation. The elution sequence of the components is shown in Figure (47). The first trace of solute was detected in fraction 38, i.e. after an elution volume of 26 ml (fraction volume of 0.69 ml). This later elution of solutes observed when using chloroform instead of THF suggests that there is an increase in the adsorption of solute molecules to the gel matrix. Furthermore, components of CDE were detected almost immediately after the first traces of PICDEA were eluted even though the components of CDE are much smaller than PICDEA.

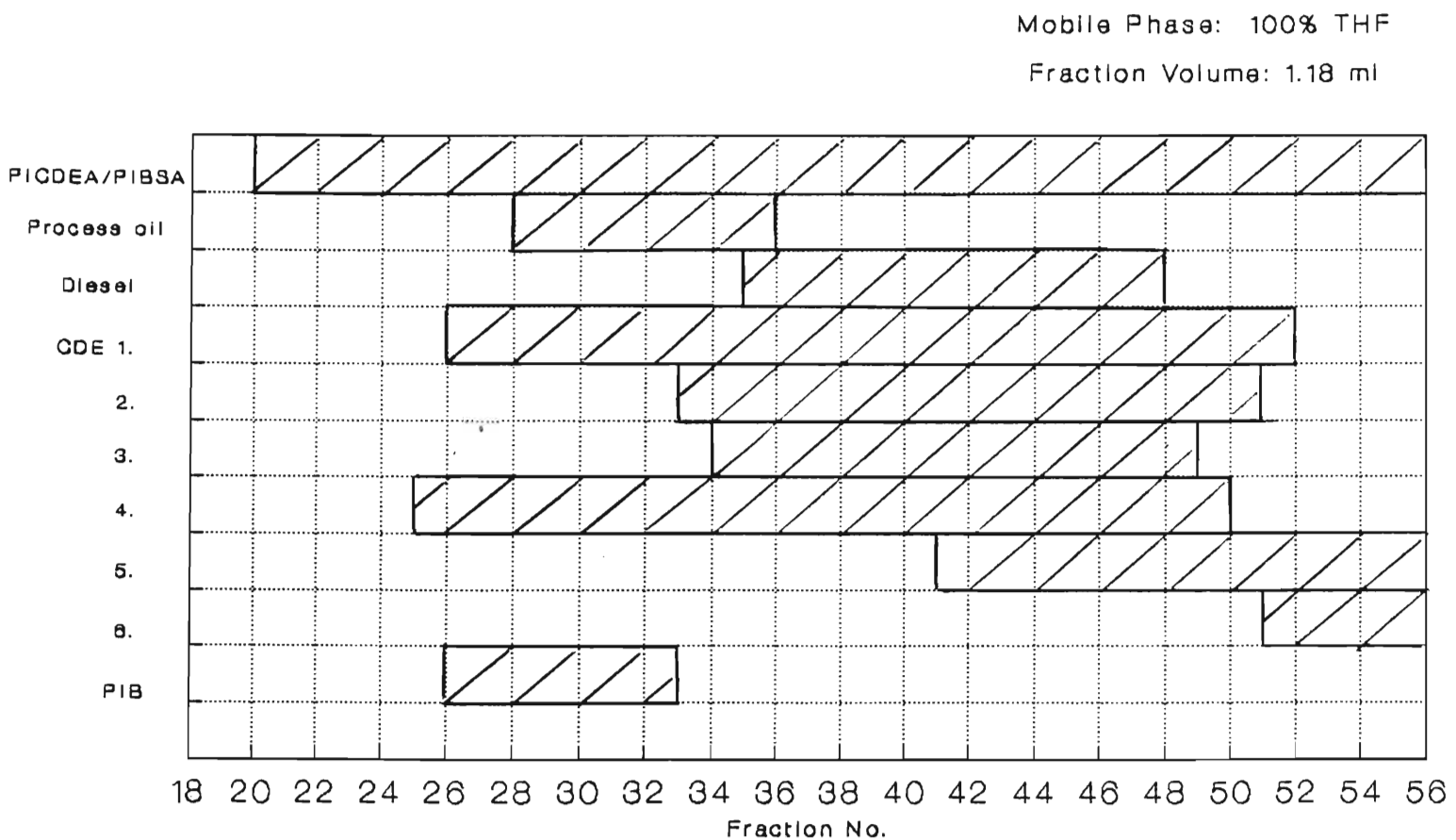

Figure 46. A bar graph showing the order of elution of the components of Aktol PICDEA from a Sephadex LH-20 size exclusion column using tetrahydrofuran as the mobile phase

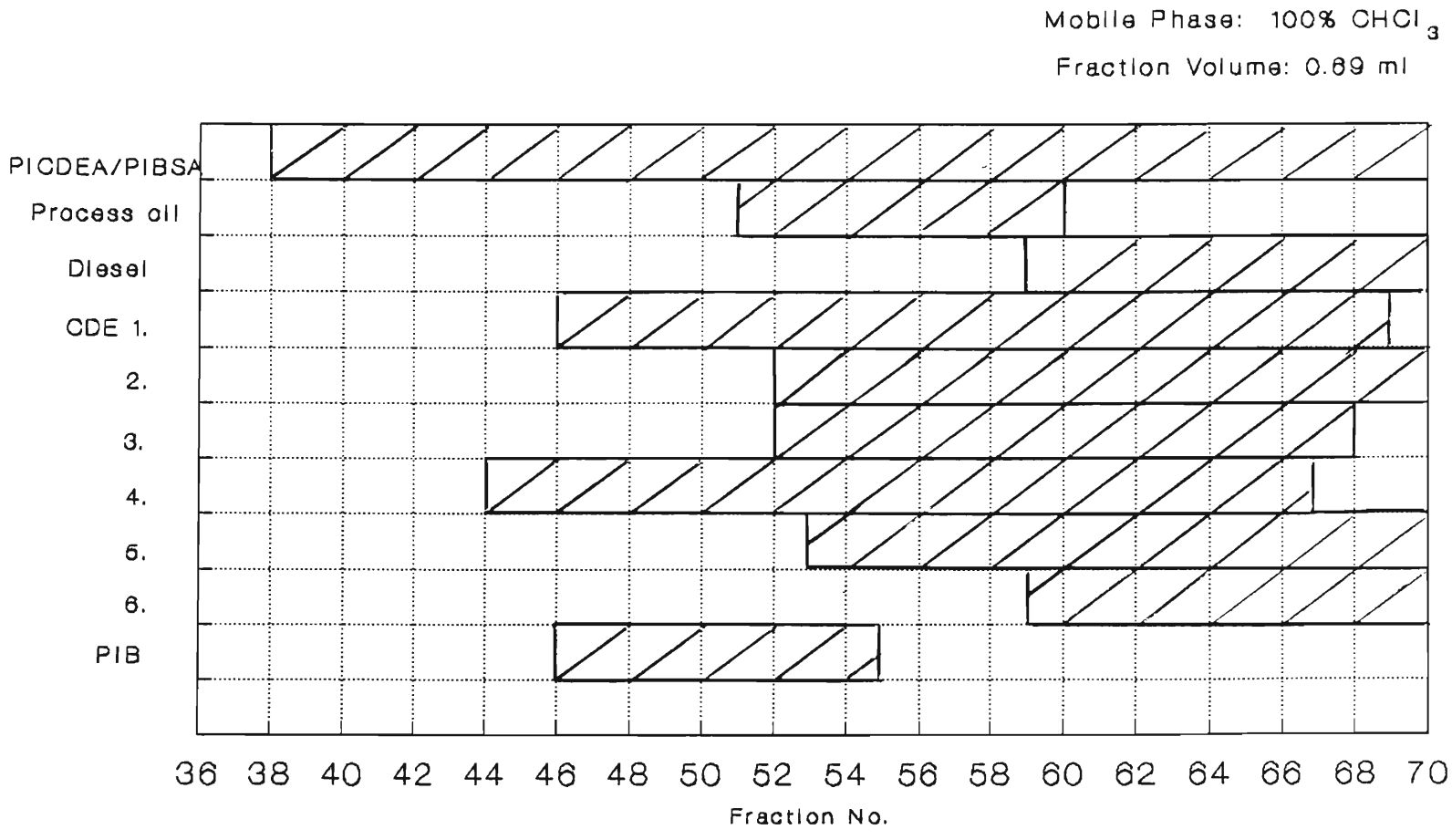

CDE component R_f values: 1 = 0.04, 2 = 0.30, 3 = 0.43, 4 = 0.52, 5 = 0.14, 6 = 0.18

Figure 47. A bar graph showing the order of elution of the components of Aktol PICDEA from a Sephadex LH-20 size exclusion column using chloroform as the mobile phase

For a separation based solely on molecular size it is essential to eliminate the adsorption of solute molecules to the gel particle surface. As already mentioned in Chapter II, Section 2.2.2.3, LH-20 has free hydroxyl and carboxyl groups which retard the migration of solutes especially when organic solvents such as chloroform are used[60]. This effect can be minimised by modifying the surface of the gel or by using a more polar solvent. Addition of a small amount of ethanol or methanol to the organic solvent blocks the polar hydroxyl and carboxyl groups and enables true size exclusion chromatography[62].

The elution sequence obtained using a 97% chloroform/3% ethanol mobile phase is illustrated in Figure (48). A total of 62 fractions were collected (fraction volume = 0.88 ml) The first traces of solute were detected in fraction 27, i.e. after the elution of approximately 23 ml of solvent. The earlier elution of solute must be due to a decrease in the adsorption of solute molecules to the gel. This is caused by the increase in solvent polarity brought about by the inclusion of ethanol.

According to the TLC results some of the CDE components (R_f values of 0.30 and 0.43) are retarded to a greater extent in the more polar solvent (Figure (48)) than in pure chloroform (Figure (47)). Although this is as predicted by Joustra[62], a study of the infra red spectra obtained for the solutes in various fractions provides some interesting results.

Figure (49) is the infra red spectrum of the solutes collected in fractions 29 to 31 using the chloroform/ethanol solvent system.

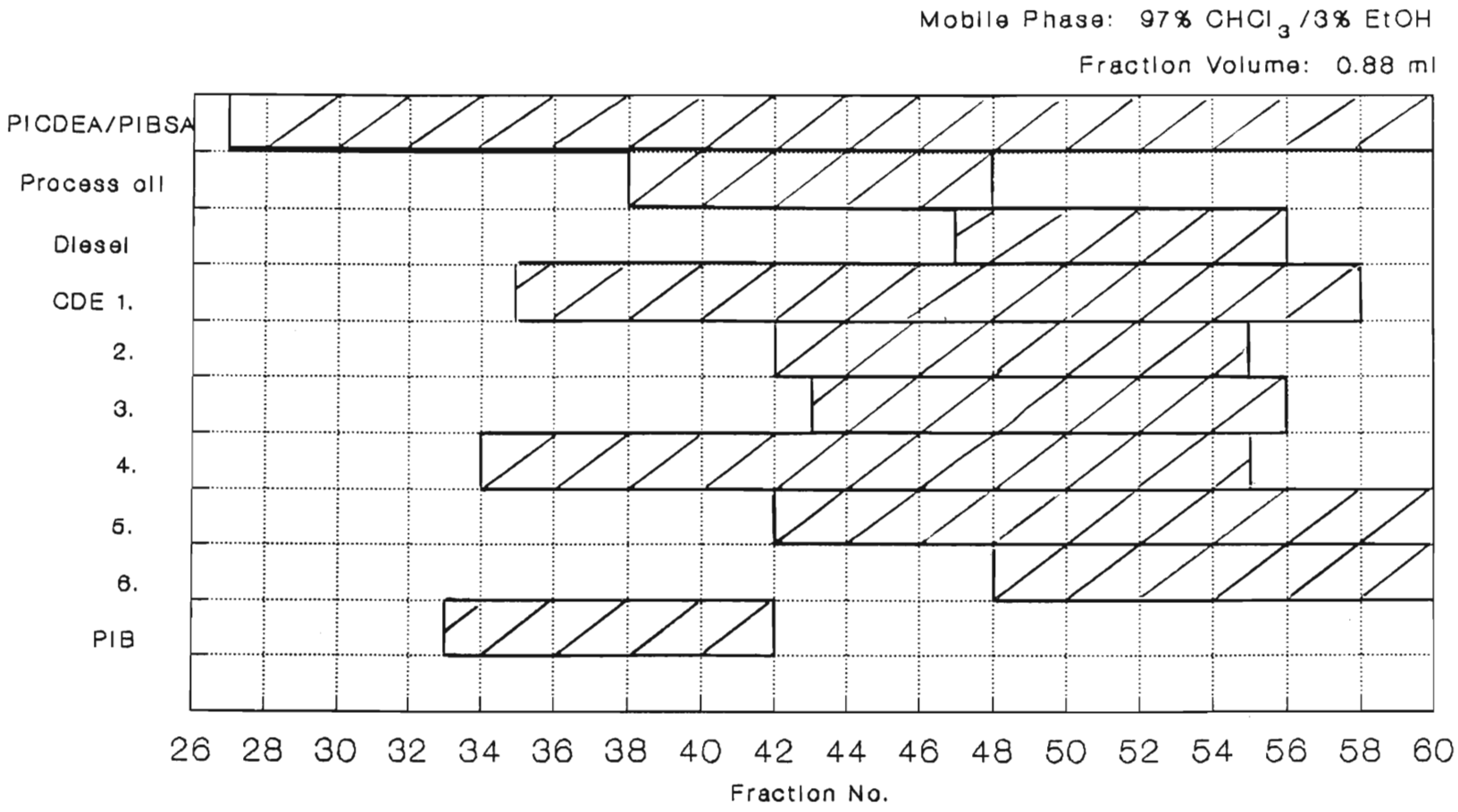

Figure 48. A bar graph showing the order of elution of the components of Aktol PICDEA from a Sephadex LH-20 size exclusion column using chloroform/ethanol (97:3) as the mobile phase

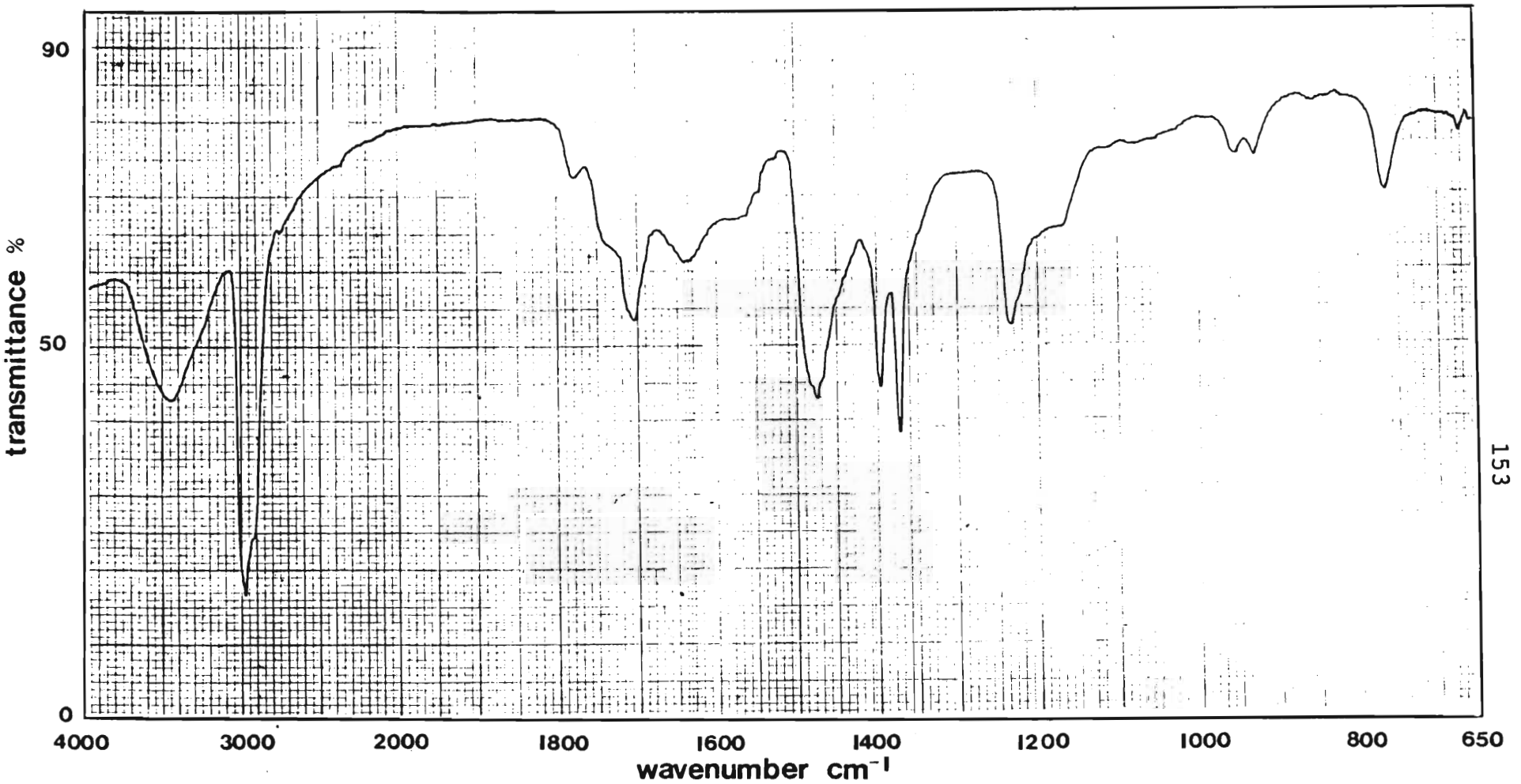

Figure 49. Infra red spectrum of the components of Aktol PICDEA eluted in fractions 29 to 31 from a Sephadex LH-20 size exclusion column using a chloroform/ethanol (97:3) mobile phase

The anhydride adsorption peak at 1780 cm^{-1} indicates the presence of PIBSA and the shoulder at 1740 cm^{-1} is due to the ester carbonyl of PICDEA. The acid carbonyl adsorption peak at 1710 cm^{-1} is proportionally larger than that produced in the infra red spectrum of 45% Aktol PICDEA in diesel displayed in Figure (39). This increased adsorption suggests that the dicarboxylic acid form of PIBSA may also be present in a higher concentration in these fractions. It is also possible that the free fatty acids present in commercial CDE (Appendix II) may also be eluted in the first fractions and thus contribute to the increased intensity of the acid carbonyl peak. However, if true size exclusion is opperative then the comparatively low molecular size of the free acids suggests that their early elution is unlikely.

The adsorption at 1640 cm^{-1} is characteristic of the amide of both PICDEA and CDE. This confirms the presence of PICDEA. TLC results showed the absence of CDE in these initial fractions and therefore it is likely that the amide peak is due to PICDEA alone.

The adsorption at 1560 cm^{-1} is characteristic of the free amine salt of diethanolamine present in Manro CDE (Appendix III). The molecular weight of the free amine is only 105 g mol^{-1} and therefore its elution in the initial fractions proves that true size exclusion chromatography has not been realised under the conditions investigated. It has been suggested by Hendrickson[100] that this phenomenon is due to the association of polar solute and polar solvent molecules.

The hydrocarbon peaks at 2950 cm^{-1} and between 1350 and 1500 cm^{-1} are proportionally smaller than those in Figure (39). This confirms that diesel and PIB hydrocarbons are absent in fractions 29 to 31 as deduced from the TLC analysis. The strong C→O→C stretching adsorption at 1235 cm^{-1} in comparison with the same peak in the spectrum for 45% Aktol PICDEA in diesel (Figure (39)) suggests that either PICDEA or PIBSA (anhydride form) or both are present in higher proportions. The characteristic CDE adsorption peak at 1060 cm^{-1} (refer to Figure (44)) due to C→N stretching is only just detectable in Figure (49). This confirms that CDE itself is more or less excluded from early elution.

The infra red spectrum shown in Figure (50) is that of the solutes collected in fractions 44 to 46. There is a large ester peak at 1740 cm^{-1} showing the presence of PICDEA. The anhydride peak at 1780 cm^{-1} also shows the presence of PIBSA. This spectrum is very similar to that of commercial Aktol PICDEA in diesel shown in Figure (39) although the free amine N-H bending vibration peak at 1540-1580 cm^{-1} is absent in Figure (50). The free secondary amine, diethanolamine, and any amine salts were probably all eluted in earlier fractions due to their association with polar solvent molecules.

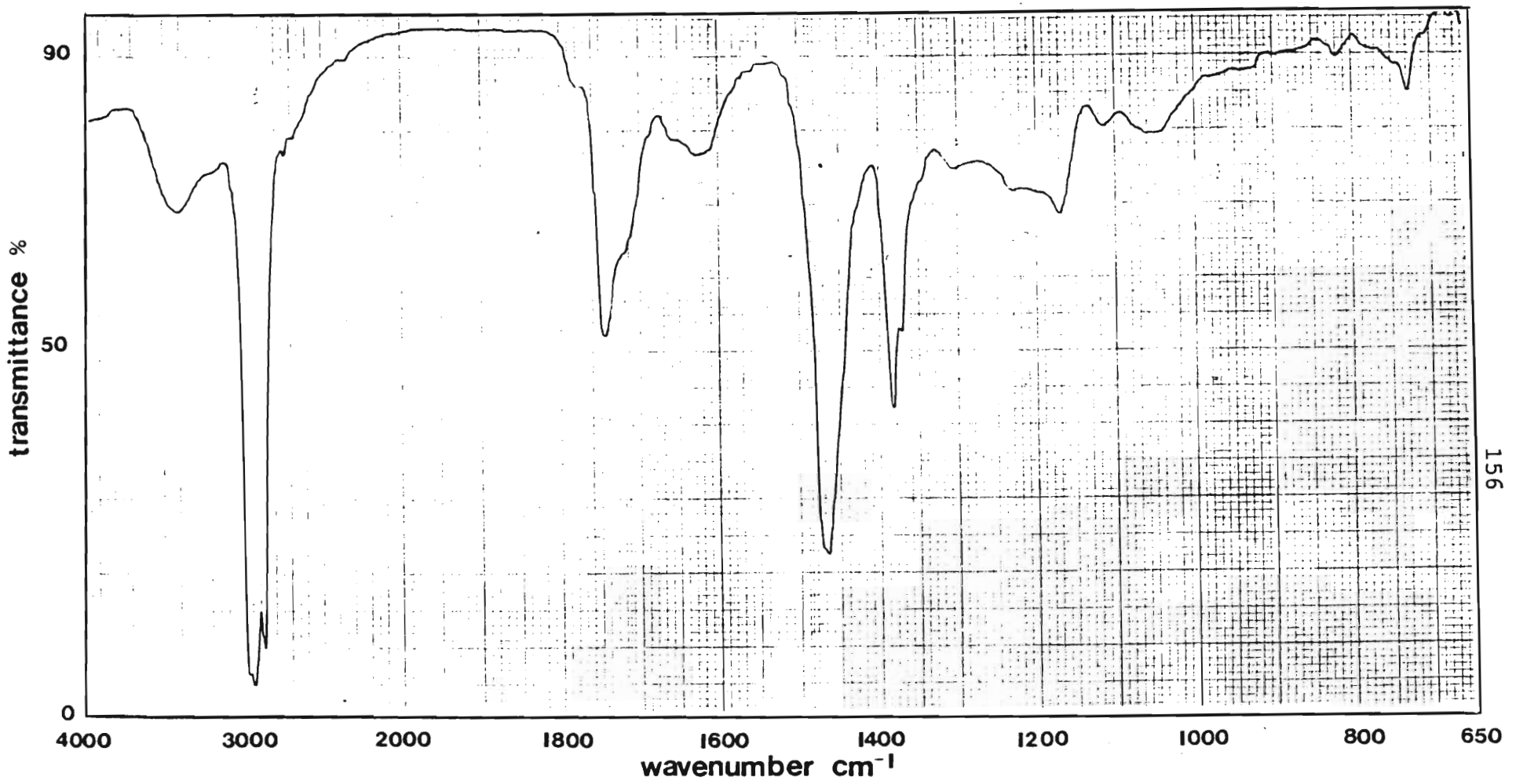

Figure 50. Infra red spectrum of the components of Aktol PICDEA eluted in fractions 44 to 46 from a Sephadex LH-20 size exclusion column using a chloroform/ehtanol (97:3) mobile phase

The infra red spectrum in Figure (51) is that of the solute collected in fractions 58 to 60. The two major peaks are characteristic of CDE as can be seen by the comparison of this spectrum with that of Manro CDE in Figure (44). The peak at 1625 cm^{-1} is due to the amide carbonyl and the peak at 1060 cm^{-1} is caused by C→N stretching. Note the absence of anhydride (1780 cm^{-1}), ester (1740 cm^{-1}), acid (1710 cm^{-1}) and free amine (1560 cm^{-1}) absorption peaks.

A suitable solvent system is yet to be found that will prevent the adsorption of the components of commercial Aktol PICDEA on to the surface of the LH-20 gel structure and at the same time prevent the accelerated elution of the smaller polar solutes such as free diethanolamine and free fatty acids. None of the solvent systems investigated were successful in providing a complete separation of the components of Aktol PICDEA which would be an essential prerequisite to a thorough qualitative study of PICDEA.

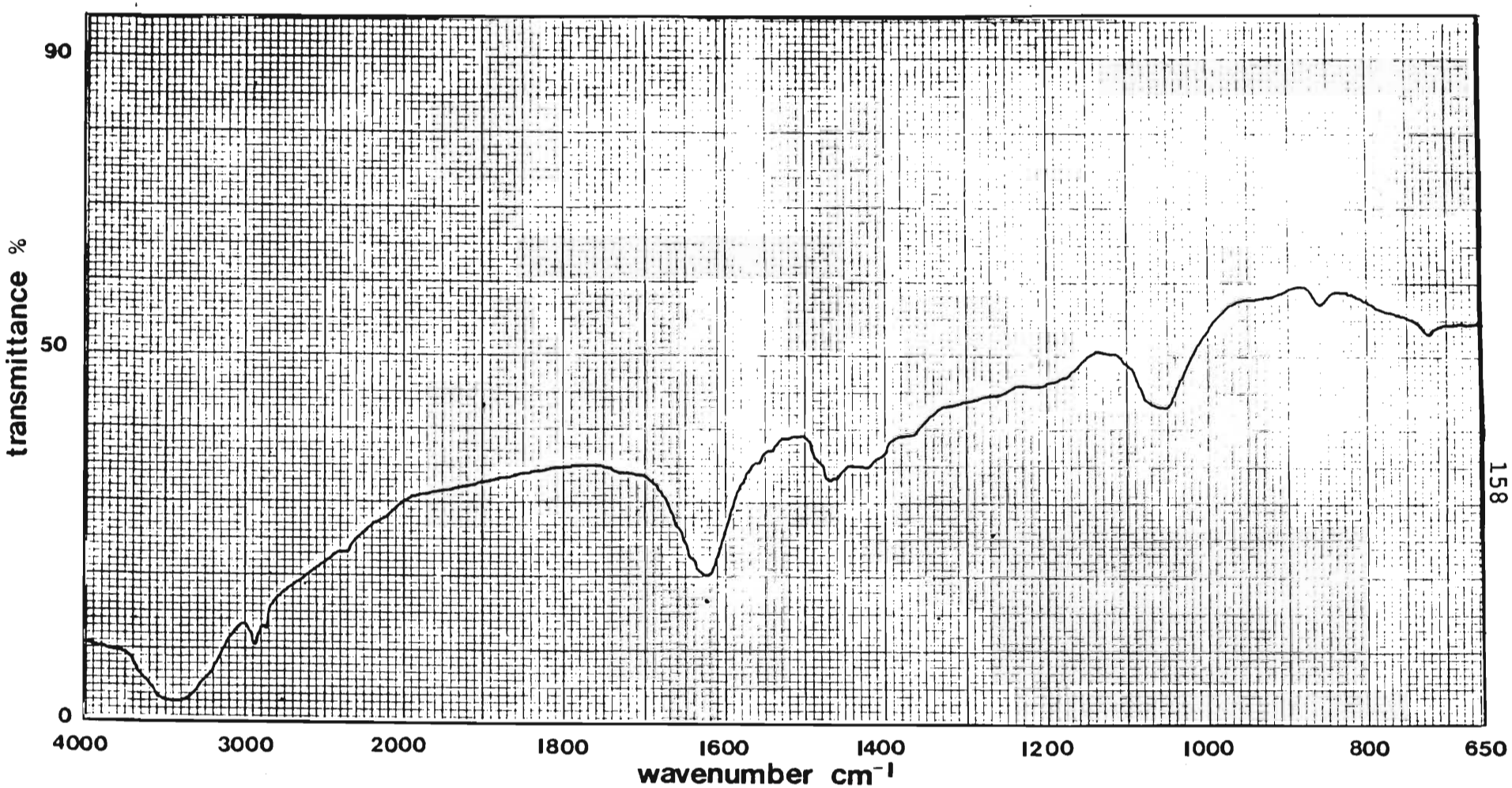

Figure 51. Infra red spectrum of the components of Aktol PICDEA eluted in fractions 58 to 60 from a Sephadex LH-20 size exclusion column using a chloroform/ethanol (97:3) mobile phase

3.3. Aqueous Droplet Coalescence

Long term stability is an essential property of emulsion explosives. Manufacturers must ensure that the product will function with the required performance after the maximum storage time. To this end the manufacturer is concerned with two major mechanisms of instability[101]: the rate of emulsion breakdown via droplet aggregation and coalescence, and heterogenous crystal nucleation of nitrate salts on dust particles. The discussion that follows is concerned with the former mechanism of emulsion breakdown involving aggregation and coalescence of droplets.

Coalescence is an undesirable property of an explosive emulsion because emulsions containing large droplets are less sensitive to detonation than those having smaller droplets. (The fuel/oxidiser reaction is slowed by the increased diffusion length[102]). Coalescence of droplets over time leads to a deterioration in detonation properties. The manufacturer's aim is therefore to produce an emulsion which experiences a minimum rate of coalescence.

The object of the investigation into droplet coalescence, described in Chapter II, Section 2.3., was to study the effect of the composition of the aqueous phase on the rate of coalescence of aqueous droplets in an emulsion stabilised with PICDEA.

3.3.1. Coagulation and Coalescence.

The breakdown of a water-in-oil emulsion is a result of the merging of water droplets to form a smaller number of larger droplets[63]. This is a two stage process[6]. During the first stage, which is either flocculation or coagulation, separated droplets approach each other and form aggregates. Flocculation is a reversible process whereas coagulation is not since coagulation involves the binding of droplets by interdroplet forces which are stronger than the forces present in flocculation. During the second stage, known as coalescence, the droplets in each aggregate combine to form single droplets.

The breakdown of the emulsion can either be simple or complex depending on the number of droplets in an aggregate and whether aggregates are formed via flocculation or coagulation. The simplest breakdown pathway assumes irreversibility (i.e. coagulation) of aggregate formation and considers the coagulation and coalescence of two droplets. A schematic representation of this process is illustrated in Figure (52)[6].

Figure 52. The coagulation and coalescence of two droplets

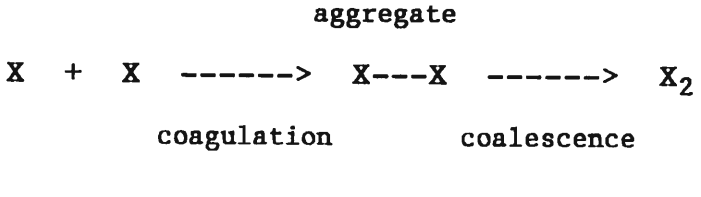

X: droplet

As can be seen from Figure (52), in order to study the process of coalescence separately from coagulation it becomes necessary to take account of the contribution of coagulation to the overall rate of emulsion breakdown.

Smoluchowski's theory[103] predicts that the rate of coagulation is proportional to the square of the droplet concentration and therefore

$$-\frac{dn}{dt} = an^2 \qquad (17)$$

or, in integrated form,

$$\frac{1}{n} - \frac{1}{n_o} = at \qquad (18)$$

where a = the rate constant, i.e. the frequency of collisions between droplets which result in coagulation

t = time

n = the number of droplets per unit volume at time = t involved in coagulation

n_o = the number of droplets at t = 0

Van den Tempel[63] used a number of approximations in order to determine an expression for the rate of droplet coalescence once coagulation had occurred. He assumed that in a coagulated emulsion, if p is the number of contact points per droplet then each droplet in an aggregate is in contact with an average of 2p other droplets. Thus the total number of contact points is $pn\ dm^{-3}$ for an emulsion which at time t contains n droplets per dm^3. Rupture of the separating film between

droplets at the contact point results in immediate coalescence. The probability of rupture is therefore the rate determining constant for coalescence, k. Van den Temple also assumed that the coalescence of two contacting droplets does not affect the stability of neighbouring contact points. Therefore the breakdown pathway which his approach describes is that illustrated in Figure (52).

The number of contact points breaking per dm^3 will be determined by

$$- \frac{d(pn)}{dt} = k.pn \qquad (19)$$

or, in integrated form after applying the assumptions stated below,

$$n = n_o \exp(-kt) \qquad (20)$$

where k = the rate constant for coalescence
p = the number of contact points
n, n_o and t are the same as previously defined

In deriving Equation (19) Van den Tempel also assumed that the average number of contact points per droplet (2p) remains constant during emulsion breakdown. This can only be true if the aggregates consist of a large number of droplets. Equation (20) shows that the rate constant for coalescence, k, is dependent on the average lifetime of the film separating the two coagulated droplets. Van den Temple points out that the rate of coalescence is simply determined from the experimental determination of the droplet concentration, n, as a

function of time, provided that all droplets are coagulated in a time which is short compared with the time in which an appreciable amount of coalescence occurs.

From Equation (20) it can be seen that the time necessary to combine half the droplets into aggregates is $(an_o)^{-1}$. On the other hand, about half the coagulated droplets will have coalesced after a time k^{-1}. The relative rates of coagulation and coalescence can therefore be determined by the ratio an_o/k.

If $an_o/k << 1$ coalescence will occur immediately after two droplets have made contact in an aggregate. Coagulation will therefore be the rate determining process and emulsion breakdown will be a second order reaction. If $an_o/k >> 1$, coagulation occurs more rapidly than coalescence and the overall rate is determined almost entirely by coalescence. In this case emulsion breakdown is a first order process. If $an_o \approx k$, the order of the reaction will be between 1 and 2.

Van den Tempel shows that the steady state rate of coagulation is about the same as the rate of coalescence at a concentration of approximately 10^9 droplets per dm^3. (Carrol[6] reports this value as being 10^{10} droplets per dm^3). Concentrations higher than this, i.e. > 10^{10} droplets per dm^3, result in a relatively rapid rate of coagulation and consequently coalescence becomes the rate determining step. Thus emulsions with droplet concentrations below 10^9 droplets per dm^3 can be expected to follow coagulation controlled breakdown kinetics.

All the emulsion systems investigated in this work were found to have droplet concentrations of 10^{11} to 10^{12} droplets per dm^3. Coagulation is therefore rapid and droplet coalescence will be the major process responsible for emulsion stability.

At this stage it is appropriate to define the limits of droplet coalescence. Although the literature offers a number of definitions[104, 105], the following definition by Carrol[7] is the only one which clearly defines the point at which coagulation ends and coalescence begins: Coalescence begins when two droplets have approached each other to a "separation corresponding to the potential energy maximum". During the onset of coalescence they tend to "draw together under the influence of the Van der Waals attractive forces until short range repulsive forces become dominant".

The following section will describe the origins of this potential energy barrier commonly referred to as the DLVO theory[106, 107].

3.3.2. DLVO Theory: Application to Oil-in-Water and Water-in-Oil Emulsions

In a water continuous emulsion, ionization of material at the interface or adsorption of free ions generally causes all of the droplets to possess an electrical double layer[108]. Overlapping of the double layers of neighbouring droplets results in a nett repulsive force, V_R.

Repulsive interactions between two such droplets whose centres are at a distance of r = x + 2a apart are given by Derjaguin's approximate expression[109]:

$$V_R = \frac{2\pi 10^{-2}}{9} \varepsilon\varepsilon_o a\psi_o^2 \ln[1 + \exp(-\kappa x)] \qquad (21)$$

where ϵ = dielectric constant of the continuous phase

ϵ_o = dielectric constant of the dispersed phase

a = radius of the particle

ψ_o = potential energy of the particle

κ = reciprocal of the double layer thickness[110]

x = particle separation

The Van der Waals' dispersion force[107, 111] is expressed as:

$$V_A = \frac{-Aa}{12x} \qquad (22)$$

where A = the Hamaker constant[111, 112]

x and a are the same as previously defined.

Combining the electrical double layer repulsive force with the attractive force due to Van der Waals' interaction gives the nett interaction energy between two particles. Both V_A and V_R are a function of the separation of the particles. The basic features of the total interaction ($V_R + V_A = V$) are shown in Figure (53)[107] which depicts the quantities V_R (curve

A), V_A (curve B) and $V = V_R + V_A$ (curve C). Curve C shows a nett repulsion between particles over certain particle separations[111] and so leads to the retardation of aggregation.

Figure 53. Schematic potential energy curves. Curve A: V_R, repulsive energy; Curve B: V_A, attractive energy; Curve C: V, nett interaction energy; and V_{max} is the potential energy barrier against coagulation.

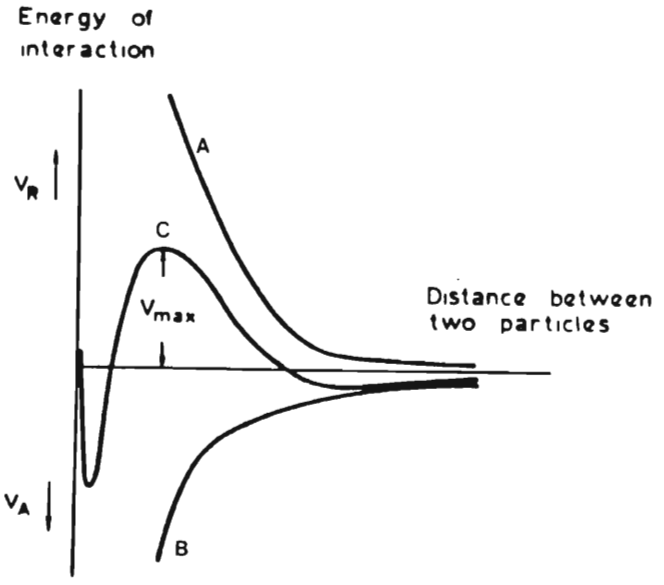

In water continuous emulsions the thickness of the double layer (κ^{-1}) is of the order of 10^{-3} - 10^{-2} μm[113], thus electrostatic interactions only take place at very short distances. Oil droplets at separation distances of several times the double layer thickness therefore have an interaction potential energy of approximately zero. For coagulation to occur the coagulating droplets have to overcome the whole potential energy barrier.

In order to assess the significance of the electrostatic potential energy barrier in terms of the possible prevention of coagulation, some estimate should be made concerning the size of the charges on surfactant stabilised water droplets in a water-in-oil emulsion. According to Schulman and Cockbain[114] water droplets in an oil continuous phase have no charge. However, Bhatnagor[115] reported measurable current flow through water-in-oil emulsions and in 1933 Fuoss and Kraus[116] demonstrated that ionisation takes place in non-polar liquids. Albers and Overbeek[117a] were also able to show that the double layer in an oil continuous system has considerable extension. In oil continuous systems the double layer may be several microns thick, i.e. of the order of magnitude of the droplet separation in a moderately concentrated emulsion. Thus two noncoagulated droplets already possess an appreciable repulsive energy at large separations and the effective barrier to coagulation is lowered.

Albers and Overbeek[117b] also determined an expression for V_R, the repulsive potential energy between a single droplet and its twelve nearest neighbours. This takes

into account the resulting coagulation if a collision were to take place causing one of the twelve droplets to come into close proximity with the central droplet. Figure (54)[117b] shows the percentage lowering of the potential barrier, as determined by Albers and Overbeek, for coagulation in concentrated emulsions as a function of the phase volume of the dispersed phase, ϕ, and of the thickness of the double layer κ^{-1}, for a drop radius of 1 μm.

Figure 54. The lowering of the energy barrier for coagulation in concentrated w/o emulsions expressed in per cent of the energy barrier in an infinitely dilute emulsion, as a function of, Φ, the phase volume, and κ, the inverse of the double layer thickness. Drop radius is taken as 1 μm.

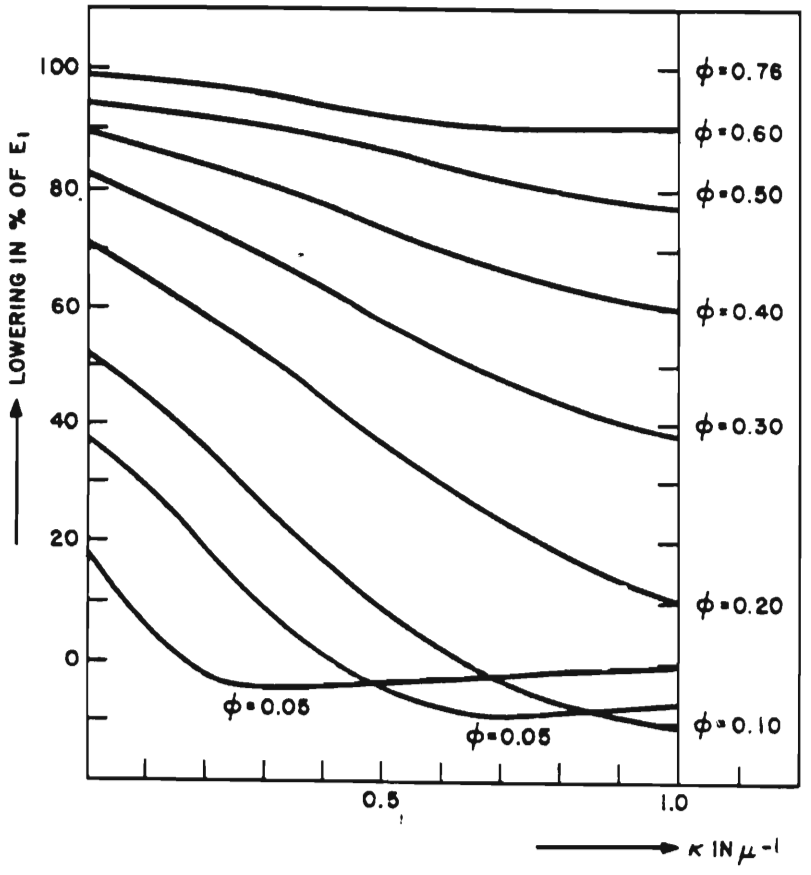

The emulsions studied in this work are high internal phase emulsions with $\phi = 0.85$. It is therefore reasonable to expect that the effect illustrated in Figure (54) will be enormous. The potential barrier will be very small and will have little effect in preventing droplet coagulation.

The discussion in this and the previous sections is an accumulation of evidence which supports the assumption that the stability of the high internal phase, concentrated water-in-oil emulsions studied in this work is not caused by the retardation of droplet aggregation by a potential energy barrier such as that illustrated in Figure (53), but rather by an energy barrier to coalescence. Coalescence is therefore taken to be the rate determining step in the overall breakdown of the water-in-oil emulsions investigated. (Inter alia, this is supported by the experimentally observed first order nature of the rate of droplet coalescence). The following section will discuss the origins of the energy barrier against coalescence.

3.3.3. Droplet Stability against Coalescence

Taking into account the discussion above it seems reasonable to assume that the stability of aqueous droplets against coalescence resides in the structural properties of the adsorbed interfacial layer. Coalescence is most likely retarded by the repulsive energies of interaction which arise from the loss of configurational entropy originating during the interpenetration of the hydrocarbon chains of adsorbed

molecules[64]. The detailed explanation of the mechanism of interpenetration is complex[118] but a few models have been postulated[119,120,121]. Due to their complexity these models are not discussed in this thesis.

According to Elworthy et al.[64] entropic repulsive forces become operative when the particles have approached to a distance equal to twice the thickness of the adsorbed surfactant layer. The hydrocarbon chains of PICDEA and E-70 originating from PIBSA extend into the oil phase by approximately 40-60 Å. Interpenetration of hydrocarbon chains between approaching droplets will therefore occur at a separation of about 120 Å. At this separation entropic repulsive forces will begin to retard the process of coalescence. This figure is in agreement with the findings of Derjaguin[122] and Israelachvili[123] who conclude that steric (or adsorption) and structural forces between droplets are effective over a distance of 100 Å.

Elworthy et al.[64] were able to derive an expression for V_{RS}, the entropic repulsive energy between droplets, and concluded that an increase in the thickness of the adsorbed layer causes an increase in V_{RS}. This is equivalent to increasing the length of the hydrocarbon chain. On addition of V_{RS} and V_A (the attractive forces due to Van der Waals interaction), the nett interaction curve predicted a higher degree of stability to coalescence. Shinoda et al.[124] were also able to show that the stability of water-in-oil emulsions increases rapidly with the molecular size of the emulsifier.

It is appropriate at this stage to refer to the discussion on interfacial tensions, specifically Sections 3.1.2.4. and 3.1.2.5. It was observed that interfacial free energy decreased more in the presence of the shorter hydrocarbon chain Adibis based surfactant molecules (both E-70 and PICDEA) than those based on Aktol PIBSA. According to basic emulsion theory[125] it is accepted that the lower the interfacial free energy the greater the thermodynamic stability of the emulsion. However, the findings of Elworthy, Shinoda and their co-workers suggest that in spite of their greater interfacial free energy the longer Aktol based molecules will be more efficient at retarding the process of coalescence than shorter Adibis molecules and hence form a more stable emulsion. These views on emulsion stability appear to contradict each other. Garti and Katz[126], however, made the following observation: Changes in interfacial tension in separated and emulsified oil-water systems do not correlate. In fact, the authors found that they change in opposite directions. If this applies to the systems studied in this work then the views above are not contradictory. Garti and Katz conclude that surfactant adsorption rather than interfacial tension should be studied in order to obtain a fundamental tool for estimating emulsion stability. The effects of different nitrate salts on the orientation and nature of PICDEA and E-70 molecules at the oil/water interface, rather than the interfacial tension of the interface (Sections 3.1.2.2. to 3.1.3.3.), should be considered in the interpretation of coalescence data.

3.3.4. The Analysis of the Change in Droplet Concentration as a Function of Time and Aqueous Droplet Composition

For the purpose of this discussion six emulsion samples will be analyzed in detail. From each of the Na^{+}, Ca^{2+} and Fe^{3+} emulsion series, those with the following aqueous nitrate concentrations were investigated: 2M, 0.8M and 0.4M. The remaining four 2M calcium nitrate emulsions which received differing degrees of mixing during emulsification are also included in this group. Each of these emulsions was stabilized with 2% (v/v) PICDEA and contained an 85 % dispersed aqueous phase. Appendix IV contains tables of droplet concentration distributions for all of the emulsions prepared. Calculations and conclusions made in the sections that follow are based on the data provided in these tables.

Sections 3.3.4.1. and 3.3.4.2. will discuss droplet size distributions. Section 3.3.4.3. will describe and attempt to explain the rapid and slow consecutive rates of droplet coalescence observed in the systems investigated. Section 3.3.4.4. explains how rate constants and coalescence rates were calculated and the remaining sections (Sections 3.3.4.5. to 3.3.4.7.) will discuss the experimental data.

3.3.4.1. Droplet Size Distributions

One of the most important aspects in the characterization of emulsions is the determination of the size distribution of the emulsion droplets. The detonation properties and stability of an explosive emulsion are largely dependent on the structure, i.e. the droplet size distribution, of the emulsion[127]. The shape of the droplet distribution is important; Muller[128] showed that the rate of coagulation can increase by up to 50% with asymmetrical droplet distribution whilst increases of only 15 % were observed with symmetrical distribution. Evidently an essentially monodisperse emulsion with a symmetrical distribution should be more stable than an asymmetrically distributed emulsion.

In the experimental section (Chapter II, Section 2.2.3.2.3.) it was explained that a conversion must be applied to the data collected from the two-dimensional photomicrographic image in order to obtain the droplet concentration of each range of particle sizes present in the sample. The conversion factor derived by Jokela et al.[69] has been applied to the droplet distribution data collected.

The conversion is performed as follows: The effective observation depth for each particle size interval was determined using the expression:

$$D_o = 2.5 D_f \qquad (23)$$

where D_f = the recorded diameter in focus

D_o = the effective observation depth

D_f was taken as the average diameter over each individual interval range, i.e. for the range 5.1 to 10 μm, D_f has a value of 7.6 μm and therefore for this interval D_o is 19μm.

V_o, the effective observation volume, was determined by multiplying D_o by the measuring frame area which was 6400 μm^2. For the interval 5.1 to 10 μm, v_o is 12.2×10^4 μm^3. Division of the number of droplets in the 6400 μm^2 measuring frame, that fall in this size interval, by V_o gives the droplet concentration.

Total droplet concentration can then be determined simply by adding the droplet concentrations obtained for each droplet size interval.

The effect of the conversion factor is clearly seen in Figure (55). Figure (55a) is a histogram showing percentage droplet distribution per unit area for a 2M calcium nitrate emulsion whilst Figure (55b) shows the percentage distribution of droplet concentration for the same emulsion system. There is a notable shift towards

smaller droplet diameters. Jokela et al.[69] observed a similar effect which they demonstrated to be a more accurate representation of the true droplet distribution by obtaining good agreement with droplet distribution data collected using laser diffraction and Coulter Counter techniques on identical emulsions.

3.3.4.2. Emulsification Time and Droplet Size Distribution

An increase in emulsification time leads to a reduction in the average droplet size[130], which is accompanied by a change in droplet distribution. Table (18) lists the initial percentage droplet concentration distributions for the five 2 M calcium nitrate emulsions as a function of emulsification time. As expected, an increase in emulsification time, beyond the minimum time required to produce the emulsion, caused a decrease in average droplet size, i.e. droplet distribution shifted to smaller droplet sizes. This was accompanied by an increase in initial droplet concentration, n_o.

The effect of increased mixing time on droplet distribution in an explosive emulsion was illustrated by Bampfield and Cooper[131]. This illustration is duplicated in Figure (56) from which it can be seen that increased mixing results in significant changes in the distribution of droplets with diameters less than 5 μm. A similar distribution was not obtained in this investigation. The photomicrographic analysis technique used in this work does not enable one to detect changes in droplet distribution below droplet diameters of approximately 5 μm.

Figure 55a. The percentage size distribution of droplet numbers for a 2M calcium nitrate w/o emulsion stabilized by PICDEA

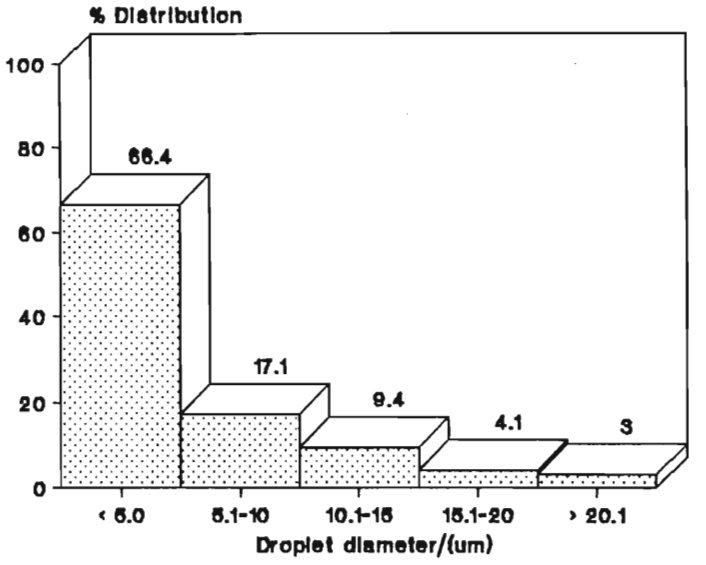

Figure 55b. The percentage size distribution of droplet concentration determined for a 2M calcium nitrate w/o emulsion stabilized by PICDEA

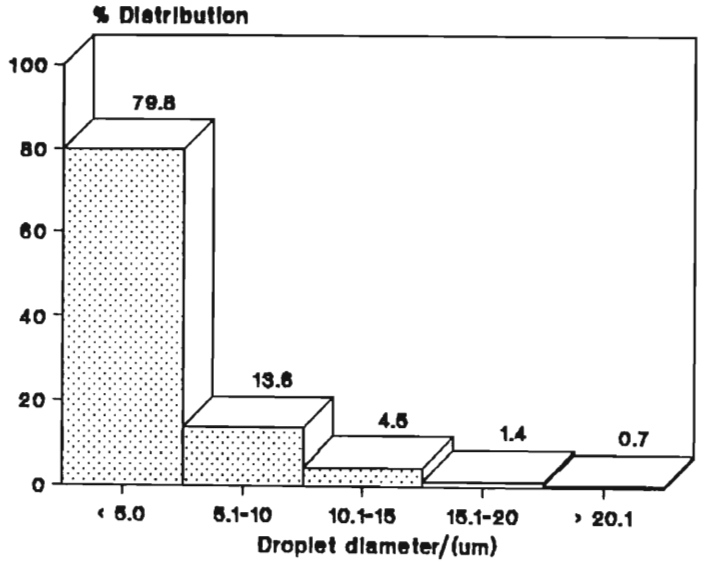

Table 18 . Initial droplet size distribution as a function of emulsification time for a series of 2M calcium nitrate emulsions

EMULSIFICATION TIME	% DROPLET SIZE DISTRIBUTION					TOTAL $n_o x\ 10^{12}$ /droplets dm^{-3}
	< 5μm	5.1-10.0μm	10.1-15.0μm	15.1-20.0μm	> 20.1μm	
Minimum time	77.54	18.36	3.26	0.67	0.17	4.275
1 minute	78.82	16.59	3.85	0.63	0.11	4.521
5 minutes	90.66	8.10	1.08	0.14	0.02	7.859
10 minutes	95.73	3.89	0.38	/	/	10.613
15 minutes	98.30	1.70	/	/	/	12.167

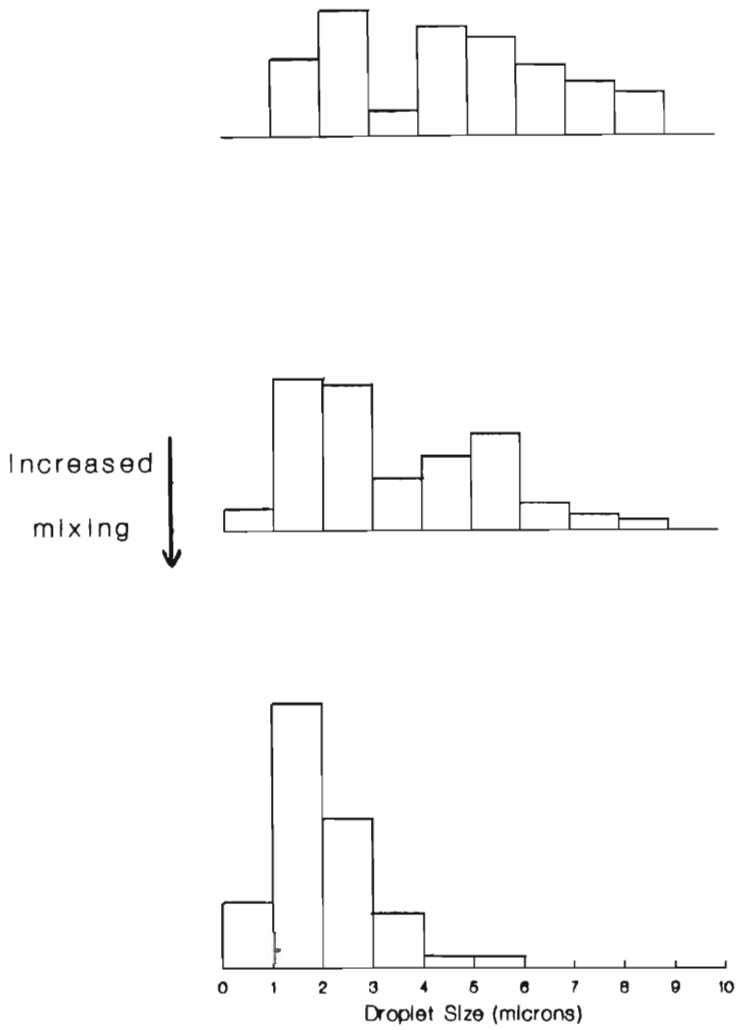

Figure 56. The effect of an increase in the time of emulsification on the droplet size distribution in an explosive emulsion[131]

With the use of computerized image analysis Jokela et al.[69] were able to divide their data into small droplet intervals as their computer software was able to distinguish between droplets with diameters less than 1 μm. In this work, however, droplets were counted manually from photomicrographs (magnification ranging between 520 and 755x) and it was therefore impossible to distinguish between droplets with diameters of less than 5 μm without introducing excessive error.

The limitations of this technique prevented the acquisition of a more detailed droplet distribution and consequently no conclusions can be made in this work as to the complete effect of prolonged emulsification on droplet distribution or the effect of different nitrate salts on the symmetry of initial droplet distribution. However, the effect of nitrate salts on initial droplet concentration and droplet coalescence rates will be discussed in Sections 3.3.4.5. to 3.3.4.7.

3.2.3.3. Rapid and Slow Consecutive Rates of Droplet Coalescence

It was concluded in Sections 3.3.1. and 3.3.2. that a highly concentrated water-in-oil emulsion is likely to follow first order reaction breakdown kinetics due to the rate determining coalescence of coagulated droplets.

The concentration of droplets, n, at any time, t, can be determined using Equation (20)[63].

$$n = n_o \exp(-kt) \qquad (20)$$

where n_0 and k are the same as previously defined. (Section 3.2.1.)

Differentiation and reorganisation of this equation gives the rate constant of coalescence:

$$k = -\frac{d\ln n}{dt} \qquad (24)$$

k can then be determined from the slope of the ln n versus t curve[63] which is expected to give a straight line of negative gradient.

Figure (57) is a plot of the natural log of total droplet concentration (ln n) versus time (in days) for the No. 4, 2M calcium nitrate emulsion. Emulsion No. 4 was emulsified for an additional 15 minutes over and above the minimum emulsification time. This emulsion was chosen to illustrate the following discussion because of

its high initial droplet concentration and pronounced changes in droplet distribution. On inspection of the plot in Figure (57) it can be seen that the rate of emulsion breakdown can be described by two rate constants. Initially, over a period of 28 to 36 days, there is a relatively rapid rate of droplet coalescence. The second rate, lasting for the remaining period, is slow and appears to be a function of the long term stability of the emulsion.

Table (19) shows the change in percentage droplet distribution and total droplet concentration as a function of time for the same No. 4 2M calcium nitrate emulsion. A thorough analysis of the data enables one to conclude that the initial rapid rate of coalescence is due to the coalescence of very small droplets with diameters of 5 μm and less. 16.5% of these small droplets disappear due to coalescence in the first 28 days. During the last 90 days both small and large droplets experience a slower rate of coalescence suggesting that the droplet distribution has reached a more favourable symmetry conducive to the stability of this emulsion system.

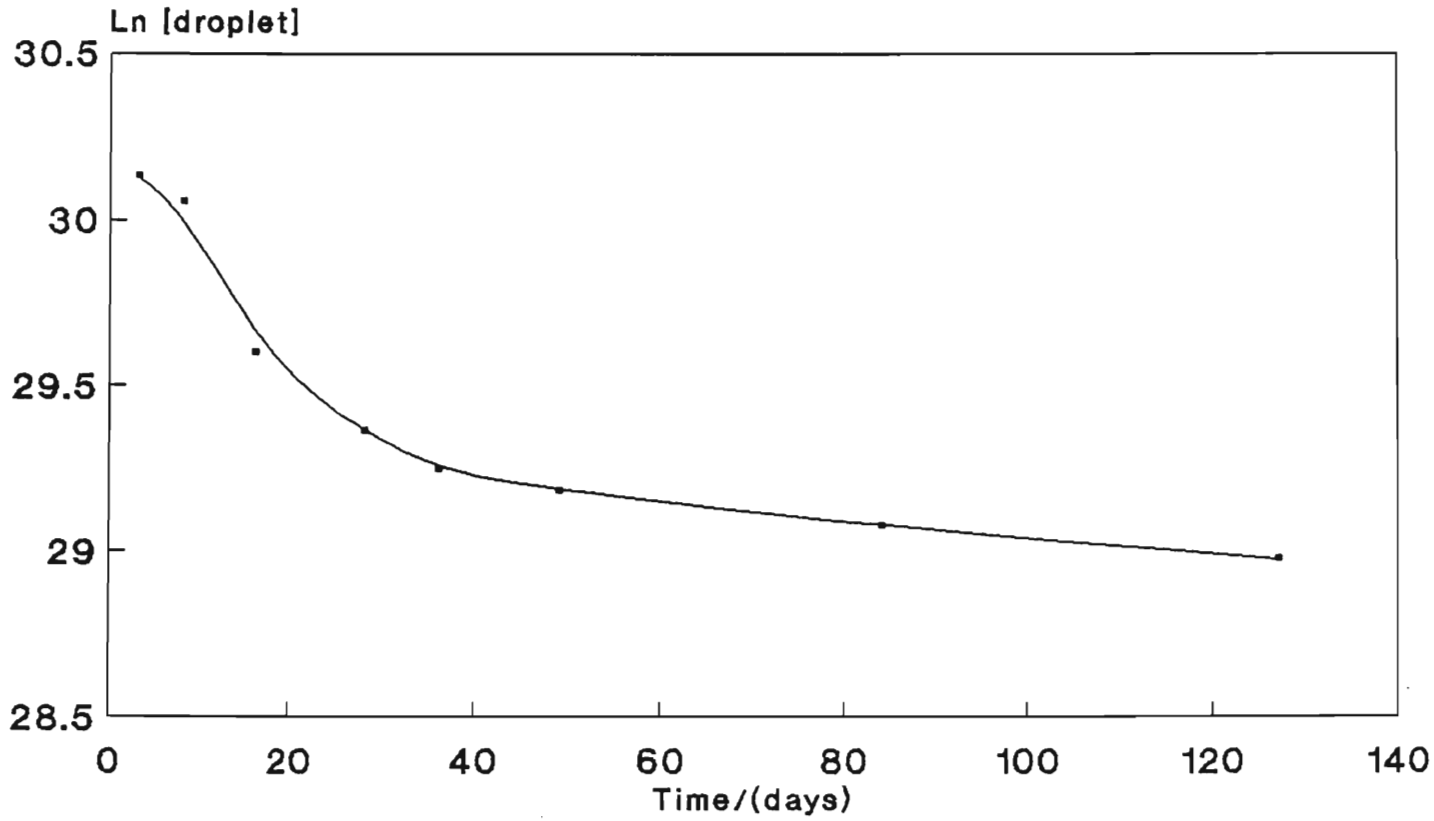

Figure 57. A plot of the natural log of total droplet concentration as a function of time for the No. 4, 2M $Ca(NO_3)_2$ emulsion

Table 19. The change in droplet distribution as a function of time for the No. 4, 2M calcium nitrate emulsion

DAYS	% DROPLET SIZE DISTRIBUTION					TOTAL n_o /x 10^{-12} Droplets dm^{-3}
	< 5.0 µm	5.1-10.0 µm	10.1-15.0 µm	15.1-20.0 µm	> 20.1 µm	
3	98.30	1.70	/	/	/	12.167
8	96.00	3.89	0.11	/	/	11.260
16	88.12	11.07	0.63	0.15	0.03	7.164
28	81.80	16.06	1.67	0.38	0.09	5.655
36	75.32	22.01	2.08	0.50	0.09	5.029
49	74.97	21.18	2.54	0.58	0.13	4.702
84	73.35	21.53	4.23	0.72	0.17	4.233

These observations suggest that coalescence may be following two or more consecutive first order reactions. The following reaction mechanism is proposed:

$$A + A \xrightarrow{k_4} A\text{-}A \xrightarrow{k_1} B$$
$$A + B \xrightarrow{k_5} A\text{-}B \xrightarrow{k_2} B'$$
$$B + B \xrightarrow{k_6} B\text{-}B \xrightarrow{k_3} B''$$

where k_4, k_5 and k_6 are second order diffusion controlled rate constants for droplet coagulation. They are considered to be equal and non rate determining.

k_1 is the initial rate constant for the coalescence of small droplets.

k_2 and k_3 are rate constants for coalescence involving at least one large droplet.

A refers to small droplets with diameters < 5 μm

B refers to droplets with diameters of 5.1 - 10 μm.

B′ and B″ refer to droplets with diameters progressively larger than 10 μm.

This description is an approximation. More detailed distribution data may have resulted in different size limits for A and B droplets.

A first order reaction is dependent on the reactant concentration. The rate of coalescence is determined using the following rate expression[132]:

$$K = -\frac{dx}{dt} = k[x]_o \qquad (25)$$

where K = the rate of coalescence (mol dm^{-3} s^{-1}).

x = the reactant concentration (mol dm^{-3})

$[x]_o$ = the initial concentration of x (mol dm^{-3})

k = the rate determining constant (s^{-1}).

From the initial percentage droplet distribution in Table (19) the concentration of A droplets is 98.3 % of the total initial droplet concentration whereas the concentration of B droplets is only 1.7 % of the total.

Therefore $K_1 >> K_2$ because $[A]_o >> [B]_o$ and $k_1 >> k_2$ (from the gradients of the plot of ln n versus time in Figure (57)). As A droplets coalesce the concentration of B droplets increases until a point is reached when the rate at which A produces B slows down, i.e. K_1 decreases and the rate of coalescence of B droplets, K_2, increases. During the last 90 days the concentration of B decreases as B′ and B″ droplets appear due to a slow coalescence determined by the rate constants k_2 and k_3.

Considering the proposed mechanism one would expect A droplets to continue to coalesce at a rapid rate for longer than was observed experimentally, since their concentration is still relatively high after the initial 28 to 36 days, i.e. 75.3 % of the total concentration. However, droplet concentration does not take into account the fact that B droplets are on average twice as big as A droplets and therefore occupy a larger volume in the

emulsion. A more realistic representation of the relative "amounts" of A and B droplets in the emulsion at any particular time would be to determine the ratio of their accumulative volumes. If the volume occupied by A droplets is less than that occupied by B droplets then the observed reduction in K_1 can be explained. This is, in fact, the case since after 36 days this ratio (V_A/V_B) is equal to 0.873, i.e. $V_B > V_A$.

When the concentration of B droplets has increased sufficiently so that they occupy more space than the A droplets (i.e. $V_B > V_A$) they become effective in separating the A droplets thereby reducing the probability of A droplet coalescence. The photomicrographs displayed in Figure (58) illustrate this point. Photomicrograph I shows the initial droplet distribution for the No. 4, 2M calcium nitrate emulsion. Note that the droplets appear to be essentially monodisperse, as indicated by the droplet distribution data in Table (19). Each A droplet is surrounded by numerous other A droplets. Photomicrograph II, on the other hand, shows the droplet distribution after 36 days. The essentially monodisperse distribution of small A droplets has been replaced by a mixture of larger B and B′ droplets and fewer small A droplets. The A droplets appear to have fewer A droplet neighbours and many A droplets have been replaced by a smaller number of larger B droplets. Note also that the A droplets tend to pack between the B droplets thus separating them. This distribution reduces the chances of two A or B droplets coalescing which would account for the observed change in the coalescence rate.

Figure 58. Photomicrographs of the No. 4, 2M calcium nitrate emulsion

Photomicrograph I: Initial droplet distribution (612 x mag)

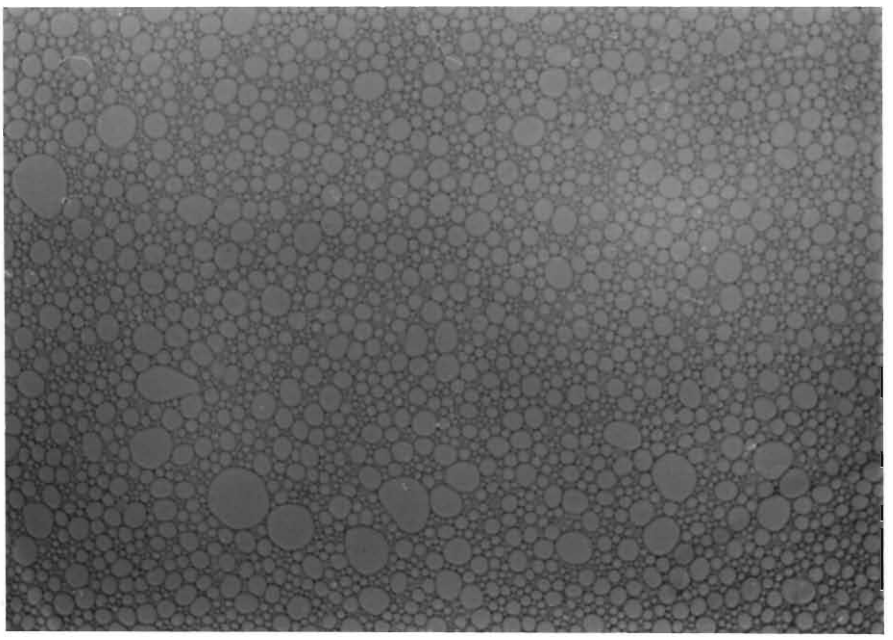

Photomicrograph II: Droplet distribution after 36 days (522 x mag)

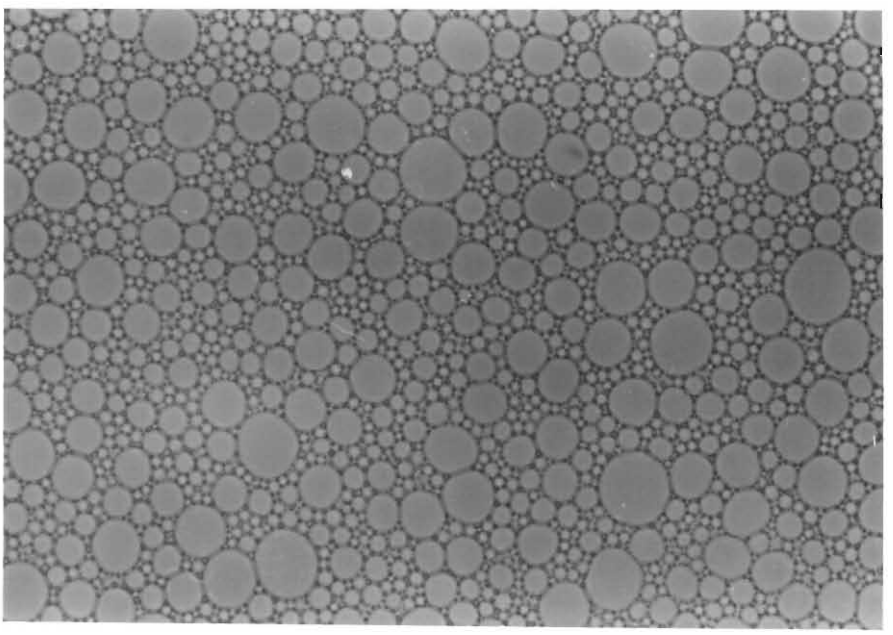

This does not, however, explain why B droplets should coalesce at a slower rate than A droplets. It is probable that this is partially related to the internal Laplace pressure of the droplets. Laplace showed that the total pressure inside a gas bubble is dependent on the radius of curvature[133], i.e.

$$\Delta P = \frac{2\gamma}{r} \qquad (26)$$

where $\Delta P = P_g + P_l$ where P_g is the pressure of gas inside the bubble

P_l is the pressure in the liquid outside the bubble

γ = surface tension of the gas-liquid interface

r = the radius of curvature of the bubble

Therefore B droplets have a lower internal Laplace pressure than the smaller A droplets. Although this may be one factor which contributes to the slower coalescence involving B type droplets, there must be some change in the structure of the interface as droplet size increases which would account for the larger energy barrier against coalescence in B droplets. The effect of droplet radius on the orientation of adsorbed surfactant molecules will be discussed in Section 3.3.4.6.

3.3.4.4. Determination of the Rate Constants, k_1 and k_2, and Rates of Droplet Coalescence, K_1 and K_2.

Application of linear regression analysis to the total droplet concentrations determined at various time intervals during the last 90 days, i.e. from 36 days onwards, provided values for a and b from the linear equation, $y = bx + a$, where a is the y intercept and b the gradient, k_2. In all cases the absolute value of the correlation coefficient, r, was greater than 0.932.

In order to determine k_1 the effect of k_2 during the first 28 days must be eliminated. The linear equation was used to obtain values of y corresponding to x values 3, 8, 16 and 28 days. These y values (which represent ln n) lie on the k_2 gradient. Anti-loging and subtracting them from the experimentally determined total droplet concentrations yielded ln n values that were then used to determine b, i.e. k_1, by linear regression analysis.

Equation (25) (Section 3.2.3.3) is used to determine the rates of coalescence. K_1 is dependent on the initial concentration of A droplets, $[A]_o$. This is not the total initial droplet concentration but rather a fraction of the concentration as determined by droplet distribution analysis. For the Number 4, 2M calcium nitrate emulsion $[A]_o$ would be 98.3% of n_o.

K_2 is dependent on the concentration of B droplets which is very small initially. K_2 is calculated using the concentration of all B droplets at 36 days ($[B]_o$) as

determined by droplet distribution analysis. This includes B droplets with diameters between 5.1 and 20.0 μm. Droplets with diameters > 20.1 μm are not included as this size interval ranges to infinite droplet size i.e. total demulsification. Consequently it is assumed that their coalescence does not contribute to k_2 (or k_3).

Table (20) lists initial A droplet concentrations, the rate constants, k_1, and the rates of coalescence, K_1, for the five 2M calcium nitrate emulsions.

The following section (Section 3.3.4.5.) refers to the data displayed in Table (20).

Table 20. Initial A droplet concentrations, rate constants, k_1, and rates of coalescence, K_1, for the 2M calcium nitrate emulsion series

EMULSION TYPE	$[A]_o \times 10^{12}$ /droplets dm^{-3}	$k_1 \times 10^{-7}$ /s^{-1}	$K_1 \times 10^{6}$ /droplets dm^{-3} s^{-1}
minimum	3.250	5.003	1.626
No. 1	3.563	8.004	2.852
No. 2	7.125	8.613	6.136
No. 3	10.16	12.03	12.23
No. 4	11.96	11.83	14.15

3.3.4.5. The Effect of Initial Droplet Concentration on the Initial Rate Determining Constant, k_1, and the Rate of Droplet Coalescence, K_1.

From Table (20) it can be seen that both k_1 and K_1 increase with increasing initial droplet concentration. Figure (59) is the graphical representation of k_1 versus $[A]_o$. Values of k_1 and $[A]_o$ were taken directly from Table (20).

From Figure (59) it can be seen that there is a linear relationship between k_1 and $[A]_o$. Therefore the higher the initial percentage of A droplets in an emulsion, i.e. the more monodisperse the original droplet distribution, the faster they will coalesce ultimately producing a more stable heterogenous distribution of droplets.

In order to determine the effects of Na^+, Ca^{2+} and Fe^{3+} nitrate salts on the initial rate constant, the effect of $[A]_o$, as illustrated in Figure (59), must be eliminated. Table (21) is a list of $[A]_o$, k_1 and K_1 values for the 0.4M, 0.8M and 2M; Na^+, Ca^{2+} and Fe^{3+} emulsions.

Figure 59. A plot of k_1 versus $[A]_o$ showing the effect of initial droplet concentration on the rate of coalescence in a 2M calcium nitrate emulsion

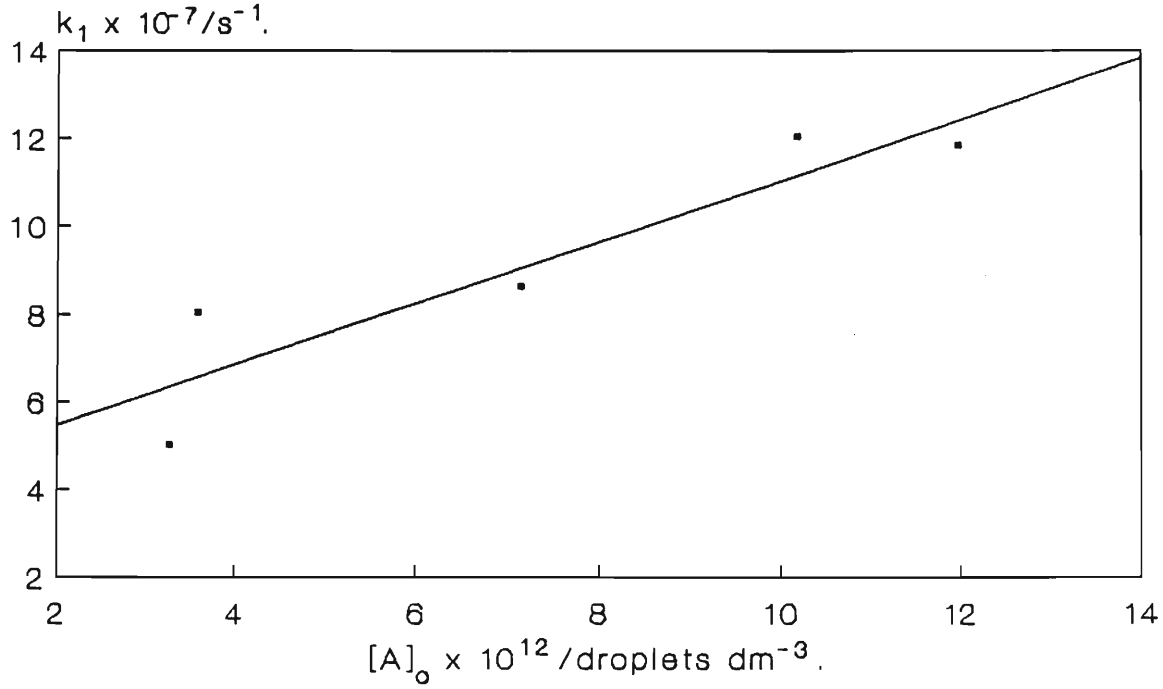

Table 21. $[A]_o$, k_1 and K_1 values for 0.4M, 0.8M and 2M emulsion systems

M^{n+}	M/mol dm^{-3}	$[A]_o \times 10^{-12}$ /droplets dm^{-3}	$k_1 \times 10^7$ /s^{-1}	$K_1 \times 10^{-6}$ /droplets dm^{-3} s^{-1}
Na^+	0.4	5.538	1.168	6.466
	0.8	4.438	9.176	4.072
	2.0	3.900	1.075	4.193
Ca^{2+}	0.4	6.323	1.264	7.992
	0.8	5.438	9.500	5.166
	2.0	3.563	6.560	2.337
Fe^{3+}	0.4	2.138	1.153	2.464
	0.8	6.625	1.288	8.533
	2.0	6.063	1.416	8.585

In order to compare the values of k_1 for the 2M emulsions, the plot in Figure (59) is used as a calibration curve. For the 2M ferric nitrate emulsion, $[A]_o$ is 6.063×10^{12} droplets dm^{-3}. Using the plot in Figure (59) and with the aid of linear regression analysis, k_1 was determined for a 2M calcium nitrate emulsion with an identical initial droplet concentration. A similar procedure was then applied to the 2M sodium nitrate emulsion. The results obtained from this analysis are shown in Table (22).

Table 22. k_1 and K_1 for emulsions of identical initial droplet concentration, $[A]_o$.

EMULSION	$[A]_o \times 10^{12}$ /droplets dm^{-3}	$k_1 \times 10^{-7}$ /s^{-1}	$K_1 \times 10^6$ /droplets dm^{-3} s^{-1}
2M Fe^{3+}	6.063	14.16	8.585
2M Ca^{2+}		8.298	5.031
2M Na^+	3.900	10.75	4.193
2M Ca^{2+}		6.795	2.650

The data in Table (22) suggest that k_1, and therefore K_1, are dependent on the type of nitrate salt in the emulsion system. k_1 values for both sodium and ferric nitrate emulsions are substantially higher than k_1 observed for calcium nitrate emulsions.

Unfortunately the effect of $[A]_o$ on k_1 was not anticipated prior to the preparation of the emulsions investigated. The effect of emulsification time was observed only for the 2M calcium nitrate emulsion series. Consequently k_1 for the 0.4M and 0.8M emulsions of the different nitrate salts cannot be compared. However, the general trend observed in Table (21) shows a decrease in coalescence as nitrate concentration increases. This is due to the reduction in electrostatic interfacial free energy at the oil/aqueous interface as the charge in the counterion layer builds up. Furthermore, calcium droplets are generally more stable than sodium and ferric nitrate droplets (assuming that k_1 increases with increasing $[A]_o$).

The fact that small calcium nitrate droplets are more stable tends to contradict the conclusions drawn from the interfacial tension data in Sections 3.1.3.2.1. and 3.1.3.2.2.

It was shown that the interfacial free energy at the aqueous calcium nitrate/oil-surfactant interface is greater than that at the sodium nitrate interface, over the concentration range investigated. This is thought to be caused by the energetically unfavourable interaction between adjacent PICDEA hydrocarbon chains brought about by the attraction of two deprotonated PICDEA molecules to a single divalent calcium cation. If this were the case then a droplet with such an interface should possess a lower energy barrier against coalescence. However, k_1 for the coalescence of small calcium nitrate droplets proves the opposite; the energy barrier against coalescence is higher than that between droplets containing sodium or ferric nitrate salts.

If one considers the effect of a small radius of curvature on the orientation of hydrocarbon chains at the interface of a small droplet, this apparent contradiction can be explained. This is discussed in the following section.

3.3.4.6. The Effect of Droplet Radius on the Entropic Repulsive Potential Energy, V_{RS}, of an Interface Stabilized with PICDEA

When the hydrocarbon chains of adsorbed surfactant molecules on neighbouring droplets overlap, the free energy change, ΔG, is the sum of the free energy changes of mixing, the excluded volume effect, the surface free energy change and the elastic free energy of repulsion[64]. Elworthy et al.[64] used the following expression for ΔG[134], i.e. V_{RS}, the entropic repulsive energy, to determine the effect of various nonionic polyethylene oxide compounds on droplet stability against coalescence:

$$\frac{\Delta G}{kT} = \frac{4\pi N c^2}{3\nu\rho_2^2}\left[\frac{1}{2} - \chi_1\right]\left[\delta - \frac{H}{2}\right]^2\left[3a + 2\delta + \frac{H}{2}\right] \qquad (27)$$

where c = the concentration of surfactant in the interfacial region (g cm^{-3})

ν = the solvent molecular volume

ρ_2 = the surfactant density

χ_1 = the surfactant-solvent interaction parameter

H = the droplet separation

δ = twice the thickness of the adsorbed surfactant layer

a = the droplet radius

From this equation it is evident that V_{RS} is proportional to the droplet radius, i.e. the smaller the droplet the lower the entropic energy of repulsion preventing droplet coalescence. This agrees with the observed rapid rate of coalescence between small A droplets as opposed to the slower coalescence rate of larger B droplets. More importantly, V_{RS} is also proportional to the square of the concentration, c, of surfactant in the interfacial region. It will be shown that c is dependent on the droplet radius and therefore the effect of droplet radius, r, on V_{RS} is more pronounced than that predicted by Elworthy et al.

Elworthy et al.[64] calculated c from the interfacial excess (Γ /moles cm^{-2}) and the thickness of the adsorbed layer (cm). Their calculation does not, however, take into account the effect of a change in the radius of curvature on the concentration. This effect is illustrated in the following determination of c for a small A and larger B droplet.

Consider an A droplet with a 1.5 μm radius. The volume of the droplet is 1.414×10^{13} Å^3. The bulky hydrocarbon chain of the PICDEA molecule (originating from Aktol PIBSA) has a maximum extension of approximately 60 Å into the oil continuous phase. The total volume, including the hydrocarbon chains, is determined for a sphere with an extended radius of $1{,}506 \times 10^4$ Å and is equal to 1.431×10^{13} Å^3. The difference in volume, i.e. the volume occupied by the adsorbed surfactant hydrocarbon chains, is the difference between the inner and outer droplet volumes and is equal to 1.701×10^{11} Å^3.

The surface area of the inner droplet is 2.827×10^9 Å^2. The number of PICDEA droplets adsorbed in a monolayer completely covering the droplet surface is equal to the total droplet surface area divided by the area occupied by a PICDEA molecule. The interfacial area per molecule was determined from the surface excess, Γ, which was obtained using the Gibbs Equation (Equation (5), Section 3.1.1.). For Aktol PICDEA (Batch B), the surfactant used in the preparation of all the emulsions investigated, the interfacial molecular area was found to be 225.7 Å^2 (Table (8), Section 3.1.2.2.). Hence it can be calculated that there are 1.253×10^7 PICDEA molecules adsorbed at the droplet interface and the concentration of surfactant molecules in the interfacial region is therefore 7.366×10^{-5} molecules Å^{-3} which is equivalent to 0.2079 g cm^{-3}.

A similar series of calculations on a B droplet with a radius of 4 μm yields a concentration of 0.2111 g cm^{-3}. These calculations show that the larger the droplet the more concentrated the interfacial region. In other words, the hydrocarbon chains are packed closer together around a relatively large droplet and should therefore be more efficient at preventing the interpenetration of hydrocarbons from approaching droplets. Since the entropic energy of repulsion is proportional to the square of c, an increase in c (for B droplets) implies a squared increase in the entropic energy of repulsion preventing coalescence.

This increase in volume and consequent decrease in surfactant concentration in the interfacial region

surrounding progressively smaller droplets may account for the observed trend in initial rate constants for coalescence. To explain this it is appropriate to illustrate the change in surfactant concentration in terms of the change in area available per hydrocarbon chain on the outer spherical surface.

Consider an A droplet with a radius of 1.5 μm. The surface area of the outer sphere, including the hydrocarbon chains, is equal to 2.850×10^9 Å^2. The total number of PICDEA molecules adsorbed at the droplet interface is 1.253×10^7 molecules (as determined previously). Therefore the end of each hydrocarbon chain has an area of 227.5 Å^2 in which to orientate itself. This area is large in comparison to the maximum cross-sectional area of the bulky hydrocarbon helix which is approximately 27.3 Å^2. This figure was determined by the summation of bond lengths and Van der Waals radii through a cross section of the helix.

The tip of a hydrocarbon chain extending from the surface of a B droplet (radius of 4 μm) has an area of 226.3 Å^2 in which to orientate itself. Therefore, a chain extending from an A droplet has an additional 1.14 Å^2 in which to move. In terms of the total area available per hydrocarbon, this additional area represents an increase of only 0.5 %. However, in terms of the cross-sectional dimensions of the hydrocarbon and the interpenetration of hydrocarbons from neighbouring droplets this increase is significant. Consider two approaching A droplets, the additional area between adjacent hydrocarbons will make interpenetration easier, i.e. the entropic repulsive

energy V_{RS}, will be reduced.

Therefore, the smaller the droplet the greater the distance between adjacent hydrocarbon tails and hence the lower the energy of repulsion between them. If this effect is sufficient to counteract the increase in interaction energy between hydrocarbons caused by the attraction of PICDEA molecules to calcium cations (refer to Section 3.1.3.2.), then it is possible that a small droplet containing calcium nitrate may be more stable than a droplet of identical size containing sodium nitrate. This would be caused by the higher ionic strength of the calcium nitrate solution which would reduce the electrostatic free energy of the interface to a larger extent than sodium nitrate and therefore create a droplet with a more energetically stable interface.

It is possible, however, that if the concentration of calcium ions in the droplet is sufficient to provide each PICDEA anion with a calcium cation then the adverse interaction of hydrocarbons would not occur. The slower coalescence observed for small calcium nitrate droplets (refer to Table (22)) would then simply be a function of the lower interfacial tension (refer to Figure (30) Section 3.1.3.2.1.) associated with relatively high concentrations of calcium nitrate.

Table (22) also shows that small ferric nitrate droplets coalesce at a faster rate than both sodium and calcium nitrate droplets. Referring to Section 3.1.3.1., it was shown that in the presence of an aqueous ferric nitrate solution (pH 1 to 2) PICDEA is protonated and the interface is therefore positively charged (on the inner

surface of the droplet interface). The counterion in this case is the nitrate anion. Referring to Figure (31) (Section 3.1.3.2.), it was suggested that a build up of nitrate anions in the counterion layer may cause the observed increase in interfacial free energy. The increase in anion concentration results in an increase in repulsive forces between anions which may account for this increase in interfacial free energy. However, comparison of Figures (30) and (31), (Section 3.1.3.2.), shows that the interfacial tension at the 2M aqueous ferric nitrate (ln n = 0.693)- diesel PICDEA interface is of a similar magnitude to that of a 2M aqueous sodium nitrate-diesel PICDEA interface. If a study of the interfacial free energy, in the presence of different nitrate salt aqueous phases, at an interface of infinite radius of curvature is representative of the effects of these nitrates on the interfacial free energy at a droplet interface, then the observed trend in coalescence rate constants would suggest that interfacial free energy is of secondary importance in the stabilisation of the aqueous nitrate droplet. This tends to support the point made by Garti and Katz[72], that it is the nature of the adsorbed surfactant interfacial film rather than the interfacial tension/free energy that should be investigated in the determination of droplet stability.

The reason why small aqueous ferric nitrate droplets should coalesce at a faster rate than droplets containing either calcium or sodium nitrate solutions is not clearly understood. Perhaps the nature of the nitrate anion or the protonated form of PICDEA adversely effect the structure and mechanical strength of the interfacial film.

3.3.4.7. The Effect of Aqueous Phase Composition on the Slow Rate Constant, k_2, and Rate of Droplet Coalescence, K_2.

Table (23) shows initial B droplet concentration, [B], (previously defined in Section 3.3.4.4.) the coalescence rate constant, k_2, and respective rates of droplet coalescence, K_2, for all of the emulsion systems under discussion. For the 2M calcium nitrate series [B] is dependent on the total initial droplet concentration, n_o, which is somewhat unexpected. It is, therefore, more appropriate to compare the percentages of B droplets present after 36 days for each emulsion in the series. This will give an indication of the type of droplet distribution which is characteristic of the long term stability of the emulsion. Table (24) is a comparison of percentage droplet size distributions for the five 2M calcium nitrate emulsions after 36 and 127 days.

The percentage distributions displayed in Table (24) are noticeably similar after the initial 36 days and even more so after the full 127 day observation period. This suggests that the droplet size distribution attained after approximately 36 days is relatively stable and characteristic of the long term stability of the emulsion system. This droplet size distribution is expected to be partially dependent on nitrate salt concentration and the type of nitrate salt in the aqueous phase.

Table 23. A list of B droplet concentrations, $[B]_o$, after 28-36 days, rate constants, k_2, and rates of coalescence, K_2.

M^{n+}		[NITRATE] /mol dm^{-3}	$[B]_o \times 10^{-11}$ /droplets dm^{-3}	$k_2 \times 10^8$ /s^{-1}	$K_2 \times 10^{-4}$ /droplets dm^{-3} s^{-1}
Ca^{2+}	min.	2.0	5.827	3.596	2.095
	No. 1		7.405	3.166	2.345
	No. 2		10.17	2.374	2.414
	No. 3		10.68	3.336	3.563
	No. 4		12.36	3.338	4.126
Ca^{2+}		0.8	8.198	3.010	2.468
		0.4	7.896	3.610	2.850
Na^{+}		2.0	7.680	2.412	1.852
		0.8	5.837	1.850	1.080
		0.4	7.397	2.137	1.581
Fe^{3+}		2.0	8.532	2.028	1.730
		0.8	11.13	1.241	1.381
		0.4	5.302	1.026	0.544

Table 24. Percentage droplet size distributions for the five 2M calcium nitrate emulsions after 36 and 127 days.

Emulsion	% Droplet Size Distribution after 36 days				
	< 5μm	5.1-10μm	10-15μm	15-20μm	> 20μm
minimum	68.6	20.06	6.56	4.13	0.65
No. 1	73.7	14.46	8.52	2.71	0.61
No. 2	71.29	23.10	4.03	1.29	0.29
No. 3	76.76	19.65	2.58	0.85	0.16
No. 4	75.30	22.00	2.10	0.50	0.10
Emulsion	% Droplet size Distribution after 127 days				
	< 5μm	5.1-10μm	10-15μm	15-20μm	> 20μm
minimum	72.69	12.70	6.27	7.23	1.11
No. 1	72.19	15.39	5.87	5.30	1.25
No. 2	71.40	22.47	3.42	2.20	0.51
No. 3	74.30	19.60	4.44	1.39	0.27
No. 4	73.60	21.30	3.76	1.11	0.23

An average percentage droplet distribution for the 2M calcium nitrate emulsion series is displayed in Table (25) together with the distributions for the 2M ferric nitrate and 2M sodium nitrate emulsions.

Table 25. Percentage droplet distributions for the 2M emulsion samples after 36 and 127 days

Emulsion 2M	% Droplet Size Distribution after 36 Days				
	< 5μm	5.1-10μm	10.1-15μm	15.1-20μm	> 20.1μm
Na^{+}	73.62	19.41	5.76	0.97	0.24
Ca^{2+}	73.13	19.85	4.76	1.90	0.36
Fe^{3+}	68.78	26.31	4.31	0.44	0.16
	% Droplet Size Distribution after 127 Days				
Na^{+}	71.81	17.50	8.92	1.45	0.32
Ca^{2+}	72.84	18.29	4.75	3.45	0.67
Fe^{3+}	66.98	22.12	9.50	1.13	0.27

It is interesting to compare these distributions in Table (25). However, as only one set of data exist for the sodium and ferric nitrate emulsions no conclusions can be made as to the effect of different nitrate salts on the type of droplet distribution attained by the emulsion. It is apparent that a 2M ferric nitrate emulsion has a droplet distribution which is less asymmetrical than those of calcium and sodium nitrate emulsions, i.e. the ferric nitrate emulsion contains a

lower percentage of both A droplets and droplets with diameters greater than 15.1 μm, and a higher percentage of B′ and B" droplets than emulsions containing calcium and sodium nitrate solutions. The relevance of this observation will become apparent in the following discussion.

From Table (23) it can be seen that k_2 is independent of $[B]_o$, unlike k_1 which is linearly related to $[A]_o$ (refer to Section 3.2.3.5., Figure (59)). Therefore, k_2 for the different nitrate salt emulsions can be compared directly, irrespective of $[B]_o$. If this is the case then the k_2 values for the 2M calcium nitrate series should be identical. This is not the case, however, on average, k_2 for a 2M calcium nitrate emulsion is 3.162×10^{-8} s^{-1}. This value has a standard deviation of 0.467×10^{-8} s^{-1}. If this deviation is applicable to the k_2 values for all of the emulsion systems (assuming that k_2 is totally independent of $[B]_o$) then no conclusive analysis can be made as to the different effects of the various nitrate salts on the long term stability of an emulsion stabilised by PICDEA.

However, a trend exists indicating that calcium nitrate droplets coalesce at a faster rate than aqueous sodium and ferric nitrate droplets, i.e. $Ca^{2+} > Na^{+} > Fe^{3+}$. The same trend is observed in the comparison of 0.8M and 0.4M emulsions in Table (23). This trend is opposite to that observed for the initial rate constant for coalescence, k_1, over the first 28 to 36 days (refer to Section 3.3.4.5., Tables (21) and (22)).

The more symmetrical distribution of droplet sizes in an emulsion containing aqueous ferric nitrate may in part contribute to the relatively slow rate of droplet coalescence. This is in agreement with Muller's[129] observation that emulsions with symmetrical droplet distributions are generally more stable than those with asymmetrical distributions.

The univalent nitrate anion, in the ferric nitrate droplet, and the univalent sodium cation, in the sodium nitrate droplet, attract individual PICDEA molecules to the droplet interface. Consequently, the PICDEA molecules are packed with their hydrocarbons protruding perpendicular to the interface into the oil continuous phase as depicted in Figure 36 (Section 3.1.3.2.3.).

Divalent calcium cations attract two PICDEA molecules resulting in the adverse interaction of their hydrocarbon tails. The hydrocarbons do not protrude straight into the oil phase but are at an angle to the perpendicular as depicted in Figure (36) (Section 3.1.3.2.3.). It is feasible that such an orientation effect will not only weaken the structure of the droplet interfacial film but also enable the closer approach of coagulated droplets through a reduction in the entropic forces of repulsion, i.e. V_{RS}, between interpenetrating hydrocarbons.

CHAPTER IV

CONCLUSIONS

The aim of this work was to evaluate the effects of various nitrate salts on the ability of PICDEA, an amphiphilic PIBSA-derived surfactant, to stabilize the droplet interface in an aqueous nitrate/ fuel oil (w/o type) emulsion. The conclusions drawn from this work are as follows:

The measurement of interfacial tension using the ring detachment method at the equilibrated aqueous/oil-surfactant interface provided the following information:

1. Batch-to-Batch variations in the quality of PICDEA. Batch A Aktol PICDEA contained excess unreacted CDE (a surface active precursor to PICDEA). The presence of CDE caused a reduction in the interfacial pressure of PICDEA at the diesel/water interface and also produced a "minimum" in the interfacial tension-concentration curve characteristic of the presence of a surface active contaminant. CDE is a water soluble amphiphile and should be eliminated as far as possible from the surfactant solution since it may lead to the breakdown of explosive emulsions[70].

2. DSA\CDE occupies a far smaller area at the interface than PICDEA. The dodecenyl hydrocarbon chain is shorter and less bulky than the PIB hydrocarbon of PICDEA, thus

enabling the closer packing of surfactant molecules at the interface.

3. Adibis E-70 has a greater interfacial pressure than Aktol E-70 at the diesel/water interface due to the preferential adsorption of Adibis E-70 which has a shorter PIB hydrocarbon chain than Aktol E-70. Both Adibis and Aktol E-70 molecules occupy the same interfacial area at the interface. Consequently (w.r.t. conclusion 2) it is thought that it is the bulkiness of the hydrocarbon chain rather than its length which effects the packing of the surfactant molecule at the interface. This explains the large differences in molecular interfacial area determined for DSA/CDE and PICDEA at the diesel/water interface.

4. E-70 and PICDEA molecules based on Adibis PIBSA have greater interfacial pressures at the aqueous/oil interface than the same derivatives based on Aktol PIBSA. This suggests that the shorter hydrocarbon chain Adibis derived molecules are more efficient at lowering the interfacial free energy than those based on Aktol PIBSA.

5. The single hydrocarbon tail E-70 molecule occupies a smaller area at the diesel/water interface than a double hydrocarbon tail PICDEA molecule. This is probably due to the smaller polar head group of the E-70 molecule and its single hydrocarbon structure which would enable the closer packing of molecules at the interface.

6. At pH values less than approximately 4.6 PICDEA is protonated producing a more surface active cationic species. At pH values greater than 4.6 PICDEA is

deprotonated producing a more surface active anionic species. At pH values less than approximately 2 E-70 is neutral, but undergoes deprotonation at higher pH values to produce the more surface active anionic species.

7. At an interface with aqueous calcium or sodium nitrate solutions (0.007M to 6M) PICDEA is deprotonated and hence the interface is negatively charged. A counterion layer of calcium or sodium cations forms in the aqueous phase.

8. The attraction of two adjacent PICDEA anions to a divalent calcium cation results in the energetically unfavourable orientation ofthe PICDEA hydrocarbon tails above the interface.

9. The calcium cation does not induce the same hydrocarbon orientation effect at an interface saturated with E-70. This is probably due to the single tail hydrocarbon structure of the E-70 molecule and its smaller interfacial molecular area, i.e. the closer packing of E-70 molecules at the interface.

10. At an interface with an aqueous ferric nitrate solution (pH 1 to 2) PICDEA is protonated and a counterion layer of nitrate anions forms below the interface. It is thought that repulsive forces between nitrate anions causes an increase in the interfacial free energy at the PICDEA-saturated interface as ferric nitrate salt concentration is increased in the aqueous phase. However, a point is reached when a further increase in nitrate salt concentration causes a decrease in interfacial free energy. This observation is not

fully understood, although it is thought to be related to the nature of the positively charged PICDEA molecule at the interface and its interaction with the nitrate anion.

11. A complex formed between a PIBSA derived surfactant such as PICDEA and the cation of a nitrate salt, e.g. a PICDEA-Ca^{2+} or Na^{+} complex, will have a positive effect on the HLB value of the surfactant. According to HLB theory[88,91] such a complex will be less efficient at stabilizing a water-in-oil type emulsion.

12. A literature study of the binding of cations to phospholipid membranes suggests that if a complex between a PIBSA derived surfactant and a cation does occur then it is likely that the surfactant will bind preferentially with Ca^{2+} rather than the Na^{+} cation.

A complete chromatographic separation of the components present in commercial PICDEA was unsuccessful. The following techniques provided limited separation.

1. Normal phase TLC (silica grade 60) using a 100 % ethyl acetate mobile phase resulted in the partial separation of CDE, diesel, process oil and PIB hydrocarbons from PICDEA and PIBSA. PIBSA and PICDEA components remained unseparated at the point of application. A number of mobile phases (Chapter II, Section 2.2.2.1. Table (3)) of varying eluent strengths were investigated with no significant improvement in the separation of PIBSA from PICDEA.

2. Reverse phase (C18) liquid chromatography was unsuccessful due to the interaction of the non-polar gel structure and the surfactant hydrocarbon tails. The large range in surfactant hydrocarbon tail lengths resulted in the spreading and overlapping of the various components over many fractions. The solvent systems investigated were: THF (100%), THF/iso-propanol (70/30), chloroform (100%), chloroform/acetone (80/20), chloroform/iso-propanol (70/30) and carbon tetrachloride (100%).

3. Size exclusion chromatography was attempted using Sephadex LH-20. True size exclusion chromatography was not achieved; PICDEA (molecular wt. 1700 g mol^{-1}), Aktol PIBSA (molecular wt. 1400 g mol^{-1}) and free diethanolamine (molecular wt. 105 g mol^{-1}) were detected in the first fractions collected using a mobile phase of chloroform/ethanol (97/3). Although hydrocarbon components were retarded by the gel, spreading and overlapping of all of the components present in Aktol PICDEA occurred. The solvent systems investigated were THF (100%), chloroform (100%) and chloroform/ethanol (97/3).

A literature survey and experimental study of aqueous droplet coalescence provided the following conclusions concerning the effect of nitrate salts on the rate of droplet coalescence in a water-in-oil emulsion system stabilized using Aktol PICDEA.

1. In the preparation of an emulsion stabilized with PICDEA emulsification time is dependent on the

interfacial free energy between the two separated phases, the type of nitrate salt in the aqueous phase and the nitrate salt concentration.

a) The greater the interfacial free energy the longer the emulsification time necessary to produce a stable emulsion.

b) The higher the concentration of nitrate salt the lower the interfacial free energy and hence a shorter emulsification time is needed to produce the emulsion.

c) A plot of emulsification time versus nitrate salt concentration (Section 3.1.3.2.1. Figure (33)) for the preparation of sodium, calcium and ferric nitrate emulsions shows a similar dependence on nitrate salt concentration and cation type as the interfacial tension-nitrate salt concentration curve (Figure (32)).

2. In the high internal phase emulsion systems studied in this work coalescence of droplets is the rate determining step in the overall breakdown of the emulsion. The coagulation of droplets is rapid and non-rate determining.

3. The stability of coagulated droplets against coalescence is largely dependent on the structural properties of the adsorbed surfactant interfacial layer.

4. PICDEA based on Aktol PIBSA rather than the shorter Adibis PIBSA will provide a larger potential energy barrier against coalescence due to the increased distance between adjacent droplets and increased repulsive forces

between interpenetrating hydrocarbon tails of two approaching coagulated droplets.

5. The adsorption of PICDEA at the droplet interface and the effects of various nitrate salts on the surfactants orientation at the interface and the interfacial structure, rather than the interfacial tension between separated phases, should be considered in the evaluation of an emulsions stability.

6. Increased emulsification time beyond the minimum time necessary to produce the emulsion results in a decrease in the average droplet diameter and hence an increase in the initial droplet concentration, n_o.

7. Coalescence may follow two or more consecutive first order reactions. The rate of coalescence can be described by two rate constants: an initial rapid rate constant lasting for approximately 28 to 36 days followed by a slow rate constant associated with the long term stability of the emulsion.

8. The initial rate constant is due to the coalescence of very small droplets with diameters of 5μm and less (A droplets). The slower rate is predominantly due to the coalescence of larger droplets (B droplets).

9. After approximately 28 to 36 days the droplet distribution attained has a symmetry conducive to a more stable emulsion.

10. When the concentration of B droplets has increased sufficiently so that they occupy a larger volume than A droplets they become effective in separating the A droplets thereby reducing the probability of rapid A droplet coalescence.

11. The initial rate determining constant, k_1, is dependent on the initial droplet concentration, n_o. The greater n_o the larger k_1 becomes.

12. The radius of curvature of a droplet effects the concentration of surfactant hydrocarbon tails in the interfacial region surrounding the droplet. The smaller the droplet the lower this concentration becomes and therefore the interpenetration of hydrocarbons between coagulated droplets becomes easier since the repulsive energy of interaction, V_{RS}, is reduced. A decrease in the radius of curvature of a droplet causes a reduction in the potential energy barrier against coalescence.

13. During the first 28 to 36 days calcium nitrate droplets coalesce at a slower rate than sodium and ferric nitrate droplets, i.e. $Fe^{3+} > Na^{+} > Ca^{2+}$. This may be associated with a lower interfacial free energy at an interface with aqueous calcium nitrate.

14. The slow rate determining constant, k_2, is independent of the initial concentration of B droplets, $[B]_o$.

15. After 36 days droplets containing calcium nitrate coalesce at a faster rate than droplets containing sodium

and ferric nitrate solutions, i.e. $Ca^{2+} > Na^{+} > Fe^{3+}$.

16. The calcium cation attracts two PICDEA anions at the interface increasing the interaction between the hydrocarbon tails of adjacent molecules. Such an orientation effect may enable the closer approach of coagulated droplets and cause a reduction in V_{RS}. This would reduce the potential energy barrier against coalescence.

17. The droplet distribution attained after 28 to 36 days is partially dependent on the type of nitrate salt in the aqueous phase. An emulsion containing ferric nitrate attains a more symmetrical distribution than calcium and sodium nitrate emulsions. This may, in part, account for the slower rate of coalescence observed in ferric nitrate emulsions.

CHAPTER V

SUGGESTIONS FOR FUTURE WORK

The emulsion systems studied in this work were stabilised using PICDEA based on Aktol PIBSA. A comparison of the stabilising qualities of Aktol PICDEA with those of Adibis PICDEA should support results obtained from the investigation described in this thesis which suggest that PICDEA based on the shorter hydrocarbon tail Adibis PIBSA will be less efficient in preventing droplet coalescence than Aktol PICDEA. Future droplet distribution studies should be performed using laser diffraction or Coulter counter techniques since the photomicrographic technique used for this work is time consuming and does not provide a sufficiently detailed distribution of droplet sizes.

A pure organic phase, such as toluene or hexane, should be used for all interfacial tension studies instead of the fuel oils used commercially. The surface activity of various aromatics and napthenes in mineral oils and diesel and variations in their proportions from one batch to the next often required experimental repetition in this investigation. The use of a pure organic solvent would enable a study of the effects of the aqueous phase composition on the PIBSA saturated interface without any interference from diluent contaminants. It is important to note, however, that the penetration of oil molecules (particularly aromatics and short chain alkanes) into the

adsorbed surfactant layer plays an important role in influencing emulsion stability[135,136]. A study of the penetration of fuel oil components into the adsorbed interfaces of various PIBSA derived surfactants should provide some interesting results and aid in the choice of a suitable fuel oil.

It has been suggested that as two coagulated droplets move closer together the surfactant molecules tend to move away from the area of contact[137]. This movement will be hindered if surface viscosity is appreciable and one might expect that the stability of the interface would parallel the surface viscosity. Wason and Mohan[138] have shown that surfactants that lower interfacial viscosity also destabilize crude oil-water emulsions. The measurement of interfacial viscosity with varying surfactant concentration and aqueous/organic phase compositions may provide some interesting information concerning the strength of the mechanical barrier against droplet coalescence in explosive emulsions. Campanelli et al.[139] found the viscous traction interfacial viscometer to be a highly reliable screening instrument.

REFERENCES

1. Alexander, J., "Colloid Chemistry", New York, D. Van Nostrand, 102, (1924)
2. Encyclopaedia Britanica, 14th Ed., 8, 416
3. Sutheim, G.M., "Introduction to Emulsions", Brooklyn, Chemical Publishing Co., 1, (1946)
4. The Concise Oxford Dictionary, 5th Ed., Oxford University Press, 398, (1964)
5. Becher, P., "Emulsions: Theory and Practise", New York, Reinhold Publishing Co., 2, (1966)
6. Carrol, B.J., "The Stability of Emulsions and Mechanisms of Emulsion Breakdown", Surfactant Colloid Science, 9, pp. 3-5, (1976)
7. Ref. 6, pp. 26-27
8. Ref. 6, p. 3
9. Aveyard, R., "Ultralow Tensions and Microemulsions", Chemistry and Industry, pp. 474-478, July (1987)
10. Quincke, Weid. Ann., 35, 571, (1888)
11. Gibbs, J.W., "Scientific Papers", Longmans and Co., 1, (1906)
12. Bancroft, J. Phys. Chem., 17, 514, (1913); 19, 275, (1915)
13. Ref. 9, p. 474
14. Harkins, W.D., and Zollman, H., J. Amer. Chem. Soc., 48, 69, (1926)
15. Ruckenstein, E., and Chi, J., J. Chem. Soc. Faraday Trans., II, 71, pp. 1690-1707, (1975)
16. Ref. 6, p. 3
17. Ref. 5, pp. 209-263

18. Winsor, P.A., "Solvent Properties of Amphiphilic Compounds", London, Butterworth Scientific Publications, 2, (1954)
19. Ref. 5, p. 20
20. Bluhm, H.F., U.S. Patent 3,447,978 (June 1969) in "Encyclopaedia of Emulsion Technology", Becher, P., Marcel Decker Inc., 3, 283, (1988)
21. Bampfield, H.A., and Cooper, J., "Encyclopaedia of Emulsion Technology", 3, 283, (1988), Becher, P., Marcel Decker Inc.
22. Wallace, B.W., "Physics and Chemistry of Explosives", AECI Explosives and Chemicals Ltd. National Symposium, Pretoria, (1987)
23. Private Communication: AECI Explosives and Chemicals Ltd. (1987)
24. Ref. 21, p. 290
25. Ref. 22, p. 6
26. Ref. 21, p. 290
27. Private communication, Knight, C., "Emulsion Explosives", July 1987
28. Cooper, J., "Fundamentals: Monolayer and Dielectric Studies", PIBSA Conference, AECI Explosives and Chemicals Ltd., Modderfontein, (1989)
29. Private communication: AECI Explosives and Chemicals Ltd., Chemical Resourses Division, (1989)
30. Chattopadhyay, A., Private communication with AECI Explosives and Chemicals Ltd., (1989)
31. Chattopadhyay, A., PIBSA Conference, AECI Explosives Division, Modderfontein, (1989)
32. Shah, D.O., and Shulman, J.H., J. Lipid Res., 8, 215, (1967)
33. Chattopadhyay, A., "PIBSA derivatives: Hydrolysis in Aqueous AN Environment", report, (1988)

34. Chattopadhyay, A., PIBSA Conference, AECI Explosives Division, Modderfontein, (1989)
35. Ref. 33, p. 1
36. Harkins, W.D., and Jordan, H.F., J. Amer. Chem. Soc., 52, pp. 1751-1772, (1930)
37. Ref. 5, p. 391
38. Harkins, W.D., Young, and Cheng, Science, 64, 93 (1926)
39. Freud, b.b., and Freud, H.Z., J. Amer. Chem. Soc., 52, pp. 1772-1783, (1930)
40. Macy, R., J. Chem. Ed., 12, 573, (1935)
41. Du Nouy, P.L., J. Gen. Phys., 1, 521, (1918-1919)
42. Padday, J.F., J. Colloid Sci., 15, 503, (1960)
43. Jaycock, M.J., and Parfitt, G.D., "Chemistry of Interfaces", John Wiley and Sons, pp. 56-57, (1981)
44. Ref. 5, pp. 398-400
45. Ref. 43, p. 64
46. White Instrumentation Company Booklet
47. Langmiur, I., J. Amer. Chem. Soc., 39, 1848, (1917)
48. McGee, C.G., Abstr. Amer. Chem. Soc., 124th meeting, (1953)
49. Harkins, W.D., and Humphrey, E.C., J. Amer. Chem. Soc., 38, 236, (1916)
50. Klopsteg, Science, 60, 319, (1924)
51. MacDougal, J. Amer. Chem. Soc., 62, 290, (1925)
52. Ref. 5, p. 397
53. Handbook of Chemistry and Physics, 64th Ed., Weast
54. Perry, S.G.; Amos, R. and Brewer, P.I., "Practical Liquid Chromatography", Plenum/Rosetta Edition, (1973)
55. Ref. 54, p. 55
56. Still, W.C., Kahn, M. and Mitra, A., J. Organic Chem., 43, No. 14, pp. 2923-2925, (1978)
57. Kremmer, T. and Boross, L., "Gel Chromatography: Methodology, Applications", Wiley, 31, (1979)

58. Sephadex Manual, "Gel Filtration in Theory and Practice", (1972)

59. Snyder, L.R. and Kirkland, J.J., "Introduction to Modern Liquid Chromatography", John Wiley and Sons, (1974)

60. Wilk, M., Rochlitz, J. and Bende, H., J. Chromatography, 24, 414, (1966)

61. Talarico, P.C. Albaugh, E.W. and Snyder, R.E., Analytical Chemistry, 40, 2192, (1968)

62. Joustra, M.K., Protides Biol. Fluids, 14, 533, (1967)

63. Van den Tempel, M., Proc. 2nd Int. Congr. Surface Activity, 1, pp. 439-446, (1957)

64. Elworthy, P.H., Florence, A.T. and Rogers, J.A., J. Colloid Interface Sci., 35, No. 1, (1971)

65. Wesley-Smith, J., "Short Notes on the Principles of Light Microscopy", Lecture notes, Biology Department, University of Natal, Durban, (1990)

66. Ref. 65

67. Spencer, M., "Fundamentals of Light Microscopy", Cambridge University Press, (1982)

68. Hedgecoe, J., "Introductory Photographic Course", Mitchell Beazley Publishers Ltd., (1983)

69. Jokela, P., Fletcher, P.D.I., Aveyard, R. and Lu, J.R., J. Colloid Interface Sci., 134, No. 2, (1990)

70. Ref. 21, p. 286

71. Adamson, A.W., "Physical Chemistry of Surfaces", Wiley, New York, 3rd Ed., 493, (1967)

72. Garti, N. and Katz, M., J. Dispersion Science and Technology, 6, No. 2, pp.149-158, (1985)

73. Aveyard, R. and Briscoe, B.J., Trans. Faraday Soc., 66, 2911, (1970)

74. Ref. 5, p. 8

75. Partington, J.R., "Advanced Treatise on Physical Chemistry", Longmans Green and Co., 2, 134, (1951)

76. McBain, J.W., Ford, T.F. and Wilson, D.A., Kolloid-Z., 78, 1, (1937)
77. Ref. 5, pp. 28-30
78. Bulkeley, R. and Bitner, F.G., Bur. Standards Journal of Research, 5, 951, (1930)
79. Reichenberg, D., Trans. Faraday Soc., 43, 467, (1947)
80. Brady, A.P., J. Phys. Chem., 53, 56, (1949)
81. Williams, E.F., Woodberry, N.T. and Dixon, J.K., J. Colloid Sci., 12, 452, (1957)
82. Miles, G.D. and Shedlovsky, L., J. Phys. Chem., 48, 57, (1944)
83. Ref. 5, p. 30
84. Ref. 5, chp. 2
85. Boyd, J., Parkinson, C. and Sherman, P., J. Colloid Interface Sci., 41, No. 2, pp. 359-370, (1972)
86. Ref. 5, pp. 234-252
87. Al-Diwan, T.A.B., Hughes, M.A. and Whewell, R.J., J. Inorganic Nuclear Chem., 39, 1419-1424, (1977)
88. Becher, P., J. Soc. Cosmetic Chemists, 11, 325, (1960)
89. Griffin, W.C., J. Soc. Cosmetic Chemists, 1, 311, (1949)
90. Ref. 5, p. 234
91. Davies, J.T., Proc. 2nd Int. Congr. Surface Activity, 1, 426, (1957)
92. McLaughlin, S., Mulrine, N., Gresalfi, T., Vaio, G. and McLaughlin, A., J. Gen. Physiol., 77, pp. 445-473, (1981)
93. Holwerda, D.L., Ellis, P.D. and Wuthier, R.E., Biochemistry, 20, pp.418-428, (1981)
94. McLaughlin, A.C., Biochemistry, 21, pp. 4879-4885, (1982)
95. Lis, L.J., Parsegian, V.A. and Rand, R.P., Biochemistry, 20, pp.1761-1770, (1981)
96. Nash, H.A. and Tobias, J.M., Proc. National Academic Sci. U.S.A., 51, pp. 476-480, (1964)

97. Abramson, M.B., Katzman, R.and Gregor, H., J. Biol. Chem., 239, pp. 70-76, (1964)

98. Papahadjopoulos, D., Vail, W.J., Newton, C., Nir, S., Jacobson, K., Poste, G. and Lazo, R., Biochemica and Biophysica Acta, 465, pp. 579-598, (1977)

99. Lis, L.J., Lis, W.T., Parsegian, V.A. and Rand, R.P., Biochemistry, 20, pp. 1771-1777, (1981)

100. Ref. 59

101. Ref. 21, p. 291

102. Ref. 21, p. 292

103. von Smoluchowski, M., Physik. Z., 17, 557-583, (1916)

104. Chen J-D, J. Colloid Interface Sci., 107, No. 1, 209-220 (1985)

105. Ref. 5, p. 170

106. Ref. 5, pp. 128-131

107. Ref. 6, pp. 10-26

108. Ref. 5, pp. 118-119

109. Derjaguin, B.V., Trans. Faraday Soc., 36, 203, (1940)

110. Bockris, J.O'M. and Reddy, A.K.N., "Modern Electrochemistry", Plenum Press, New York, 2, 730, (1977)

111. Verwey, E.J.W. and Overbeek, J.Th.G., "Theory and Stability of Lyophobic Colloids", Elsevier, Amsterdam, Chapter II, (1948)

112. Hamaker, H.C., Physica IV, 10, 1058, (1937)

113. Ref. 5, p. 204

114. Schulman, J.H. and Cockbain, E.G., Trans. Faraday Soc., 36, 661, (1940)

115. Bhatnagar, S.S., J. Chem. Soc., 117, 542, (1920)

116. Fuoss, R.M. and Kraus, C.A., J. Amer. Chem. Soc., 55, 3614, (1933)

117a. Albers, W. and Overbeek, J.Th.G., J. Colloid Sci., 14, 501, (1959)

117b. Albers, W. and Overbeek, J.Th.G., J. Colloid Sci., 14, 510, (1959)

118. Becher, P., Surfactant Science Series (Interfacial Phenomena Apolos. media), 21, pp. 257-280, (1987)

119. Hesselink, F.Th., J. Phys. Chem., 75, 65, (1971)

120. Hesselink, F.Th., Vrij, A. and Overbeek, J.Th.G., J. Phys. Chem., 75, 2094, (1971)

121. Sherman, P., J. Colloid Interface Sci., 45, 427, (1973)

122. Derjaguin, B.V. and Churaev, N.V., J. Colloid Interface Sci., 49, 249, (1974)

123. Israelachvili, J.N., Philos. Mag. A, 43, 753, (1981)

124. Harusawa, F. and Mitsui, T., Progress in Organic Coatings, Elsevier, Amsterdam, 3, pp. 177-190, (1975)

125. Ref. 5, Chapter I

126. Garti, N. and Katz, M., J. Dispersion Sci. and Technology, 6, No. 2, pp. 149-158, (1985)

127. Ref. 21, p. 286

128. Ref. 5, p.184

130. Ref. 5, pp. 271-277

131. Ref. 21, p. 287

132. Capellos, C. and Bielski, B.H.J., "Kinetic Systems", Wiley Interscience, U.S.A., (1972)

133. Ref. 43, p. 41

134. Ottewill, R.H. and Walker, T., Kolloid Z. Z. Polm., 108, 227, (1968)

135. Kunieda, H., Yano, N. and Solans, Colloids and Surfaces, 36, 313, (1986)

136. Williams, J.M., Langmuir, 4, 44, (1988)

137. Ref. 6, p. 29

138. Srivastava, S.W. and Haydon, D.A., Proc. 4th Int. Congr. Surface Activity, 2, 1221, (1964)

139. Biswas, B. and Haydon, D.A., Kolloid-Z., 185, 31, (1962)

APPENDIX I

The molecular structures of various PIBSA-derived surfactants.

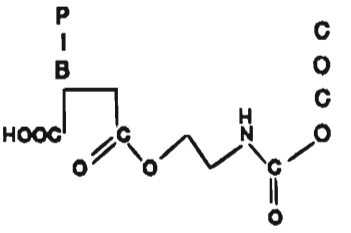

PICMEA

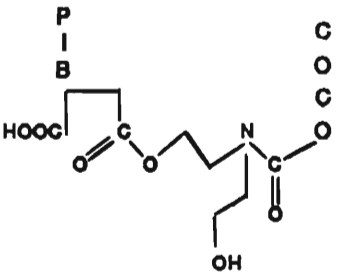

PICDEA

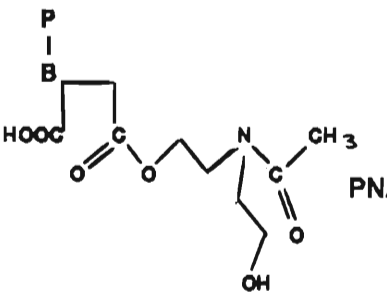

PNADEA

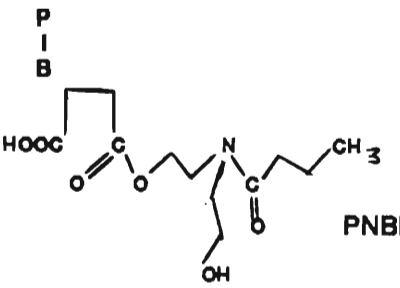

PNBDEA

E-70 (E475-high imide)

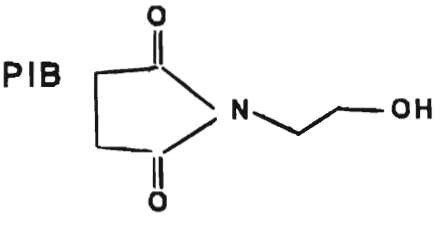

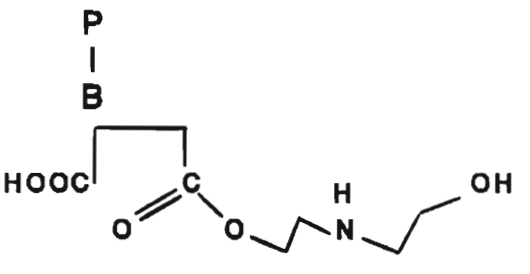

E476

APPENDIX II

Commercial Coconut acid contains:

		No. Carbons	Double bonds
1 %	Caprylic Acid	8	0
7 %	Cupric Acid	10	0
49 %	Lauric Acid	12	0
17 %	Myristic Acid	14	0
9 %	Palmitic Acid	16	0
2 %	Stearic Acid	18	0
6 %	Oleic Acid	18	1
2 %	Linoleic Acid	18	2

Average Carbon chain length = 12.3

Empirical Formula of CDE = $C_{16}H_{33}NO_3$

CDE Average Molecular Weight = 287 g/mole

APPENDIX III

Manro Coconut-diethanolamide

Typical Data:	Appearance	: Clear golden liquid
	Viscosity	: 800 cps
	Free Amine	: 8 % max.
	Free Alkali	: 6 % max.
	Free Fatty Acid	: 2 % max.

Minimum Assay of CDE = 84 %

Table 1. Droplet Distribution: 2M $Ca(NO_3)_2.4H_2O$ Emulsion

DAYS	% DROPLET SIZE DISTRIBUTION					DROPLET CONC. x 10^{-12} / DROPLETS dm^{-3}
	< 5.0 µm	5.1-10.0 µm	10.1-15.0 µm	15.1-20.0 µm	> 20.1 µm	
3	77.27	17.88	4.02	0.76	0.06	4.206
8	73.89	20.62	4.57	0.84	0.08	3.807
16	70.77	22.79	5.34	1.03	0.07	3.445
28	70.81	21.22	5.26	2.42	0.29	2.648
36	68.6	20.06	6.56	4.13	0.65	1.895
49	72.8	15.90	5.73	4.70	0.87	1.819
84	72.79	14.69	5.49	6.11	0.92	1.632
127	72.69	12.70	6.27	7.23	1.11	1.428

Table 2. Droplet Distribution: 2M $Ca(NO_3)_2.4H_2O$ No. 1

DAYS	% DROPLET SIZE DISTRIBUTION					DROPLET CONC. x 10^{-12} / DROPLETS dm^{-3}
	< 5.0 µm	5.1-10.0 µm	10.1-15.0 µm	15.1-20.0 µm	> 20.1 µm	
3	78.81	16.59	3.85	0.63	0.12	4.521
8	76.37	18.58	4.27	0.68	0.10	4.198
16	70.03	24.52	4.22	1.08	0.15	3.303
28	70.84	19.13	7.63	2.10	0.30	2.541
36	73.7	14.46	8.52	2.71	0.61	2.103
49	71.61	16.02	8.65	3.09	0.63	1.955
84	72.89	15.09	7.02	3.86	1.14	1.842
127	72.19	15.39	5.87	5.30	1.25	1.611

Table 3. Droplet Distribution: 2M $Ca(NO_3)_2.4H_2O$ No. 2

DAYS	% DROPLET SIZE DISTRIBUTION					DROPLET CONC. x 10^{-12} / DROPLETS dm^{-3}
	< 5.0 µm	5.1-10.0 µm	10.1-15.0 µm	15.1-20.0 µm	> 20.1 µm	
3	90.66	8.10	1.08	0.14	0.02	7.859
8	88.39	10.38	1.05	0.15	0.03	7.086
16	80.18	17.34	1.89	0.50	0.09	5.005
28	75.88	20.61	2.58	0.75	0.18	4.250
36	71.29	23.10	4.03	1.29	0.29	3.577
49	70.26	24.60	3.33	1.51	0.30	3.292
84	70.55	23.32	3.94	1.80	0.39	3.154
127	71.40	22.47	3.42	2.20	0.51	2.906

Table 4. Droplet Distribution: 2M $Ca(NO_3)_2.4H_2O$ No. 3

DAYS	% DROPLET SIZE DISTRIBUTION					DROPLET CONC. x 10^{-12} / DROPLETS dm^{-3}
	< 5.0 µm	5.1-10.0 µm	10.1-15.0 µm	15.1-20.0 µm	> 20.1 µm	
3	95.73	3.89	0.38	/	/	10.613
8	94.09	5.33	0.47	0.11	/	9.618
16	87.45	11.41	0.83	0.27	0.04	6.590
28	78.99	18.21	2.04	0.69	0.07	5.103
36	76.76	19.65	2.58	0.85	0.16	4.625
49	76.26	19.39	3.20	0.98	0.17	4.347
84	75.22	19.56	3.79	1.22	0.21	3.802
127	74.30	19.60	4.44	1.39	0.27	3.583

Table 5. Droplet Distribution: 2M $Ca(NO_3)_2.4H_2O$ No. 4

DAYS	% DROPLET SIZE DISTRIBUTION					DROPLET CONC. x 10^{-12} / DROPLETS dm^{-3}
	< 5.0 µm	5.1-10.0 µm	10.1-15.0 µm	15.1-20.0 µm	> 20.1 µm	
3	98.30	1.70	/	/	/	12.17
8	96.00	3.89	0.11	/	/	11.26
16	88.10	11.12	0.58	0.16	0.04	7.164
28	81.80	16.06	1.67	0.38	0.09	5.655
36	75.30	22.00	2.10	0.50	0.10	5.029
49	74.97	21.18	2.54	0.58	0.13	4.702
84	73.35	21.53	4.23	0.72	0.17	4.233
127	73.60	21.30	3.76	1.11	0.23	3.837

Table 6. Droplet Distribution: 0.8M $Ca(NO_3)_2.4H_2O$

DAYS	% DROPLET SIZE DISTRIBUTION					DROPLET CONC. x 10^{-12} / DROPLETS dm^{-3}
	< 5.0 µm	5.1-10.0 µm	10.1-15.0 µm	15.1-20.0 µm	> 20.1 µm	
3	88.15	9.24	2.26	0.35	/	6.169
8	85.02	12.37	2.13	0.38	0.10	5.795
16	80.78	15.55	2.56	0.96	0.15	4.763
28	74.90	19.60	4.44	1.26	0.09	3.367
36	72.00	22.50	3.04	2.11	0.35	2.965
49	71.10	20.59	4.35	2.90	1.06	2.779
84	71.15	19.12	5.54	2.77	1.33	2.502
127	70.40	16.54	5.51	5.95	1.60	2.326

Table 7. Droplet distribution: 0.4M $Ca(NO_3)_2.4H_2O$

DAYS	% DROPLET SIZE DISTRIBUTION					DROPLET CONC. x 10-12 / DROPLETS dm^{-3}
	< 5.0 µm	5.1-10.0 µm	10.1-15.0 µm	15.1-20.0 µm	> 20.1 µm	
3	89.10	10.35	0.43	0.12	/	7.096
8	84.15	14.95	0.65	0.25	/	6.495
16	77.98	18.53	1.56	1.03	0.90	4.721
28	73.39	19.95	2.87	2.09	1.70	3.347
36	71.80	19.98	4.16	2.41	1.65	2.974
49	70.05	20.10	5.23	2.56	2.06	2.866
84	71.12	18.35	6.00	2.80	1.73	2.683
127	69.90	17.00	7.15	3.36	2.59	2.223

Table 8. Droplet Distribution: 0.4M $Fe(NO_3)_3.9H_2O$

DAYS	% DROPLET SIZE DISTRIBUTION					DROPLET CONC. x 10-12 / DROPLETS dm^{-3}
	< 5.0 µm	5.1-10.0 µm	10.1-15.0 µm	15.1-20.0 µm	> 20.1 µm	
1	70.72	23.24	3.78	1.77	0.49	3.023
9	69.18	24.13	3.95	2.00	0.74	2.633
21	64.52	23.30	8.59	2.49	1.10	1.725
28	64.10	21.50	10.94	2.51	0.95	1.517
41	63.91	20.02	12.19	2.78	1.10	1.456
77	63.05	19.98	12.25	2.60	2.12	1.443
119	63.26	17.89	12.55	3.65	2.65	1.384

Table 9. Droplet Distribution: 0.8M $Fe(NO_3)_3.9H_2O$

DAYS	% DROPLET SIZE DISTRIBUTION					DROPLET CONC. x 10^{-12} /DROPLETS dm^{-3}
	< 5.0 µm	5.1-10.0 µm	10.1-15.0 µm	15.1-20.0 µm	> 20.1 µm	
1	91.04	7.50	1.03	0.43	/	7.277
9	78.50	17.52	2.74	1.00	0.24	5.286
21	71.69	25.63	2.63	1.11	0.24	3.857
28	69.90	23.50	4.00	1.65	0.95	3.819
41	68.91	23.60	4.21	1.88	1.40	3.785
77	69.15	22.05	6.09	1.70	1.01	3.691
119	68.78	20.56	7.37	2.19	1.10	3.462

Table 10. Droplet Distribution: 2M $Fe(NO_3)_3.9H_2O$

DAYS	% DROPLET SIZE DISTRIBUTION					DROPLET CONC. x 10^{-12} / DROPLETS dm^{-3}
	< 5.0 µm	5.1-10.0 µm	10.1-15.0 µm	15.1-20.0 µm	> 20.1 µm	
1	95.93	2.88	1.02	0.17	/	6.320
9	85.39	12.04	2.10	0.38	0.09	4.743
21	79.51	16.75	3.18	0.49	0.07	3.601
28	73.36	21.81	4.02	0.66	0.15	3.221
41	68.78	26.31	4.31	0.44	0.16	3.235
77	68.11	24.05	6.78	0.83	0.23	3.010
119	66.98	22.12	9.50	1.13	0.27	2.829

Table 11. Droplet Distribution: 0.4M $NaNO_3$

DAYS	% DROPLET SIZE DISTRIBUTION					DROPLET CONC. x 10^{-12} / DROPLETS dm^{-3}
	< 5.0 µm	5.1-10.0 µm	10.1-15.0 µm	15.1-20.0 µm	> 20.1 µm	
1	86.87	10.50	2.03	0.56	0.04	6.375
6	84.11	11.56	3.50	0.81	0.02	4.913
14	79.98	14.99	4.10	0.90	0.03	3.751
26	72.54	18.79	5.90	2.20	0.57	2.930
34	71.90	20.03	6.45	1.12	0.50	2.680
47	70.32	21.00	7.25	1.13	0.30	2.675
82	69.51	19.10	7.95	2.42	1.02	2.497
125	69.90	16.50	9.31	3.19	1.10	2.282

Table 12. Droplet Distribution: 0.8M $NaNO_3$

DAYS	% DROPLET SIZE DISTRIBUTION					DROPLET CONC. x 10^{-12} / DROPLETS dm^{-3}
	< 5.0 µm	5.1-10.0 µm	10.1-15.0 µm	15.1-20.0 µm	> 20.1 µm	
1	88.47	6.83	4.02	0.67	0.01	5.317
6	86.12	8.19	4.65	0.86	0.18	4.978
14	77.94	16.00	5.83	0.23	/	3.297
26	73.91	18.25	5.65	1.89	0.30	2.179
34	72.15	19.98	6.53	1.00	0.34	2.096
47	71.23	19.90	7.58	0.86	0.43	1.972
82	69.25	17.50	9.25	2.10	1.90	1.906
125	70.01	17.00	8.86	2.23	1.90	1.784

Table 13. Droplet Distribution: 2M $NaNO_3$

DAYS	% DROPLET SIZE DISTRIBUTION					DROPLET CONC. x 10^{-12} /DROPLETS dm^{-3}
	< 5.0 µm	5.1-10.0 µm	10.1-15.0 µm	15.1-20.0 µm	> 20.1 µm	
1	89.24	6.95	3.05	0.70	0.06	4.370
6	81.18	13.76	3.41	0.70	0.12	3.905
14	76.34	18.00	4.53	1.04	0.09	3.406
26	73.98	19.94	4.77	1.06	0.25	3.025
34	73.62	19.41	5.76	0.97	0.24	2.938
47	74.36	17.95	6.38	1.14	0.17	2.808
82	73.89	17.54	7.17	1.21	0.19	2.639
125	71.81	17.50	8.92	1.45	0.32	2.455